JOURNAL OF APPLIED PHYSICS

JOURNAL OF APPLIED
PHYSICS

OCTOBER, 1940 Vol. 11, No. 10

In This Issue

	Page
"The Irresponsibles"	625
New Books	626
Resumés of Recent Research	628

Contributed Original Research

Cuprous-Cupric Oxide Films on Copper — C. G. Cruzan and H. A. Miley	631
On the Resistance to the Uniform Motion of a Solid Through a Viscous Liquid — Raymond B. Block	635
Preparation of High Melting Alloys with the Aid of Electron Bombardment — Ralph Hultgren and M. H. Pakkala	643
Measurement of Solid Friction of Plastics — Andrew Gemant	647
Optical Properties of Colloidal Suspensions in Relation to the Measurement of Particle-Size Frequency — E. G. Richardson	653
Velocity of Compressional Waves in Petroleum Fractions at Atmospheric and Elevated Pressures — Robert Matteson and C. J. Vogt	658
Electric Oscillations and Surges in Subdivided Windings — Reinhold Rüdenberg	665
Dielectric Properties of the Rutile Form of TiO_2 — L. J. Berberich and M. E. Bell	681

In Every Issue

Contributors to This Issue	693
Here and There	694
Index to Advertisers	viii

BOARD OF EDITORS

Elmer Hutchisson, *Editor*

Associate Editors

F. Bitter
W. E. Forsythe
L. A. Jones
B. E. Warren
J. B. Whitehead

Publication of the American Institute of Physics

ADMINISTRATIVE STAFF

Henry A. Barton, *Director*

Madeline M. Mitchell, *Publications Manager*

John T. Tate, *Adviser on Publications*

GOVERNING BOARD

Paul E. Klopsteg, *Chairman*
George B. Pegram, *Secretary*
Karl T. Compton
Wheeler P. Davey
Floyd A. Firestone
Harvey Fletcher
R. C. Gibbs
Arthur C. Hardy
George R. Harrison
A. Stuart Hunter
H. R. Lillie
Frederic Palmer, Jr.
George B. Pegram
W. B. Rayton
John T. Tate
Wallace Waterfall

The Journal of Applied Physics, published monthly at Prince and Lemon Sts., Lancaster, Pa., is devoted to physics in its role as the science basic to other natural sciences and to the arts and industries. Previous to 1937 this publication was known as Physics. It aims to be of service not only in physical laboratories, but also in the laboratories of industrial, chemical, geological, geophysical, meteorological, radio, and similar concerns. The Journal of Applied Physics publishes editorials, news of physicists and reviews, as well as technical papers of applied physics.

Manuscripts should be submitted to Elmer Hutchisson, Editor, University of Pittsburgh, Pittsburgh, Pennsylvania.

SUBSCRIPTION PRICE

	U. S., POSS. AND CANADA	FOREIGN
To members of scientific societies	$5.00	$5.70
To all others	7.00	7.70

Single copies are $.70 each.

Changes of address and proofs should be addressed to the Publications Manager.

Subscriptions and orders for back numbers should be addressed to Prince and Lemon Streets, Lancaster, Pa. or to the American Institute of Physics, 175 Fifth Avenue, New York, N. Y.

Advertising rates supplied on request. Orders, advertising copy and cuts should be sent to the American Institute of Physics.

Entered as second class matter at the Post Office at Lancaster, Pennsylvania, under the Act of March 3, 1897.
Accepted for mailing at the special rate of postage provided for in the Act of February 28, 1925, authorized May 2, 1932.

Copyright 1940, by the American Institute of Physics.

Journal of Applied Physics

Volume 11 October, 1940 Number 10

"The Irresponsibles"

ARCHIBALD MacLeish* has made a declaration and a challenge. He accuses physicists and scholars in all fields of having divided learning into narrow cubicles; each particular scholar being conscientious, laborious, competent and supreme in his own little section but absolutely disinterested in the society or the culture that has made his bit of freedom possible or in his responsibility for its continuation. MacLeish deplores the fission of the man of letters into the scholar on one hand and the writer on the other, neither of whom accepts the responsibility for the defense of the common culture of the West.

One would like to refute this powerful little essay. It would be comforting to be able to say: "No, he just doesn't know scientists." Unfortunately he knows them only too well. Which of us has not given thanks that we have not been driven out of our laboratories, and yet has never given a thought as to what we ourselves can do today to prevent this same catastrophe from overtaking us tomorrow?

On many sides men of science have even been accused of contributing to the possibility of their own downfall. Because of the applications of science we live in an entirely different world from that of the "men of letters" who wielded the pen so mightily in the cause of freedom in the seventeenth, eighteenth and nineteenth centuries. Civilization has been furnished with great sources of energy to ease man's physical work, with artificial light to extend the hours of his activities, fast methods of transportation to all corners of the earth and new systems of communications that enable him to talk to a million people thousands of miles away with no more effort than to a friend across the table. Unfortunately these very achievements have enabled a few selfish individuals to rise to great heights of power; to use the newly-developed sources of energy to build hideous weapons of destruction; to use the faster methods of transportation to bomb civilians and to level great cities; and to use the broader means of communication to spread lies in an attempt to erase completely the rights of human beings to think for themselves.

What can the scientist do about all this? Only the most narrow minded person would propose a scientific holiday. Scientific research must go forward as never before. Yet along with this increased activity scientific men and other scholars must also take out time to study the problems of government and to become leaders in preserving truth and freedom. The development of science in the past few years has given evidence of the great progress which is possible under an entirely democratic system. This progress has occurred in peace time and has its basis primarily in the enlightened membership of scholars who hold the truth above everything else. Can not scientists learn to use the essay, the radio, the movies, the dynamic museums and some of the other tools with which they have provided society to educate the lay members of this society in the method and goal of science? If that could be done surely a better world would result.

* Archibald MacLeish, *The Irresponsibles* (Duell, Slone and Pearce, New York, 1940).

New Books

Mechanics Applied to Vibrations and Balancing

By D. Laugharne Thornton. Pp. 529+xii, Figs. 186, 16×25½ cm. John Wiley and Sons, Inc., New York 1940. Price $7.50.

Chapter I gives Newton's laws of motion and applies them to the calculation of inertia reactions in crank engine systems. The character of the unbalance of various types of engine systems, including *opposed*, *vee*, and *radial* types, is treated. Generalized coordinates are described and Lagrange's equations derived. With this mathematical basis, a formula is developed for the fly-wheel effect of reciprocating engine parts. In another paragraph headed *Motion of Reciprocating Engines*, Lagrange's formula is again made use of. The paragraph proceeds into a mathematical haze, no clear result being obtained until the analysis is restarted on the basis of a simple single degree of freedom differential equation. Expressions for the stability of governors are derived in Chapter I by again using generalized coordinates. The treatment is difficult to follow, not only because of the unnecessary complication introduced by the use of generalized coordinates, but also because of lack of clarity in the diagrams and in the definitions of terms. This same criticism applies to Chapter II in which the subject is balancing of locomotives.

In Chapter III the solutions of the simple differential equations of a spring-mounted vibrating mass are given. Several simple vibrating systems are illustrated. Next, a general theory of vibration is given, using generalized coordinates and the concept of normal coordinates developed. Application is made of these results to the vibration of frames.

The subject of Chapter IV is the propagation of stress waves in elastic materials. The equations for wave propagation are developed for both longitudinal, transverse and torsional waves; applications of the former to pile driving, water hammer, and the fuel systems in internal combustion engines are made. The propagation of waves in reinforced concrete is treated. An interesting failure of concrete which took place twenty-four hours after an impact is described, yet no satisfactory explanation is offered. Spherical wave equations are derived and earthquakes are discussed briefly.

Chapter V deals with the vibration of beams, plates, frame structures and membranes. Nodal patterns and natural period formulae are developed. Hamilton's equations are derived and discussed. Another paragraph is devoted to the principle of least action.

Chapter VI is a complicated treatment of the vibration of rotating shafts and disks and relevant gyroscopic effects.

Chapter VII, headed "General survey," is a rambling discussion of subjects from ignorable coordinates to the physiological effect of vibration.

J. G. Baker
Baker Manufacturing Co.

The Perception of Light

By W. D. Wright. Pp. 100+iv, Figs. 49, 13×19 cm. Chemical Publishing Company, New York, 1939. Price $2.50.

This is a condensed summary of visual phenomena for illuminating engineers and for those interested in physiological optics. It discusses the effects of lighting and the peculiarities of vision on industrial efficiency and on the hazards of driving. The contents include a general account of visual phenomena, vision at low intensities, vision at high intensities, glare, visual sensations, and a summary of recent researches with a bibliography.

The recommendation as to what constitutes adequate illumination seems to be based on a faulty premise: "at certain times of the day and year we are in fact accustomed to working under daylight illuminations of several thousand footcandles." This may be true for farmers and day-laborers, but the reviewer has yet to see an office or home where the illumination actually used rises to such high values at any time.

Those who design or install lighting equipment for factories, homes, theaters, and highways will find much of value in this small book pertaining to the limits set by the properties of vision in regard to what constitutes adequate and safe lighting.

Joseph Valasek
University of Minnesota

(1) Mathematical Methods in Engineering

By T. v. Kármán and M. A. Biot. Pp. 505+xii, Figs. 172, 23½×16 cm. McGraw-Hill Book Company, Inc., New York, 1940. Price $4.00.

(2) Mathematics Applied to Electrical Engineering

By A. G. Warren. Pp. 384+xv, Figs. 131, 14½×22½ cm. D. Van Nostrand Company, Inc., New York, 1940. Price $4.50.

(1) This book, by the famous aeronautical engineer, and a professor of mechanics at Columbia, is really, as its title states, not concerned with mathematics but with mathematical methods. Presupposing a knowledge of only elementary calculus, it manages to teach a great deal of pure mathematics along the way; but its emphasis is continually on the methods of solution of physical problems of engineering interest. The reviewer believes that this represents the soundest pedagogy in the instruction of engineers and physicists.

The title is somewhat more general than the contents. *The book is essentially an introductory treatise, and an excellent one, on all phases of the theory of small oscillations, mechanical and electrical.* From the mathematical point

of view it gives an adequate working knowledge of ordinary differential equations, algebraic equations, matrices, Bessel's functions, elliptic integrals and functions, Fourier series, the complex representation of periodic phenomena, Heaviside's operational methods, and finite differences. It omits almost entirely such subjects as scalar and vector fields, partial differential equations, Legendre polynomials, conjugate functions, calculus of variations, and numerical integration. But this is as well, for in spite of its 500 pages it gives the impression of being condensed in style.

Each chapter terminates with a useful set of references to textbooks and articles, and with an extensive set of problems, almost all of which are practical examples drawn from many branches of engineering and physics.

For engineering students, a course from this book could well replace much of the differential equations and advanced calculus taught at present; the reviewer knows of one school where this has been tried successfully.

(2) The second book, written by a member of the research department at Woolwich and printed in England, differs from the first in many respects. It is concerned with electrical theory of all types: electromagnetic fields, radiation, steady and transient electric currents, oscillating circuits, skin effect, etc. At the same time, it starts from scratch to develop elementary and advanced calculus, differential equations, Fourier series, Bessel functions, operational calculus, and conjugate functions. Since it does all this in 360 pages, about half pure-mathematics and half electrodynamics, and contains no sets of problems, it is hardly suitable for use as a textbook. Neither its mathematical nor physical sections contain sufficient *introductory* material. But it is clearly written and should be valuable for purposes of review and reference in regard to both the mathematical and physical parts of its contents.

G. H. SHORTLEY
Ohio State University

The Microscope

BY R. M. ALLEN. Pp. 286+viii, Figs. 82, Plates XVII, 16×23½ cm. D. Van Nostrand Company, New York City, 1940. Price $3.00.

This is a book which users of microscopes will find profitable to read. Following an historical introduction and survey of optical principles, there are chapters on the types of modern instruments, illumination, the efficient use of a microscope, and preparation of material for examination.

Although it is not essential that a book of this type include a complete discussion of optical principles, certain mistakes in their statement should not have appeared. The statement that an object subtending less than 1.4 minutes of arc is invisible is obviously incorrect. It is another instance of the too common confusion between the requirement for resolving *two* objects and for just detecting a *single* small object. It is well to emphasize this because of the recent impossible claims for a supermicroscope which even appeared in a reputable optical journal. The statement that field brightnesses vary inversely as the square of the magnification, should have been qualified by a mention of "normal magnification," even though this is usually exceeded in practice. Abbe's diffraction theory of resolution is considered beyond the scope of the book. There is a footnote which comments on the theory but contains some misstatements as to how the requirement of coherent wavelets may be satisfied. A somewhat more detailed discussion of the subject would probably have led to a more accurate presentation. Photomicrography is only given passing notice. It is unfortunate that a chapter could not have been devoted to this important subject, though, as the author says, a complete discussion would require an entire volume.

JOSEPH VALASEK
University of Minnesota

Fundamentals of Photography

BY PAUL E. BOUCHER. Pp. 304+lii, FIGS. 94, 16×23½ cm. D. Van Nostrand Company, New York, 1940. Price $3.00.

Elementary Photography

BY GILFORD G. QUARLES. Pp. 350+x, Figs. 84, 16×23½ cm. McGraw-Hill Book Company, New York, 1940. Price $3.00.

Both of these books have been written mainly to serve as textbooks suitable for a first course in photography at the college level. An acquaintance with the fundamentals of optics, chemistry, and algebra is desirable but not essential. While both give complete directions for carrying out the principal photographic processes, only that by Boucher contains instructions for a set of formal laboratory experiments.

In general, Boucher places more emphasis on the scientific basis of photography. For example, the section on optics is carried far enough to include a derivation of the formulae for depth of field. Factors affecting tone reproduction, such as developer composition, concentration, and temperature are discussed with the aid of characteristic curves obtained by the author. The procedures followed in making such studies are adequately outlined. The chemical reactions of development, fixation, reduction, intensification, and toning are given where possible. The chapter on 2″×2″ film-slides is timely because of their low cost and usefulness in education, as well as their convenience in preserving and showing records of trips, experiments, and the like. At the end of each chapter is a set of references for those who wish to extend their study of some particular topic. There are many excellent illustrations of apparatus and procedures. The seventeen laboratory experiments are well chosen.

Quarles does not stress scientific basis so much, but gives much useful advice on the art or practice of photography. This will appeal more to students who do not find the natural sciences attractive, but will be unsatisfying to those who do. This book contains a good, short summary of the essentials of composition, and the controls that may be exercised in projection printing to secure an attractive print. The careful, critical study of well-made proofs which are mounted where one may see them frequently

over a period of several days or weeks before making the final print is an excellent recommendation. It is more likely to lead to successful results than any amount of study of characteristic curves. However, a thorough understanding of scientific fundamentals will reduce the number of unsuccessful attempts consigned to the waste-basket. Quarles discusses the use of paper negatives in pictorial photography and gives a good chapter on the coloring of prints and transparencies. The chapter on color photography is inadequate for there is no discussion of color printing.

It is odd that Boucher, who specializes in the study of contrast or gamma, states two incorrect definitions in words before giving the correct definition by means of an equation. Naturally, one advantage of mathematics is the precision with which one can make statements, but there seems to be no reason why definitions in words should be given in such a way that if translated literally into mathematical symbols, the resulting formulas would be incorrect. Both authors stumble on the use of brightness units. Boucher gives brightnesses in footcandles, while Quarles states that the units are foot-lamberts.

Both books fill a definite need for textbooks in a subject which is being increasingly recognized as a suitable addition to the college curriculum and is a fascinating hobby to many.

JOSEPH VALASEK
University of Minnesota

Resumés of Recent Research

Packed Fractionating Columns and the Concentration of Isotopes

The separation of isotopes in large quantities is based on a process closely analogous to fractional distillation. The theoretical problems arising during the operation of exceptionally long fractionating columns for the concentration of N^{15}, C^{13} and S^{34} are discussed by Karl Cohen.[1] The discussion is expressly fashioned to be of immediate applicability not to isotope separation alone, but to any problem of fractional distillation or counter-current washing.

The usual plate-to-plate treatment of distilling columns found in engineering manuals is replaced by the solution of simultaneous partial differential equations. In this way more practical solutions of problems involving long columns are obtained. Subjects considered include the relation between fractionation and the rate of production, and the hitherto unconsidered problem of the rate of approach to equilibrium. The results are condensed wherever possible into graphs, and illustrated by applications to the separation of isotopes.

The chief novelties of the treatment, aside from the divorce of packed columns from cramping analogies to plate columns, are the emphasis and method. Whereas the usual engineer's problem is the construction of a column to produce a given material at a given rate, the paper reported considers the performance of a single column under varying conditions. The application of more flexible mathematical methods permits the hope that considerable new knowledge may yet be extracted from the theory of fractionating columns.

[1] K. Cohen, "Packed fractionating columns and the concentration of isotopes," J. Chem. Phys. **8**, 588 (1940).

Mass Spectrometer for Routine Isotope and Gas Analyses

Since the discovery of the isotopic nature of the stable elements by J. J. Thomson in 1912 many improvements have been made in the technique of determining masses and relative abundances of isotopes. Recently, Alfred O. Nier[1] of the University of Minnesota described a new mass spectrometer suitable for routine isotope abundance measurements of those elements which conveniently may be put in a gas or vapor form.

As in most mass spectrometers the new apparatus produces positive ions by the controlled bombardment of a gas by an electron beam. The ions formed are drawn from the ionizing region and sent through a suitable analyzer which separates the various masses. The ion currents are measured by means of an electrometer tube amplifier.

Usually a 180° magnetic analyzer is employed to perform the mass analysis. This entails the use of either a large electromagnet or solenoid. Both the initial cost and power consumption are high

[1] A. O. Nier, Rev. Sci. Inst. **11**, 212 (1940).

for these. The principal virtue of the new apparatus lies in the fact that by employing a small electromagnet with wedge-shaped pole faces it is possible to obtain essentially as good resolution at a much lower initial cost. In addition, the power consumption is extremely low. The analyzer makes use of the well-known theorem that if ions are sent into the homogeneous magnetic field between two V-shaped poles there is a focusing action, provided the source, apex of V, and the collector lie along a straight line.

The mass-spectrometer tube housing is made entirely of glass and metal, with glass to metal seals connecting the various sections. As no grease or wax joints are employed, the tube may be outgassed, and hence, impurities are reduced to a minimum.

When heavy carbon, C^{13}, and heavy nitrogen, N^{15}, are used as tracers in biological and chemical problems it is necessary to make abundance measurements of the isotopes in order to determine the location of the "planted" heavy isotopes. The present apparatus has been found to perform this task very satisfactorily.

Because of the small amount of material necessary for an analysis the apparatus should also prove useful as a tool for performing routine purity analyses of either inorganic or organic gases.

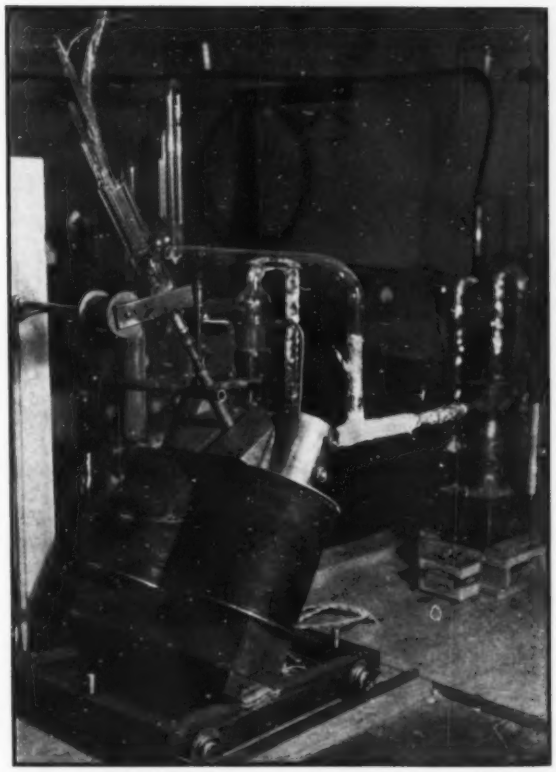

Mass spectrometer for routine isotope and gas analyses. Upper left: ion source; center: analyzer and magnet; far right: electrometer tube for measurement of ion currents.

A New Electron Microscope

Electrons of all speeds have come to be, in recent years, among the most valuable tools for exploring atomic and molecular dimensions. High speed electrons have been used mainly in connection with atomic and nuclear work, whereas electrons of lower speeds ($\beta = 0.3$ to 0.5) have been used in electron diffraction experiments which have become equal in rank to x-ray diffraction for exploring molecular structure. Bridging the gap between the dimensions covered by the fields above mentioned and that covered by light microscopy, an electron microscope, using electrons of the same speed as those used in electron diffraction, has been recently developed.

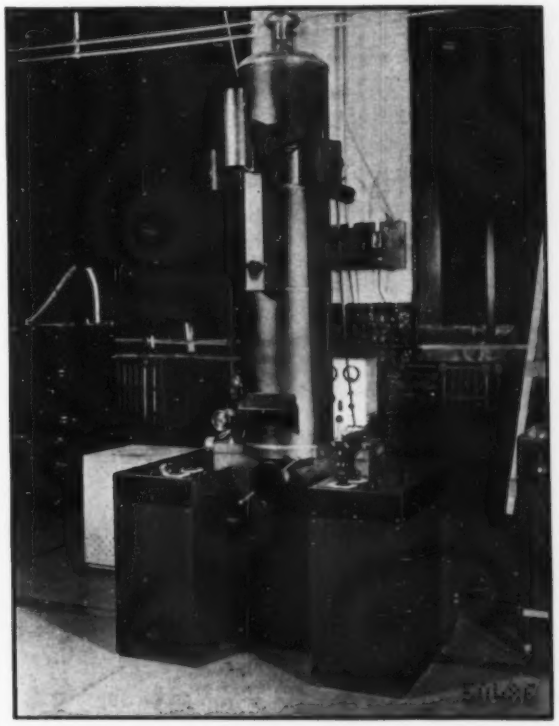

FIG. 1.

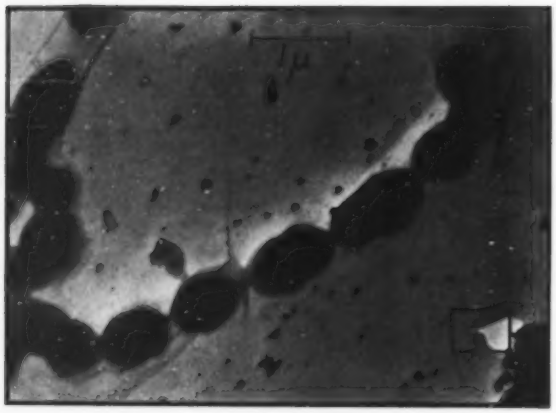

(a)

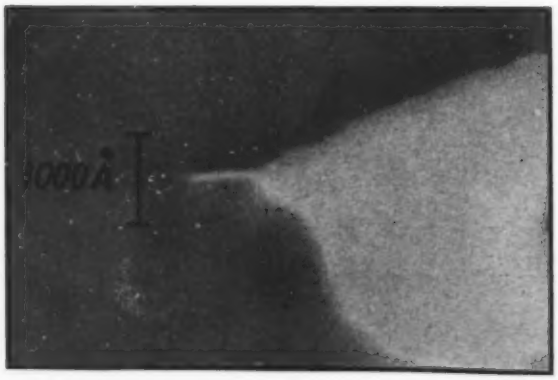

(b)

FIG. 2.

Of the different possible forms of electron microscopes, only the transmission type magnetic microscope has reached a stage of development where it can successfully be used as a research tool in biological, bacteriological, and colloidal research.

An improved form of such an instrument has been recently constructed in the RCA Research Laboratories (Fig. 1).[1] The electron beam is generated by means of a single potential electron gun provided with a hot cathode, which is completely adjustable for centering the beam along the optical axis of the instrument. The optical system, consisting of three iron-clad coils corresponding to the condenser, objective, and projection lenses, is built into the main tube of the microscope. Because the coils are housed inside the vacuum, they must be completely sealed to prevent excessive pumping time. The instrument is provided with air locks for the specimens and photographic plates to allow them to be rapidly changed without breaking the vacuum. Vacuum-tight adjustments move the "stage" in both horizontal and vertical directions. Two large windows are provided for visual observation of the highly magnified image on the main fluorescent screen. After focusing, photographic plates can be substituted for the fluorescent screen. A periscope-like system permits observation of the intermediate image (first-stage magnification) from the same window from which the highly magnified image is viewed, by means of an additional fluorescent screen placed between the objective and the projection lens. The adjustments of the instrument are placed so that the observer sitting in front of the main window can manipulate from one spot all focusing knobs and the adjustment of the "stage."

The results are best illustrated by Figs. 2 and 3. Figure 2 shows streptococcus bacteria taken at

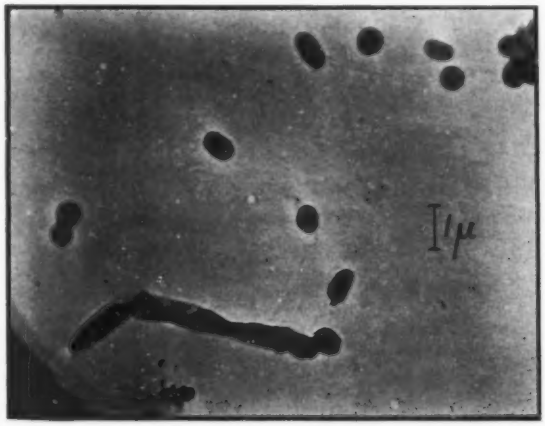

FIG. 3.

a direct magnification of 20,000, with the instrument. Resolving power can best be estimated from a defect of the bacteria-supporting nitrocellulose film shown separately enlarged, where the edges of a little crack in the film are 100A apart. From microphotometric measurements of the intensity distribution across the edges, a resolving power of at least 50A can be estimated. Figure 3 shows a bacteriological specimen of whooping cough germs, giving details of internal structure for an organism which itself is pretty close to the limit of visibility of light optical systems.

[1] L. Marton, Phys. Rev. **58**, 57 (1940).

Cuprous-Cupric Oxide Films on Copper

C. G. Cruzan and H. A. Miley
Physics Laboratory, Oklahoma Agricultural and Mechanical College, Stillwater, Oklahoma
(Received February 28, 1940)

The influence of film thickness on the formation of cupric oxide in cuprous oxide films on an abraded copper surface was studied from measurements obtained by the electrolytic reduction method. The critical thickness value for the formation of cupric oxide in the films appeared to be near 600A for a commercial copper, and the critical thickness range was found to be approximately 400 to 800A. The thicknesses resulting from heating specimens in different atmospheres, for a given time, increase with the oxygen concentration. The time required to produce films of a given thickness decreases as the oxygen concentration increases. Murison's observations concerning the conditions favorable to the formation of cupric oxide in the films at a higher temperature were extended to include the proper period of heating and film thickness as well as oxygen concentration. Dunholter and Kersten's electron diffraction analyses of copper oxide films on mirror-like surfaces were considered to be in satisfactory agreement with the present results.

Introduction

SINCE the electrolytic reduction method[1] has made it possible to measure the respective amounts of each oxide in cuprous-cupric oxide films,[2] it was employed in the present work for studying the influence of film thickness on the composition of the copper oxide films. This method requires that the time be observed for the cathodic reduction of a film from a fixed area by a constant current, and from the millicoulombs thus obtained the thickness is determined by means of one of Faraday's laws.

Procedure

Sheets of a good grade of commercial copper (99.99 percent pure), which had been rolled to a thickness of 0.5 mm, were obtained from the Central Scientific Company, and abraded with flint paper No. 0, cut into strips measuring 1.75×5.5 cm, washed in benzene, and rubbed dry with chemically pure cotton. Other experimental factors were similar to those described elsewhere,[2] except the electrolyte employed was 0.1 *M* ammonium chloride solution and the constant current of 1 to 0.5 milliamperes[3] per square cm was provided by applying 220 volts through a resistance of 100,000 to 200,000 ohms. A larger current value involves a smaller time for an experiment and accordingly increases the effectiveness of any observational or instrumental error in the time measurement. Smaller current values cause a decrease in the sharpness of the end points, and magnify the influence of any tendency of the films to dissolve in the electrolyte. The error due to the reduction of any of the oxygen, dissolved in the electrolyte, is very small when reduction currents of the order of those mentioned above are employed. Ammonium chloride solution gives much sharper end points for the copper oxide experiments than potassium chloride or any other electrolyte that was tried.

[1] H. A. Miley, Iron and Steel Inst., Carnegie Schol. Mem. **25**, 197 (1936).
[2] H. A. Miley, J. Am. Chem. Soc. **59**, 2626 (1937).
[3] The current value was fixed at the lower part of this range only for the measurement of the thinner films.

Results

Critical thickness range

Copper oxide films of different thicknesses were prepared by heating specimens in air at 240°C for various periods of time. Figure 1 shows the great influence of film thickness on the composition of the films. Cuprous oxide films of thicknesses less than 400A contained no cupric oxide. Only a part of the films in the thickness range 400 to 800A possessed some of this oxide while all of those above 800A contained some cupric oxide. The thickness range which provides both cuprous oxide and cuprous-cupric oxide films is defined in this paper as the *critical thickness range*, CTR, of Fig. 1. The probability of obtaining cuprous-cupric oxide films in this range

increases with the thickness while that of obtaining cuprous oxide films decreases. Hence there must be some intermediate thickness value in the range at which the simple and duplex films are equally probable, and this value is defined as the *critical thickness* of cuprous oxide films. It is probably near 600A for the films formed under the present conditions.

The critical thickness value and range would be expected to vary some with conditions.

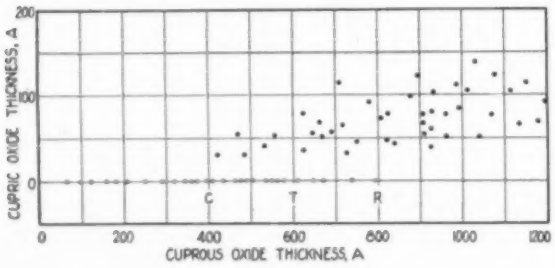

FIG. 1. Composition of some air-formed copper oxide films prepared at 240°C, each circle being obtained from a single experiment. White circles represent cuprous oxide films containing no cupric oxide. The abscissa and ordinate values of the black circles represent the respective amounts of cuprous and cupric oxide in these films.

Clearly anything that alters the perviousness of the films affects the critical thickness values. As the film thickens diffusion through it becomes increasingly more difficult and when the critical thickness range is reached the cuprous oxide is expected to begin competing with the base metal for the attacking oxygen. For the experiments of Fig. 1 such factors as nature of the material, treatment of the surface, purity of the air, temperature at which the films were formed, and oxygen concentration in the furnace atmosphere were kept constant. The different thicknesses were provided by heating the specimens for various periods of time. Similar thickness effects were obtained by keeping the period of time constant and varying the temperature at which the films were prepared. It seems reasonable to expect the temperature at which the films are formed to have some influence on the formation of cupric oxide in the cuprous oxide films, but its influence on the perviousness of the films measured in the range 150 to 350 °C appeared to be small.

A series of copper oxide films of increasingly thicker values are easily obtained by heating similar specimens in pure air (1) at a given temperature for successively increasing periods of time, or (2) for a given time through a chosen range of temperatures. Thickness-time curves for copper oxide films produced at ordinary and several higher temperatures have been given elsewhere.[2] Since the effect of oxygen concentration was not studied in this former work, some observations were made in the present work.

Oxygen concentration

The electric furnace was kept at 240°C while some specimens were heated in air, others in air rich in nitrogen, and still others in air rich in oxygen. These conditions were provided by conducting nitrogen or oxygen into the furnace through a glass tube. The small diffusion through the asbestos door of the furnace made it possible to keep the gas replenished without disturbing the temperature equilibrium appreciably.

In Table I it can be seen that the thickness resulting from heating specimens in different atmospheres, for a given time, increases with the oxygen concentration. Table II shows that the time required to produce films of similar thicknesses decreases as the oxygen concentration increases.

This variation of the oxidation rate with the pressure of the attacking gas appears to be in general agreement with C. Wagner's theory of oxidation for copper discussed by Price.[4] The thickness-time curves obtained were similar to those already given,[2] with the ones for the greater oxygen concentration displaced towards the larger thickness values and those for the lesser oxygen concentration displaced towards the smaller thickness values.

TABLE I. *Copper oxide thicknesses produced at 240°C by varying the oxygen concentration.**

Time in Minutes	Thickness† of Films, A			Atmosphere
	Cu_2O	CuO	Total	
6	1005	95	1100	Air rich in oxygen
6	905	75	980	Air
6	545	0	545	Air rich in nitrogen

* It is to be understood that the oxygen pressures must be above the decomposition pressure of cupric oxide.
† Single values, representative of the respective types of experiments described.

[4] L. E. Price, Chem. and Ind. **56**, 769 (1937).

Discussion of the Results

Comparison with Murison's observations

Murison's electron diffraction patterns[5] indicated that the occurrence of cupric oxide in cuprous oxide films on copper was influenced by the atmosphere in the heating furnace. (1) When he heated the specimens in pure air cuprous oxide and "3-ring" (interpreted here as cuprous-cupric oxide) electron diffraction patterns were equally probable. (2) When the concentration of oxygen was increased by blowing air or oxygen through the furnace tube the patterns were invariably of the "3-ring" type. (3) The patterns were of the cuprous oxide type when carbon dioxide or sulphur dioxide was blown through the furnace. He did not mention any period of time during which his specimens were heated.[6]

These general observations of Murison, concerning the composition of the films formed on copper at a given temperature, were confirmed as follows: The conditions of (1) above were provided by choosing periods, for heating the specimens in pure air, sufficient to give thickness values near that of the critical thickness of cuprous oxide (see Fig. 1, about 600A), thereby making the cuprous and the cuprous-cupric oxide compositions appear to be equally probable. The conditions of (2) were obtained by conducting oxygen into the furnace until the oxygen concentration was increased enough to provide, in the same periods of time, thickness values well above that of the upper limit of the critical thickness range (see Fig. 1, above 800A). These films were accordingly always of the cuprous-cupric oxide composition. The conditions of (3) were attained by conducting nitrogen into the furnace until the oxygen concentration was decreased enough to lead to film thickness values less than that of the lower limit of the critical thickness range. These films were less than 400A in thickness and contained only cuprous oxide.

Clearly the period of heating the specimens could have been chosen so short that even the highest oxygen concentration employed would have produced films containing only cuprous oxide. On the other hand, the period could have been made so long that the lowest oxygen concentration would have developed a cuprous-cupric oxide film. Thus it appears that the period of heating a specimen at a given temperature, as well as the oxygen concentration, greatly influences the thickness of the film and hence the composition of the film.

Comparison with Dunholter and Kersten's results

Dunholter and Kersten[7] studied the kinds of electron diffraction patterns obtained from copper oxide formed on evaporated copper films by heating them in oxygen at several temperatures, in the range 50° to 300°C, for various lengths of time, in the range 0 to 120 minutes. Their temperature-time graph of the results reveals five zones, each containing only one of the following types of patterns: (1) Copper, (2) copper and cuprous oxide, (3) cuprous oxide, (4) cuprous-cupric oxide, and (5) cupric oxide.

When these observations are interpreted in the light of the present thickness-composition results, the cuprous oxide films in zone (1) were too thin to produce any noticeable effect[8] in the patterns

Table II. *Comparison of the times required to produce similar films under the same conditions of temperature and oxygen concentration represented in the above table.*

Time in Minutes	Thickness† of Films, A			Atmosphere
	Cu_2O	CuO	Total	
6	1005	95	1100	Air rich in oxygen
9	1010	105	1115	Air
25	995	100	1095	Air rich in nitrogen

† Single values, representative of the respective types of experiments described.

[5] C. A. Murison, Phil. Mag. **17**, 96 (1934).

[6] It is assumed that Murison's comparison of films obtained from the different atmospheres involved equal periods of heating at the same temperature. It is also assumed that blowing oxygen or air through his furnace increased the oxygen concentration and that blowing carbon dioxide or sulphur dioxide through it decreased the oxygen concentration, or the oxygen available for either reaction.

[7] H. Dunholter and H. Kersten, J. App. Phys. **10**, 523 (1939).

[8] For the production of electron diffraction patterns the surface films must be at least a small number of atoms in thickness (see H. R. Nelson, J. App. Phys. **9**, 627 (1938). W. E. Campbell and U. B. Thomas, Nature **142**, 253 (1938); Trans. Electrochem. Soc. **76**, 303 (1939)) have adapted the electrolytic reduction method to the accurate measurement of cuprous oxide films of atomic dimensions. Whereas their finely abraded copper surfaces carried 30–70A of cuprous oxide at ordinary temperatures, the films on freshly reduced copper after one-half hour's

characteristic of the base metal. In zone (2) the cuprous oxide films were thick enough to add their characteristic effects to the patterns of the base metal. In zone (3) the cuprous oxide films had become thick enough to eliminate the pattern of the underlying base metal, but their thickness values were still below the critical thickness value. In zone (4) the thickness values were greater than the critical thickness value,[9] but not great enough for the overlying cupric oxide to control the pattern. In zone (5) the cupric oxide had become thick enough to obscure the effects of any cuprous oxide on the patterns.[10]

The belief that these zones representing different film compositions are also film thickness zones is supported by certain evidence presented by the graph of Dunholter and Kersten's results. (1) The zones extend obliquely across the graph so that, within a given zone, the respective temperature values decrease as the times of heating increase. (2) At a given temperature the changes in the film composition with increase of the period of heating indicate the thickening of the film; e.g., at 175°C films produced from very short exposures yield cuprous oxide patterns, while those exposed longer give cuprous-cupric oxide patterns, and those heated for still longer periods give cupric oxide patterns. (3) For any given period of heating the characteristic series of compositions is obtained by successively increasing the temperatures. Thus it seems that the results of Dunholter and Kersten are in general agreement with the conclusions reached in the present study of the influence of thickness on the composition of copper oxide films.

Conclusion and General Remarks

When diffusion through cuprous oxide films becomes sufficiently difficult some cupric oxide is developed in the films, presumably through the oxidation of cuprous oxide. In this way, the composition of the oxide films formed on copper is determined largely by the thickness of the films, those of thickness values below the critical thickness range being of the cuprous oxide composition, and those of values within the range being of either the cuprous or the cuprous-cupric oxide composition while those of values above the critical thickness range are always of the cuprous-cupric oxide composition. The thickness of a film is a function of the temperature at which it is produced, the period of time during which it is formed, the oxygen concentration in which it is developed, and any factor[11] that may alter the perviousness of the film. The presence of any cupric oxide nuclei, due to previous heat treatment in the manufacture of the metal or otherwise, might cause the secondary reaction to start more readily and thus affect the location of the critical thickness range for such a material. Accordingly, the critical thickness range for one material and set of conditions should not be expected to duplicate that of another.[12] Hence the critical thickness range for the oxide films on a given material is determined directly by the thickness of the films and indirectly by all of the factors that affect the thickness.

exposure to air or oxygen were only 10–20A thick. Dunholter and Kersten's still smoother mirror-like surfaces possibly contained very thin films under the conditions of zone (1).

[9] The critical thickness value may differ from the one obtained in the present work, but the same general influence of thickness on composition is to be expected. The perviousness of films formed on mirror-like surfaces may differ considerably from that of less perfect films developed on abraded surfaces containing corrugations, shattered metal and stresses resulting from the abrasion treatment (see U. R. Evans and J. Stockdale, J. Chem. Soc. 2651 (1929); also U. R. Evans, Nature **128**, 1062 (1931)). The more perfect films might be expected to lead to greater consistency in the composition of the films in the region of the critical thickness value and to a reduced critical thickness range. This range should incorporate the boundary between zone (3) and zone (4) in the graph, with the critical thickness values on the boundary. It is considered that the well-defined arrestments in the potential-time curve, reference 2, for a cuprous-cupric oxide film indicate two separate phases for the oxides, and that the pattern of such a duplex film consists of two overlying separate patterns.

[10] On prolonged heating of thick specimens, the cupric oxide layer becomes thick enough to be separated mechanically from the underlying cuprous oxide layer.

[11] Such as nature of the material, treatment of the surface, and purity of the atmosphere in which the film is formed.

[12] Previous measurements made by one of the authors (H. A. M.), in other studies, indicate critical thickness ranges that do not coincide with the one found for a commercial copper under the conditions of the present experiments.

On the Resistance to the Uniform Motion of a Solid Through a Viscous Liquid

RAYMOND B. BLOCK
Wright Field, Dayton, Ohio
(Received April 9, 1940)

This paper is a report on an experimental investigation of the resistance to the uniform motion of a solid through a viscous liquid, the results of which appear to indicate that the liquid slipped on the surface of the solid. The apparatus was a straight, closed, glass tube containing a steel ball and the liquid being studied. The tube was arranged so that it could be inclined at various angles with the horizontal, and the only motion of the ball that was considered in working up the observations was one of pure rolling. The liquids employed were mixtures of glycerine and methyl alcohol. The analysis of the data is based upon Stokes' and Oseen's forms of Rayleigh's law of resistance, and the results of the investigation are interpreted in the light of theories due to A. B. Basset and to H. Brillié.

I. INTRODUCTION

IN most theoretical investigations on the motion of a solid body through a viscous liquid the assumption is made that the liquid adheres so firmly to the solid as to have no movement relative to the surface of the body at that surface. Attempts to modify the theory in order to take into account the possible slipping of the liquid on the surface of the solid have been made by A. B. Basset[1] and by H. Brillié.[2] This paper constitutes a report on some experiments whose results appear to support the hypothesis of slipping. Rayleigh's law of resistance[3] formed the basis of the experimental work and it also suggested how the observed quantities should be combined in the analysis of the data.

II. DESCRIPTION OF THE APPARATUS AND OF THE LIQUIDS

The apparatus used in the investigation was a straight, closed, glass tube containing a steel ball. The tube was fastened to the upper surface of a somewhat longer wooden arm that was hinged at one end to an upright bar so that it could be given various angles of inclination. This equipment and its arrangement have the following four advantages for the study described here: (1) The speed of the moving body can be easily controlled (by altering the angle of inclination of the tube); (2) The body is free from wobbling while in motion; (3) There is a definite and known relation between the linear speed of the center of gravity of the body and the angular velocity of rotation about an axis through the c.g., namely, $v = r\omega$, provided that the motion of the ball is one of rolling without sliding; (4) The resistance to the motion of the body can be accurately determined. (It is numerically equal to the component of the weight of the ball acting down the tube minus the component of the buoyant force of the liquid acting up the tube.)

The tube was 54 cm long and had an average internal diameter of 1.240 cm. The variation of the bore along the axis of the tube is shown in Table I. The mean deviation from the average internal diameter is less than 0.4 percent and there is no consistent change in diameter from one end of the tube to the other.

TABLE I. *Variation of the tube's internal diameter with distance along its axis.*

DISTANCE FROM LOWER END OF THE TUBE CM	INTERNAL DIAMETER CM
4.27	1.243
7.49	1.251
12.17	1.240
17.86	1.236
24.05	1.245
28.83	1.239
31.40	1.246
34.39	1.241
37.96	1.236
40.81	1.223
43.40	1.240
47.98	1.239

[1] A. B. Basset, *A Treatise on Hydrodynamics*, Vol. 2 (Deighton, Bell and Co., Cambridge, 1888), chapter XXI.
[2] H. Brillié, *Proceedings of the General Discussion on Lubrication and Lubricants*, Vol. 2 (The Institution of Mechanical Engineers, London, 1937), pp. 248–250.
[3] See Lord Rayleigh's note attached to the paper of A. F. Zahm, Phil. Mag. **8**, 58–66 (1904); or H. Lamb, *Hydrodynamics*, sixth edition (Cambridge University Press, 1932), article 371, Eq. (2).

The data of Table I were secured by opening one end of the tube and then mounting the hollow cylinder vertically with the closed end down. A burette filled with water was then set up directly over the open end, so that the axes of the tube and burette lay in the same vertical line. Successive, known, small quantities of water were then put into the tube from the burette a drop at a time, great care being taken that the drops did not strike the inner wall but fell straight into it. As each amount of water was added, the height of the meniscus in the tube was measured by means of a cathetometer, the initial reading being taken near the stopper which closed the lower end of the tube. The readings were made on a brass scale mounted beside the tube and in a plane containing its axis. Assuming the tube to have a circular cross section, a simple arithmetical calculation gave the mean diameter of each of these short cylinders of water. The data in the first column of Table I are the distances from the lower end of the tube to the middles of the successive portions of it, whose average internal diameters are listed in the second column.

TABLE II. *Densities at +30°C and average thermal coefficients of cubical expansion of the glycerine-methyl alcohol mixtures.*

LIQUID, % BY WEIGHT	ρ_{30} IN G PER CC	$\alpha \times 10^3$ PER °C
glycerine	1.246	0.45
90% glyc. 10% m.alc.	1.185	0.51
80% glyc. 20% m.alc.	1.132	0.57
70% glyc. 30% m.alc.	1.082	0.64
60% glyc. 40% m.alc.	1.034	0.71

The mass of the ball was 3.50 grams, diameter 0.953 cm, and density 7.72 grams per cc. Its surface was bright and smooth.

The liquids used in this investigation were glycerine and four mixtures of it with methyl alcohol in the proportions in percent by weight shown in Table II. The methyl alcohol was of reagent purity. Commercial glycerine generally contains water. The sample used in this work was found by measurement to have a kinematic viscosity of 4.04 c.g.s. units at +20°C. From data given by J. W. Lawrie[4] it has been estimated by graphical interpolation that this value of kinematic viscosity corresponds to a glycerol-water solution containing 95.4 percent glycerol by weight.

The kinematic viscosities of these liquids at several temperatures in the neighborhood of those anticipated during the tests were measured by means of the modified Ostwald capillary viscometer described by Houseman and Keulegan,[5] and then by plotting the values for each liquid against temperature it was possible to secure the viscosity corresponding to the temperature at which the liquid was used.

The densities of the liquids were computed by means of the formula

$$\rho_\theta = \rho_{30}[1+\alpha(30-\theta)], \qquad (1)$$

in which ρ_θ = density at θ°C, ρ_{30} = density at +30°C, α = average thermal coefficient of cubical expansion in the range 0°C to +30°C. The values of ρ_{30} and of α were secured in the customary manner. They are listed in Table II.

The hygroscopic nature of the glycerine used was carefully guarded against by keeping the liquids in tightly stoppered containers.

The temperature of a liquid under test was known from a mercurial thermometer that was completely immersed in a sample of it contained in a closed, hollow, glass cylinder of practically the same internal diameter and wall thickness as the tube of the rolling-ball apparatus, which was set up in the immediate vicinity of the same. No special effort was made to maintain the apparatus at a constant temperature. The reason for this will be evident from the discussion in Section IV.

III. EXPERIMENTAL PROCEDURE

The experiments consisted of measurements of the times of travel of the ball through 40 cm of the tube when the latter was completely filled with the liquids described in Section II and inclined at various angles. This interval was located so that its center was approximately coincident with the midpoint of the tube. Both the tube and the ball were clean and dry to start with. Between liquids the tube was thoroughly flushed out with methyl alcohol and then with

[4] J. W. Lawrie, *Glycerol and the Glycols*, first edition (Chemical Catalog Co., New York, 1928), Chapter 6, Tables 21, 51, and 52.

[5] M. R. Houseman and G. H. Keulegan, N. A. C. A. Technical Report No. 398 (1931).

the liquid about to be used. The ball, before being transferred from one liquid to the next, was wiped with clean cotton, washed in methyl alcohol without being touched by hand, and then allowed to dry by evaporation. It was not touched by hand while being put into the tube.

IV. Analysis of the Data

(a) Introduction

Rayleigh's law of resistance suggests that there should be a relation between the two variables

$$\Pi_1 \equiv \frac{F}{\rho v^2 d^2} \quad \text{and} \quad \Pi_2 \equiv \frac{dv}{\nu}, \tag{2}$$

in which

F = the total drag on the ball,
ρ = the density of the liquid,
v = the linear speed of the ball,
d = the diameter of the ball,
ν = the kinematic viscosity of the liquid.

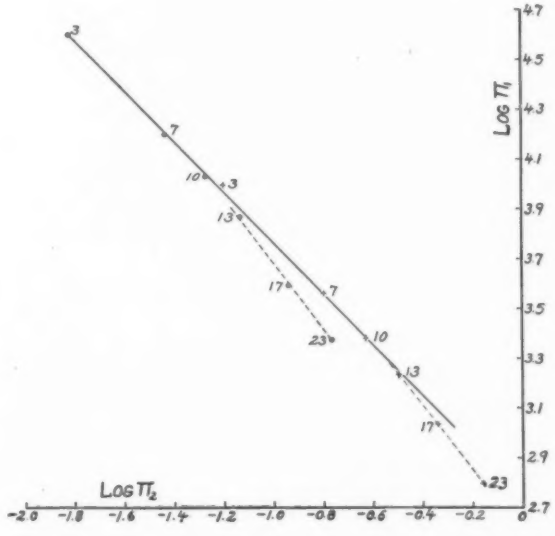

FIG. 1. The motion of the ball was known to be rolling, only, at 3-, 7-, and 10-degree inclinations of the tube, and to be rolling and sliding, together, at 13-, 17-, and 23-degree inclinations. The liquid was glycerine.

In working up the data of this investigation the assumption was made that the ball had no linear acceleration throughout the distance over which the times of travel were observed. This assumption was not checked directly, but subsequent comparison of the results with the forms of Rayleigh's law due to Stokes[6] and to Oseen[6] verified the correctness of it. Thus, the total drag on the ball was considered to be numerically equal to the net driving force on the same, which in turn was equal to the component of the weight of the ball acting down the tube minus the component of the buoyancy of the liquid acting up the tube. Hence,

$$F = (w_2 - w_1)\left(\frac{\pi}{6} d^3\right) \sin\theta, \tag{3}$$

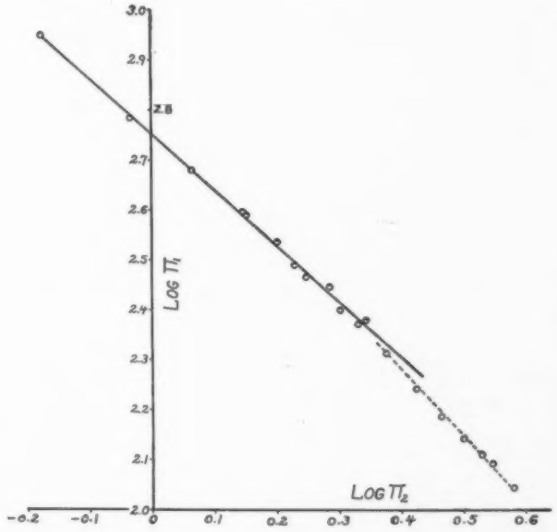

FIG. 2. By comparison with Fig. 1 it is concluded that the ball must have been rolling, only, for the data on the full line, and rolling and sliding, together, for the data on the dotted line. The liquid was a mixture of 90 percent glycerine and 10 percent methyl alcohol, by weight.

in which

w_2 = the weight per unit volume of the ball,
w_1 = the weight per unit volume of the liquid,
d = the diameter of the ball,
θ = the angle of inclination of the tube.

Note that $w_2 = \sigma g$ and $w_1 = \rho g$, in which σ and ρ are the densities of the ball and of the liquid, respectively, and g is the acceleration of gravity.

Also on the basis of this assumption

$$v = \frac{40}{t}, \tag{4}$$

in which t was the measured time of travel of the ball through the 40-cm interval marked off on the

[6] H. Lamb, reference 3, article 337, Eq. (10); article 343a, Eq. (16).

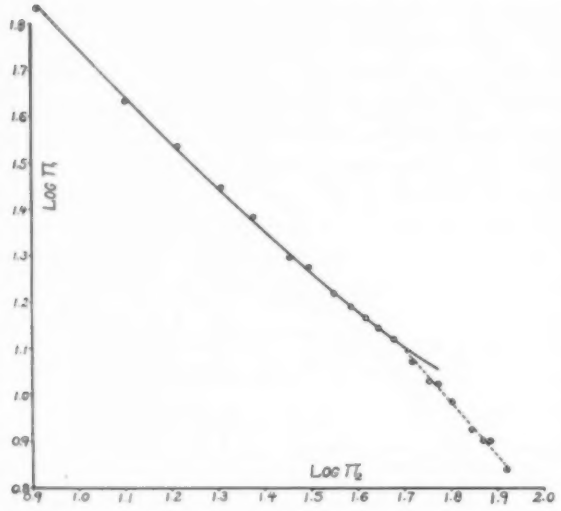

FIG. 3. This figure, like Figs. 1 and 2, illustrates the method used to separate the data for which the motion of the ball was pure rolling from that for which it was a combination of rolling and sliding. The liquid was a mixture of 70 percent glycerine and 30 percent methyl alcohol, by weight.

tube. Only those values of θ and t were used in the computation of the variables Π_1 and Π_2, for which the motion of the ball was rolling without sliding. Because of the consequent rigid connection between the linear speed v and the angular velocity $\omega(v=r\omega$, in which r is the radius of the ball) it was unnecessary to measure the angular velocity of the ball, as well. The value of v from Eq. (4) then gave a complete kinematical specification of the motion of the ball. If sliding as well as rolling had been permitted, this would not have been so.

It is now easy to understand why no special effort had to be made to keep the apparatus at a constant temperature during the experiments. All that was wanted was a set of corresponding values of Π_1 and Π_2 for each liquid. The only quantities appreciably affected by temperature that enter into Π_1 and Π_2 are ρ and ν, and therefore it was required that the temperature remain unchanged merely throughout the time t used in Eq. (4) to compute v for a pair of corresponding values of these variables. The values of ρ and ν at this temperature for the liquid employed were then secured from Eq. (1) and the plots of kinematic viscosity against temperature mentioned in Section II. Time t never exceeded 6 minutes—it was generally much smaller than this—and experience showed that the temperature of the laboratory did not change noticeably over such short periods of time.

When a ball rolls down an inclined tube filled with liquid, the viscous drag of the liquid on the surface of the ball acts to restrain the ball from rotating. As the angle of inclination of the tube is increased the rate of rotation of the ball tends to increase with it, until eventually at some angle the resultant moment of the viscous shearing stress about the instantaneous axis of rotation balances the moment of the weight of the ball about the same axis but acting in the opposite direction. At this angle of inclination the ball begins to slide.

In order to check this conclusion in the present case, and also to provide a means for separating the data for which the motion of the ball was rolling without sliding from that for which it was a combination of rolling and sliding, the following experiment was performed. The ball was marked with a small spot of black India ink. It was then put into the tube and the latter was filled with glycerine. The time required by the ball to travel through the 40-cm interval in the tube was then measured at angles of inclination of 3, 7, 10, 13, 17, and 23 degrees; and in addition measurements were made at each angle of the distance covered by the ball in a known number of complete revolutions determined by counting the successive appearances of the ink spot. From the diameter of the ball it was possible to compute the distance the ball should have traveled in the observed number of revolutions if its motion was pure rolling. For the first three angles of inclination the distance traveled was found to be just equal to that expected for pure rolling. For the last three angles of inclination the distance was always greater than this. The increase in the distance traveled at these higher angles of inclination could have been due to no other cause than sliding combined with the rolling of the ball. Glycerine was used because of the slow motion of the ball through it, which resulted in more accurate measurements of the distance traveled. This experiment was made at a liquid temperature of $+21°$C and then again at one of $+31°$C. The values of $\log \Pi_1$ are plotted against those of $\log \Pi_2$ in Fig. 1. The open circles represent the data at $+21°$C, and the numbers alongside of the points

are the corresponding angles of inclination of the tube in degrees. It is seen that when the data are plotted logarithmically the points for which the motion of the ball was a combination of rolling and sliding lie on a line that has a steeper slope than the line on which lie the points for which the motion of the ball was rolling, only.

Typical logarithmic plots of the data on the liquids employed in this investigation are shown in Figs. 2 and 3. On the basis of the criterion described in the last paragraph it appears that the points lying on the full line in each figure represent data for which the ball had a motion of pure rolling. In a similar manner for the three other liquids the values of Π_1 and Π_2 for pure rolling of the ball were separated from the values for combined rolling and sliding. Only the former sets of data were used in the computations that are now about to be discussed.

(b) Computations

The forms of Rayleigh's law of resistance due to the theoretical work of Stokes[6] and of Oseen[6] furnished the particular relations between the variables Π_1 and Π_2 that were used in the detailed examination of the data of the present study. In terms of these variables as defined by Eqs. (2) Stokes' law takes the form

$$\Pi_1 = A\Pi_2^b \tag{5}$$

or

$$\log \Pi_1 = a + b \log \Pi_2, \tag{6}$$

and Oseen's law takes the form

$$\Pi_1 = A\Pi_2^b + c \tag{7}$$

or

$$\log (\Pi_1 - c) = a + b \log \Pi_2. \tag{8}$$

When $\log \Pi_1$ was plotted against $\log \Pi_2$ as abscissa it was found that for each of the first three liquids listed in Table II the points representing the observations lay on a straight line (Fig. 2), in accordance with Eq. (6); but that for each of the two remaining liquids the points lay on a curve that was concave upward (Fig. 3). The value of c in Eq. (7) was determined for each of these latter liquids by the method described in the next paragraph, and then in both cases plots of $\log (\Pi_1 - c)$ against $\log \Pi_2$ turned out to be straight lines, in accordance with Eq. (8).

The procedure employed for evaluating c will now be given. Π_1 was plotted against Π_2 as abscissa and a smooth curve was faired in among the points. Taking formula (7) to represent this curve, the following equations must be satisfied at any three points on the curve:

$$\begin{aligned} \Pi_1' &= A\Pi_2'^b + c, \\ \Pi_1'' &= A\Pi_2''^b + c, \\ \Pi_1''' &= A\Pi_2'''^b + c. \end{aligned} \tag{9}$$

If, now, Π_2'' is chosen to be the geometric mean between Π_2' and Π_2''', the relation

$$\Pi_1'' - c = [(\Pi_1' - c)(\Pi_1''' - c)]^{\frac{1}{2}} \tag{10}$$

holds. Therefore,

$$c = \frac{\Pi_1'\Pi_1''' - \Pi_1''\Pi_1''}{\Pi_1' + \Pi_1''' - 2\Pi_1''}. \tag{11}$$

An attempt was made to secure a representative value of c for each of the liquids in question by choosing the first and third points for Eqs. (9) to satisfy, at the beginning and end, respectively, of the faired curve for the liquid.

The constants a and b in Eqs. (6) and (8) were determined from the observations on each liquid

TABLE III. *The weighted mean values of a and b, and the values of c [Eqs. (5) to (8), inclusive], together with their precision measures.**

LIQUID, % BY WEIGHT	a	b	c
glycerine	+2.632±0.016	−1.1077±0.0072	0
90% glyc. 10% m.alc.	+2.755±0.012	−1.136 ±0.012	0
80% glyc. 20% m.alc.	+2.776±0.017	−1.0460±0.0084	0
70% glyc. 30% m.alc.	+2.810±0.033	−1.090 ±0.012	+3.65±0.26
60% glyc. 40% m.alc.	+2.821±0.021	−1.0717±0.0084	+3.22±0.32

* In order to clarify the meaning of the phrase "weighted mean values of a and b" that is used in Section IV (c) and in the title of Table III, the following explanation is appended. The weighted normal equations for a and b derived from the observation Eqs. (6) and (8) were formed upon the assumption that $\log \Pi_2$ was without error, in accordance with the usual practice. (Bartlett, reference 7, pp. 28–32, especially article 41.) From these normal equations the values of a and b were calculated, together with their precision measures. Equations (6) and (8) were then solved for $\log \Pi_2$, giving

$$\log \Pi_2 = \alpha + \beta \log \Pi_1$$

and

$$\log \Pi_2 = \alpha + \beta \log (\Pi_1 - c),$$

where $\alpha = -(a/b)$ and $\beta = +(1/b)$. Weighted normal equations for α and β were formed from these observation equations, assuming this time that $\log \Pi_1$ and $\log (\Pi_1 - c)$ were without error; and from them the values of α and β were calculated together with their precision measures. From α and β and their precision measures it was a simple matter to find the values of a and b themselves and their precision measures. In this way there were secured "measurements" of a and b that were independent of the "measurements" of these quantities embodied in the weighted normal equations formed from the observation Eqs. (6) and (8). The two values of a and the two values of b thus determined differed merely because of a different effect in each case of the accidental errors in the basic, direct measurements by means of which Π_1 and Π_2 were evaluated from Eqs. (2), (3), and (4). The weights of the two values of a were thus inversely proportional to the squares of their precision measures, and the weighted mean value was a more reliable indication of the true value of a than either one alone. Similarly, the weighted mean of the two values of b was a closer approximation to the true value of b than either of them alone. In calculating the precision measures of the "observations" $\log (\Pi_1 - c)$, the percentage error in c was considered to be equal to the average percentage error in all of the values of Π_1 that determined the curve of Π_1 vs. Π_2 from which c was found.

separately by the method of least squares,[7] the word "observations" meaning here the values of log Π_1 and log Π_2 in the case of Eq. (6), and the values of log $(\Pi_1 - c)$ and log Π_2 in the case of Eq. (8). The first step was to make an estimate of the errors in the basic measurements in order to evaluate the relative weights of these observations. Referring to Eq. (3) the ball diameter, d(0.953 cm), and the acceleration of gravity, g (980 cm per sec. per sec.), were considered to be without error. The error in σ was computed from the estimated uncertainty in the total mass of the ball (3.50 g). The total mass of the ball was determined to the nearest 5 milligrams, but to be conservative the uncertainty was taken to be twice this amount. Hence, the percentage error in σ was $\pm(100/350) = \pm 0.286$. Now, $\sigma = 7.72$ g per cc. Therefore, $d\sigma = \pm 7.72 \times 0.00286 = \pm 0.0221$ g per cc. The error in ρ was assumed

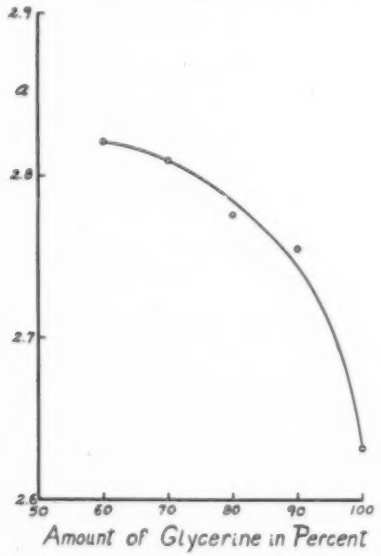

FIG. 4. The variation of a with the amount of glycerine in the glycerine-methyl alcohol mixtures in percent by weight.

to be ± 1 percent of ρ. The angle of inclination of the tube, θ, was measured by means of a protractor level whose least graduation was 1°. It is believed that the level could be read to 0.25°, and this value was taken as the error in θ. Thus, $d\theta = \pm 0.25$ degree $= \pm 0.0044$ radian. Referring now to Eq. (4) the error in the 40-cm path-length

[7] The text used for reference was D. P. Bartlett, *The Method of Least Squares*, third edition (The author, Boston, 1915).

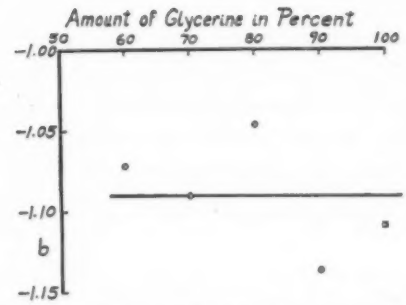

FIG. 5. The variation of b with the amount of glycerine in the glycerine-methyl alcohol mixtures in percent by weight.

was considered to be ± 1 mm. The time of roll was measured with a stop-watch graduated to fifths of a second, and the measurement of t was assumed to be good to ± 0.2 sec. The component errors in v were then

$$\pm\frac{\partial v}{\partial l}dl = \pm\frac{0.1}{t} \quad \text{and} \quad \pm\frac{\partial v}{\partial t}dt = \pm\frac{8}{t^2},$$

and the resultant error, dv, was the square root of the sum of the squares of these two components. The uncertainty in v was assumed to be ± 1 percent of v.

(c) Results

The weighted mean values of a and b, and the values of c [Eqs. (5) to (8), inclusive] together with their precision measures are given in Table III for each of the liquids studied in this investigation. The weighted mean values of a and b are presented graphically in Figs. 4 and 5. It appears that a varies systematically with the glycerine content of the liquids, whereas b exhibits no systematic change with the composition of the liquids. In the case of the two liquids for which the constant c had to be introduced, the value of this parameter increases with the glycerine content of the liquids.

V. Discussion of the Results

According to the laws of Stokes and of Oseen the values of a, b, and c should be independent of the liquid. In the present investigation it has been found that whereas b appears to be independent of the liquid, the same certainly cannot be said of a and c. A fundamental assumption in the theory underlying the laws of Stokes and

of Oseen is that the liquid has no motion relative to the surface of the sphere at that surface. It will be shown in the following paragraphs that if the theory is modified merely to the extent of permitting a tangential slipping of the liquid on the surface of the sphere, formulas are secured by which the experimental results reported here can be accounted for.

Referring then to Fig. 6, if a solid is moving toward the right with the speed $|u'|$ through a viscous liquid initially at rest, the relative velocity of the liquid with respect to the solid at the surface is $u-u'$, in which $|u|$ is the speed of the layer of liquid in immediate contact with the solid, and its value is negative (i.e., it is directed toward the left). If, now, T is the shearing stress exerted upon the liquid by the solid, its magnitude is proportional[8] to this relative velocity, but its direction is toward the right (otherwise the liquid would not be urged toward the right by the motion of the solid). Therefore, $T=-\beta(u-u')$. Now, the layer of liquid in immediate contact with the solid exerts a shearing stress upon the layer of liquid just above it, whose magnitude is $\mu(\partial u/\partial y)$,—a negative value since u decreases outward from the surface of the solid. Hence, the shearing stress of the layer 1 upon the layer 2 is $-\mu(\partial u/\partial y)$ in direction (i.e., toward the right) as well as magnitude. The shearing stress of the layer 2 upon the layer 1 is thus $-[-\mu(\partial u/\partial y)]=\mu(\partial u/\partial y)$. This stress represents a drag upon the layer 1, and it acts toward the left. Consequently, for the equilibrium of the layer of liquid in immediate contact with the solid it is necessary that

$$-\beta(u-u')=\mu\frac{\partial u}{\partial y}. \qquad (12)^{9}$$

From this equation it is seen that $\beta=\infty$ is the condition that layer 1 have no tangential motion relative to the surface of the solid, for otherwise the value of $\mu(\partial u/\partial y)$ would not be finite there.

If Stokes' law is now re-derived, using the boundary condition (12) for the tangential velocity of the liquid at the surface of the sphere instead of the usual one that $u=u'$, the relation between the variables Π_1 and Π_2 as defined in Eqs. (2) turns out to be

$$\Pi_1=\frac{3\pi}{\Pi_2}\left(\frac{2\mu-\beta r}{3\mu-\beta r}\right) \qquad (13)^{10}$$

or

$$\log \Pi_1=\log\left[3\pi\left(\frac{2\mu-\beta r}{3\mu-\beta r}\right)\right]-\log \Pi_2, \qquad (14)$$

in which μ = the absolute viscosity of the liquid,

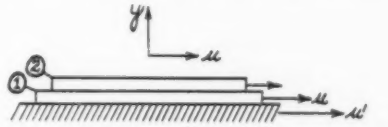

FIG. 6. A solid moves with velocity u' through a viscous liquid, dragging with it a thin layer of liquid, 1, at velocity u, which in turn drags with it the thin layer of liquid, 2. If there is slipping at the boundary between the solid and the liquid, $|u|<|u'|$. The equilibrium between the shearing stresses on the upper and lower surfaces of liquid layer 1 results in the boundary condition given by Eq. (12).

and r = the radius of the sphere. By using condition (12) in the theory underlying Oseen's formula[11] the author has found the relation

$$\Pi_1=\frac{3\pi}{\Pi_2}\left(\frac{\mu-\beta r}{2\mu-\beta r}\right)+\frac{9\pi}{16}\left(\frac{\mu-\beta r}{2\mu-\beta r}\right)^2 \qquad (15)$$

or

$$\log\left[\Pi_1-\frac{9\pi}{16}\left(\frac{\mu-\beta r}{2\mu-\beta r}\right)^2\right]=\log\left[3\pi\left(\frac{\mu-\beta r}{2\mu-\beta r}\right)\right]-\log \Pi_2. \qquad (16)$$

If $\beta=\infty$ in Eqs. (13) and (15), these formulas reduce to the laws of Stokes and of Oseen, respectively.[6]

By comparison with Eqs. (6) and (8) it is seen that if there was slipping of the liquid on the surface of the sphere, for the first three liquids listed in Table III the following relations should hold approximately:

$$a=\log\left[3\pi\left(\frac{2\mu-\beta r}{3\mu-\beta r}\right)\right] \quad \text{and} \quad b=-1; \qquad (17)$$

[8] A. B. Basset, reference 1, article 475; or H. Lamb, reference 3, article 327.

[9] A. B. Basset, reference 1, article 487, Eq. (17); or H. Lamb, reference 3, article 337, Eq. (36). Note that the sign of β in both of these equations should be negative.

[10] A. B. Basset, reference 1, article 495, Eq. (44); or H. Lamb, reference 3, article 337, Eq. (38). The sign of β in both of these equations should be negative.

[11] Wien-Harms, *Handbuch der Experimentalphysik*, first edition, Vol. 4, Part 1 (Akademische Verlagsgesellschaft, Leipzig, 1931), pp. 212–220.

and that for the last two liquids in the table the following relations should hold approximately:

$$a=\log\left[3\pi\left(\frac{\mu-\beta r}{2\mu-\beta r}\right)\right], \quad b=-1,$$

and

$$c=\frac{9\pi}{16}\left(\frac{\mu-\beta r}{2\mu-\beta r}\right)^2. \tag{18}$$

The corresponding relations for no slipping are secured by setting $\beta=\infty$ in these formulas. These relations do not hold exactly for the reason that the numerical data in Table III apply to the combined translation and rotation of a sphere through a comparatively small quantity of liquid confined in a closed tube, whereas Eqs. (14) and (16) apply to the uniform translation, only, of a sphere through a liquid of infinite extent. The fact that a and c as given in Table III do vary progressively from liquid to liquid, whereas b seems to be constant and approximately equal to -1, appears to support the hypothesis of slipping. From the numerical values in the table and Eqs. (17) and (18) the values of β for the liquids have been computed. They are listed in Table IV. For the last two liquids the value of β from c serves as a check on the value determined from a. In each case the order of magnitude of the two values of β is the same, as is also the order of magnitude of the changes in β as computed from the two values of a and as computed from the two values of c. The direction of the change in β is likewise the same in both cases.

TABLE IV. *Approximate values of the coefficient of slip, β, for glycerine-methyl alcohol mixtures against steel.*

LIQUID, % BY WEIGHT	AVERAGE TEMP. OF THE TEST, +°C	ABSOLUTE VISCOSITY, C.G.S. UNITS	β COMPUTED FROM a	β COMPUTED FROM c
glycerine	30.3	2.32	14.72	—
90% glyc. 10% m.alc.	31.4	0.760	4.81	—
80% glyc. 20% m.alc.	25.1	0.400	2.53	—
70% glyc. 30% m.alc.	27.4	0.155	0.65	1.39
60% glyc. 40% m.alc.	22.9	0.0935	0.40	0.95

Note: $\beta=\infty$ corresponds to no slipping of the liquid on the surface of the sphere.

According to Brillié[12] slipping of a liquid on the surface of a solid moving through it always occurs in the case of a polar liquid, but never when the liquid is nonpolar. He believes it to be due to the neutralization of the field of force emanating from the surface of the solid, by the adsorbed layer of polar molecules on the boundary between the liquid and the solid, which results in a local reduction in the internal friction (viscosity) of the liquid in the immediate neighborhood of the surface. There is perfect adherence of this adsorbed boundary layer to the solid, as in the usual hydrodynamical theory, the slipping taking place actually in a thin "zone of oiliness" between the layer and the main body of liquid, in which the local value of the viscosity is much less than that in the main body of liquid.

The liquids used in the investigation reported here were mixtures of glycerine and methyl alcohol. It is not known for certain whether glycerine contains dipoles or not,[13] but methyl alcohol is well known to be a highly associated, polar compound. According to Kyropoulos[14] the existence of dipoles in a liquid is not of itself sufficient to cause the formation of an adsorbed boundary layer, but association of the polar molecules must also obtain. Those polar molecules which have formed complexes by association are adsorbed in preference to the other molecules in the liquid. It would be expected that the amount of slipping of a liquid on the surface of a solid moving through it, if such a phenomenon exists, would vary with the composition of the boundary between the liquid and the solid, and it is interesting to note that the value of β as given in Table IV decreases as the proportion of methyl alcohol increases, i.e., the slipping of the liquid increases with the amount of methyl alcohol present. This effect is consistent with Brillié's theory.

[12] H. Brillié, Mémoires de la Société des Ingénieurs Civils de France **88**, 623 (1935).
[13] W. Graffunder, Ann. d. Physik **70**, 225–249 (1923).
[14] S. Kyropoulos, *Proceedings of the General Discussion on Lubrication and Lubricants*, Vol. 2 (The Institution of Mechanical Engineers, London, 1937), pp. 346–353, especially p. 351.

Preparation of High Melting Alloys with the Aid of Electron Bombardment

RALPH HULTGREN AND M. H. PAKKALA
Graduate School of Engineering, Harvard University, Cambridge, Massachusetts
(Received April 24, 1940)

An electron bombardment furnace was constructed for high temperature melting. The temperature attainable is limited only by the refractoriness of the crucible; a tantalum cup (m.p. 2850°C) was melted with the expenditure of only 700 watts. Degassing of sample and surroundings causes gas discharge if the rate of heating is too rapid. Metals volatile at their melting point cannot be melted, but this applies to only a few metals such as manganese and palladium. Alloys of platinum with tungsten, molybdenum, and cobalt are now being successfully prepared for x-ray investigation. The tendency of some metals to react with available refractory crucibles needs further study before their alloys can be prepared.

COMPARATIVELY little is known of the phase diagrams and properties of alloys with melting points higher than that of iron. Technical difficulties in preparing the alloys without contamination combined with the fact that many of the constituent metals have only recently become available in a pure form has made much of this work impossible in the past. However, successful commercial applications of high melting metals and alloys such as tungsten filaments, tungsten carbide cutting tools, platinum-rhodium resistance wire, iridium pen points, and materials for electrical contacts have indicated fields of application of much promise. We have felt that systematic x-ray studies should not only yield results in a nearly untouched scientific field, but might bring nearer important practical applications.

The most direct method of preparing alloys is to melt the constituent metals together, followed by a homogenizing anneal of the solid ingot. A temperature well above the melting point is desirable to insure thorough mixing. It is with this method which we shall deal, although powder metallurgy has had important successes.

To obtain an uncontaminated alloy, the melting must be carried out in a vacuum or inert atmosphere in a refractory crucible which does not react with the melt. Leaving aside the important question of suitable refractories, we shall concern ourselves with the attainment of temperature.

The most common means of attaining high temperatures in a vacuum are electric resistance elements or high frequency induction. Tungsten or molybdenum resistance elements can be used as high as 1700°C without excessively shortening their lives, while carbon can be used at higher temperatures. However, carbon has the disadvantage of absorbing large quantities of air when the furnace is open, which may be given off as CO on subsequent heating. This reacts with the high melting transition metals. High frequency induction is more popular and is admirably suited to samples of moderate size. However, power cannot be efficiently transmitted to small samples because of coupling difficulties, so that an induction sleeve becomes necessary if the sample is small. Thus, a considerable volume must be heated, requiring large power expenditure for high temperatures and increasing the difficulty of insulation. Suitable induction furnaces are expensive, a 20-kw outfit costing $3500, exclusive of cost of installation. Furthermore, a considerable power supply must be available.

Since very small samples (a fraction of a gram) are suitable for x-ray study, a method was sought whereby power could be directly transmitted to the small crucible alone. Electron bombardment accomplishes this admirably.

We have constructed an electron bombardment furnace which proved to be convenient for heating small samples. The total cost of materials, including shop time, was about $500, and this could be decreased by simplifying the apparatus. This does not include the cost of mounting the parts or the wiring. Operation was simple except that the heating had to be slow to allow for outgassing. Since melting must be done in a vacuum, a few metals, like manganese and

palladium, are too volatile at the melting point to be easily melted. The maximum temperatures attainable with the electron furnace are limited only by the refractoriness of the crucible. A tantalum shell, (melting point 2850°C) was melted with a power expenditure of only 700 watts.

In principle, electron bombardment[1] is very simple. A hot filament is placed near a positively charged crucible in a vacuum. Electrons from the filament are accelerated by the voltage drop and strike the crucible. The kinetic energy of the electrons is given up in the form of heat. Thus all the power goes directly to the crucible, which may be made as small as desired.

Description of the Apparatus

Pumping equipment

Care was taken to secure a diffusion pump with high pumping speed. This is necessary to remove the considerable quantity of gas given off by most metals on heating. If the pressure becomes too high (above perhaps 3×10^{-4} mm for air), gas discharge may occur, which leads to a flash-over and trips the circuit breakers. The rate of heating the sample is limited by the pumping speed.

We were fortunate in securing an oil diffusion pump with a pumping speed of 77 liters per second, compared with perhaps 1 liter per second for an ordinary mercury diffusion pump. This was a duplicate of a pump designated by C. M. and L. C. Van Atta[2] and was constructed under the supervision of Professor C. M. Van Atta of the Massachusetts Institute of Technology, whose valuable assistance is greatly appreciated. Oil diffusion was chosen because of its low vapor pressure at room temperature, which makes it possible to dispense with a cold trap. The use of oil also allowed the pump to be made entirely of brass, with all joints sealed with lead gaskets. Against these advantages must be set the high cost of the oil and its liability to be oxidized and ruined if air is admitted to the system while the oil is hot. The temperature of the oil was determined as a function of heating current by a thermocouple placed in a recess designed for the purpose. Thereafter, the optimum heating current was always used. The diffusion pump was backed by a Cenco Megavac pump, connected with a one-inch pipe and sylphon bellows. A large globe valve allowed this pump to be shut off, which was convenient in testing for leaks. The Megavac was run at a high speed, which increased its capacity to 57 liters per minute. Above the diffusion pump was placed a chamber of the same diameter, which contained three baffles to trap oil molecules, and the electrical leads. The leads entered through six Lavite plugs, also constructed in the shop of Professor Van Atta. Seals were made with lead gaskets and the plugs were painted with glyptal on the outside. A thermocouple vacuum gage was connected just above the baffles. Above this was the bombarding chamber with a somewhat larger diameter. This

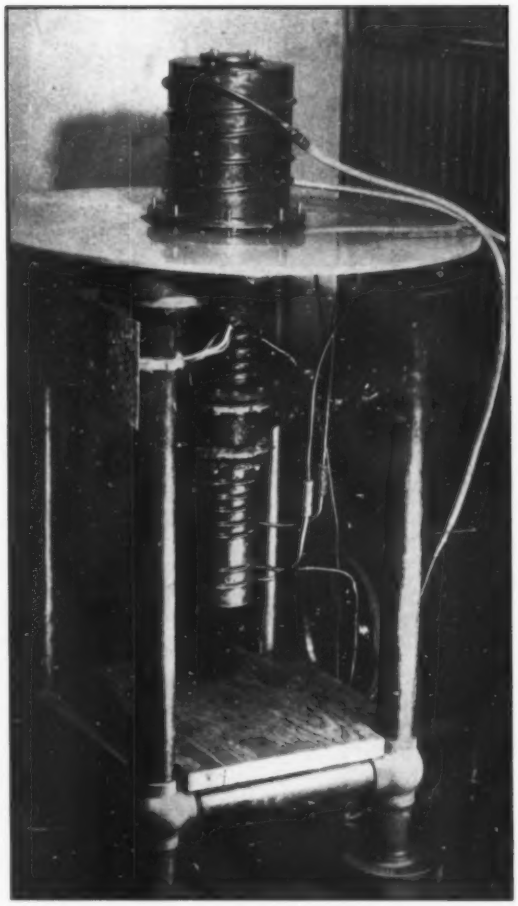

Fig. 1. Electron bombardment furnace. The bombarding chamber is above the table level, the high potential leads (not visible), thermocouple vacuum gage, and diffusion pump below.

[1] H. M. O'Bryan, Rev. Sci. Inst. **5**, 125 (1934).
[2] C. M. Van Atta and L. C. Van Atta, Phys. Rev. **51**, 377 (1937).

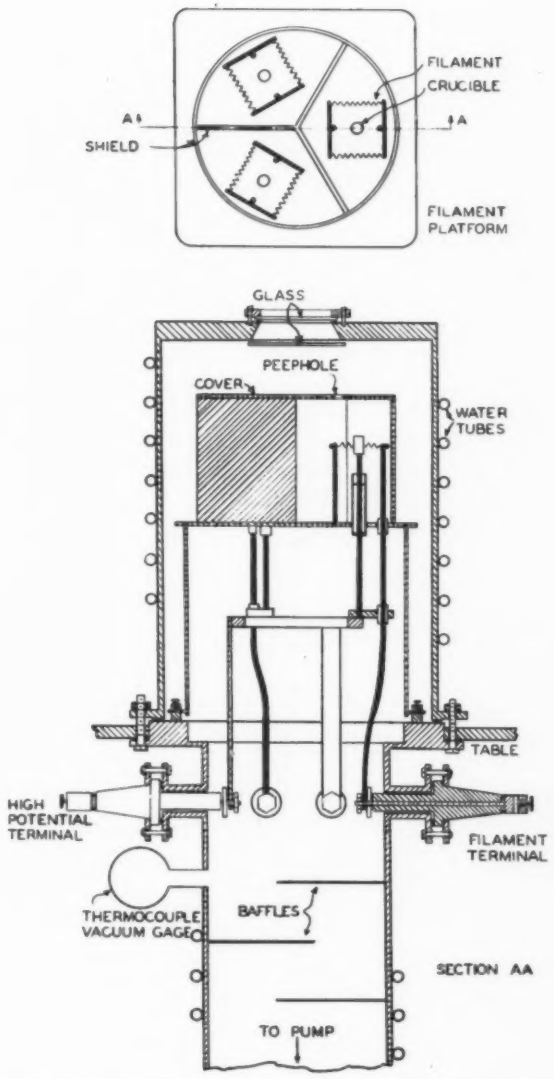

FIG. 2. Section and plan of bombarding chamber.

chamber was bolted on with lead gaskets and could be removed. At the top was a window of Pyrex glass through which the melts could be observed. A second piece of glass within the vacuum protected the window from much of the radiant heat. The general arrangement of the apparatus is shown in Figs. 1 and 2.

Bombarding apparatus

The heating units are shown in Fig. 3. A tantalum cup serves as target for the bombarding electrons. It is spot welded to a tungsten rod which is connected to the high potential. The crucible containing the sample is placed within the cup, which heats it by radiation and thermal conduction. The crucibles were made of pure oxides of zirconium or aluminum, made without a binder. The tantalum cups were purchased from Fansteel Metallurgical Corporation, North Chicago, Illinois; the zirconia crucibles, which were 6 mm OD×10 mm tall, from Saxonburg Potteries, Saxonburg, Pennsylvania; and the alumina crucibles 12 mm OD×10 mm tall from Lava Crucible Company of Pittsburgh, Pennsylvania. However, it is possible to make crucibles of these materials or of the more refractory thoria by simple laboratory technique, since little mechanical strength is necessary.

Filaments are composed of two tungsten wires 0.010 inch in diameter and $2\frac{3}{8}$ inches long connected in parallel. These wires are coiled into a spiral by wrapping them around a stiff rod of small diameter and are hooked over the ends of the supports. This avoids spot welding, which is inconvenient unless a portable spot welder is available. (For design of filaments to secure sufficient electron emission, see the excellent tables of Jones and Langmuir.[3]) Three heating

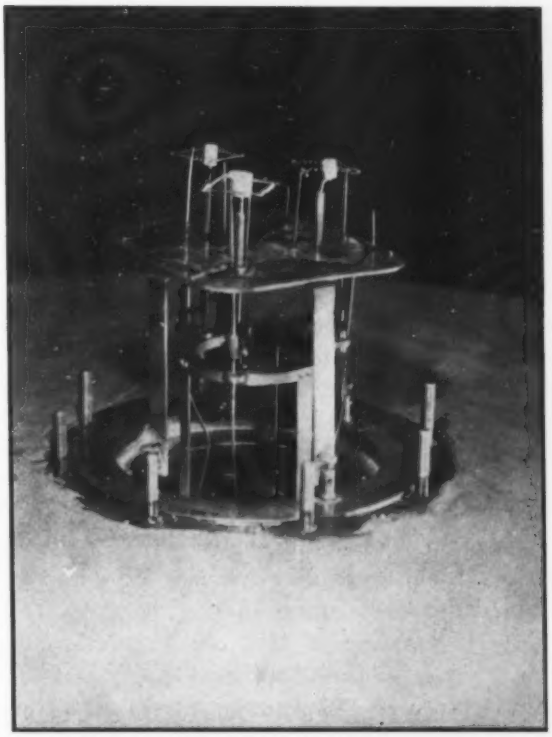

FIG. 3. Bombarding chamber with cover and shield removed.

[3] H. A. Jones and I. Langmuir, Gen. Elec. Rev. **30** 310–319, 354–361, 408–412 (1927).

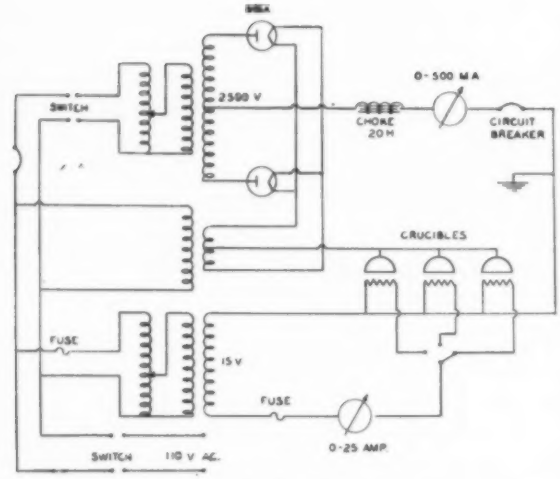

FIG. 4. Power supply for bombardment furnace.

units were placed in the bombarding chamber so that three melts may be made with one evacuation. The crucible cups are connected in parallel while the filament to be heated is chosen by a selector switch. They are surrounded by a molybdenum radiation shield divided into three compartments by partitions. The base is a nickel plate.

Electrical system

The wiring diagram is shown in Fig. 4. Full-wave rectified voltage is applied to the tantalum cups. A 20-henry choke helps to smooth out operation and decrease surges. Circuit breakers in both primary and secondary interrupt the primary current when gas discharge occurs. The bombarding voltage is regulated by a Variac in the primary; full voltage is +2500 r.m.s. volts. The space current is controlled by the temperature of the filament through a Variac in the filament circuit.

Operation

The main difficulty encountered in operation was gas discharge caused by the gas given off by sample and surroundings during heating. This makes it necessary to heat slowly so that the pump may have time to remove the gas as fast as it is given off. Gas discharge forms an arc with an accompanying surge of current which trips the circuit breakers. It is best to begin with a low voltage (perhaps 250 volts) while considerable gas is expelled with the first heat. Then voltage and milliamperage may be slowly increased, while the thermocouple vacuum gage is watched for signs of too rapid an increase of pressure. After a long period of disuse or after new metal is added to the surroundings, the first melt may require an hour or more, but conditions improve with use and the time per melt becomes considerably less. The time required will also depend on the amount of gas in the sample.

If the sample has a high vapor pressure at the melting point, it will be difficult or impossible to melt it. Thus great difficulty was experienced with palladium and a large part of the sample was lost before melting was accomplished. On the other hand, no difficulty was experienced with iron, which has the comparatively high vapor pressure[4] of 0.0001 atmos. 30°C above the melting point.

Platinum (m.p. 1755°C), iridium (m.p. 2350–2450°C), iron (m.p. 1535°C), cobalt (m.p. 1480°C), vanadium (m.p. 1715°C), titanium (m.p. 1800°C), and zirconium (m.p. 1700°C) were melted without difficulty, although vanadium, titanium, zirconium, and iridium appear to have reacted with the zirconia crucibles. Chromium (m.p. 1810°C), and columbium (m.p. 1950°C) were not melted even at very high wattages, no doubt because of strong protective coatings of oxide around the grains. Ruthenium also failed to melt, although the temperature was raised so high that the tantalum shell melted. The power used for melting is rather small, thus platinum melted with 150 watts, the tantalum shell (m.p. 2850°C) melted with 700 watts. The rated capacity of our electrical equipment is 1250 watts, 500 ma at 2500 volts. It could be readily increased, if necessary.

We are indebted to the Milton Fund of Harvard University for a stipend which made possible the construction of the furnace. Dr. H. M. O'Bryan and Dr. D. A. Lyon gave much valued advice, while Dr. Howard Tatel assisted in the design of the electrical circuit. We are also indebted to several graduate students in the Laboratory of Physical Metallurgy, particularly to Haim H. Chiswik and Robert Jaffee for help in construction and operation of the furnace.

[4] K. K. Kelley, U. S. Bur. Mines Bull. 383 (1935).

The Measurement of Solid Friction of Plastics

ANDREW GEMANT*
Department of Electrical Engineering, University of Wisconsin, Madison, Wisconsin
(Received May 9, 1940)

In view of the increasing importance of synthetic plastic materials, a method is developed to measure their vibrational damping in a wide range of temperature up to fairly high plasticity. The method and its results should be useful both from a physical and technical standpoint.

1. INTRODUCTION

IN some recent papers the importance from a metallurgical standpoint of the measurement of internal friction has been pointed out.[1,2] The author has shown the significance of this conception in the interpretation of the behavior of plastic dielectrics.[3] There is no doubt that internal friction is just as essential in understanding some mechanical, especially vibrational characteristics of plastics.

In view of the ever increasing technical significance of these materials the methods of measuring their internal friction ought to be given ample consideration. Generally speaking, the same methods as used for metals can be applied also for plastics. Among these methods the one used by Förster (see below) appears rather simple and still satisfactory. It is, however, restricted to rigid bodies, and this imposes a certain limitation with regard to its use for plastics.

It is desirable, namely, to carry out measurements on plastics in a temperature range in which the plasticity of the material becomes appreciable. This might be required from a technical standpoint in cases where plastics are used at fairly high temperatures, and also from a theoretical standpoint, aiming at a physical interpretation of the mechanism of internal friction in contradistinction to that of plasticity (see Section 4, *c*). In this temperature range the material does not behave as a rigid body, and the method of Förster would not be applicable.

It is the purpose of this paper to describe a variation of the method applicable to highly plastic materials, like soft wax, for instance. In the following pages the theory and then the praxis of the method will be described. Measurements on glass and polystyrene at room temperature, carried out in order to check the method, will follow. Results obtained with paraffin wax at different temperatures up to its softening range will conclude the paper.

2. PRINCIPLE AND THEORY OF THE METHOD

The method as developed by Förster[1] utilizes forced flexural vibrations of cylindrical bars with free ends, suspended at nodal points. Oscillations at varying frequencies are set up at one point, picked up and measured at another, and the resonance curve of the response taken, in determining the width of the frequency range w_f in which the amplitude drops to a fraction $1:\sqrt{2}$ of the maximum, obtained at frequency f. The sharpness or rather bluntness b is then defined as

$$b = w_f/f. \tag{1}$$

There are several notations in use to measure the internal friction. One is the decay factor Δ, as occurring in the exponential term $e^{-\Delta t}$ (t = time). The relation between Δ and b is given by

$$\Delta = \pi f b. \tag{2}$$

Another is the logarithmic decrement δ as given by

$$\delta = \pi b. \tag{3}$$

A third is the specific loss θ, being the loss of energy per cycle, expressed as a fraction of the total energy. It is given by

$$\theta = 2\pi b. \tag{4}$$

Finally we have η the "equivalent viscosity," being

$$\eta = Eb/2\pi f. \tag{5}$$

* This work has been carried out at the Department of Electrical Engineering, The University of Wisconsin, Madison, Wisconsin. Author's present address: Detroit Edison Co., Detroit, Michigan.

[1] F. Förster and W. Köster, J. I. E. E. **84**, 558 (1939).

[2] R. H. Randall, F. C. Rose and C. Zener, Phys. Rev. **56**, 343 (1939).

[3] A. Gemant, J. App. Phys. **10**, 508 (1939).

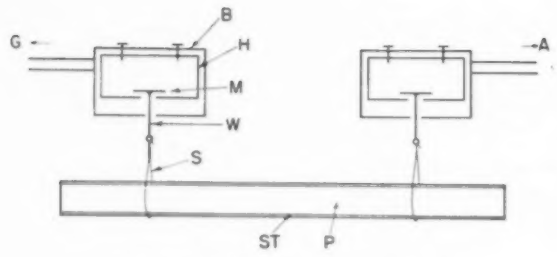

FIG. 1. Diagram of apparatus.

(E=elasticity modulus.) η is not a constant resistance unit, like the plastic resistance η_0; it varies with the frequency, and has no physical reality. For a given frequency it can be thought of as a viscous element, connected mechanically parallel to the elasticity modulus. It appears that the specific loss θ is the most appropriate quantity, in case a physical explanation is sought for. In the following either θ or η will be used.

In order to evaluate η, the knowledge of E is required. The latter is connected with the natural frequency f by the equation:

$$f=0.88(E/\rho)^{\frac{1}{2}}d/l^2, \tag{6}$$

where ρ=density of the material, d=diameter and l=length of the cylinder. If f is measured, E, the Young modulus, can be computed. In Eq. (6) f is the fundamental frequency, but any other harmonic can be used as well. In order to obtain the first, second, third . . . harmonic, the right side of (6) has to be multiplied by 2.76, 5.41, 8.94, 13.3 etc.[4]

The material will vibrate as a rigid cylinder as long as its plasticity is negligible. Mathematically this condition is given by

$$\eta_0 \gg E/2\pi f. \tag{7}$$

If, with increasing temperature and decreasing η_0, the two sides of (7) become comparable, the method described above must fail. In order to overcome this difficulty, the following is suggested.

Instead of a solid cylinder a rigid cylindrical hollow tube is used as a kind of reference. This tube has to be made of a suitable standard material of high E and low η. Steel is well suited for the purpose. After obtaining θ or η for the reference tube, it has to be filled with the plastic in question, and the total damping determined again. From the total damping and that of the steel tube alone that of the plastic can be computed. In following this procedure, the plasticity of the filler will not obviate the measurements, since the rigidity of the specimen is maintained at the required level by the use of the external steel tube.

In evaluating the damping of the plastic, first the data for the tube alone have to be considered. As to Eqs. (1) to (5), they are valid for a hollow tube as well as for a solid. Equation (6), on the other hand, has to be modified, and it can be shown that it will take the form

$$f=0.88\left(\frac{E}{\rho}\right)^{\frac{1}{2}}\frac{(d_0^2+d_i^2)^{\frac{1}{2}}}{l^2}, \tag{6a}$$

where d_0=outer diameter and d_i=inner diameter. In case the tube wall is thin compared with the average diameter d, we have

$$f=0.88\left(\frac{E}{\rho}\right)^{\frac{1}{2}}\frac{\sqrt{2}d}{l^2}. \tag{6b}$$

From (6b) E can be computed and used in (5). In cases where otherwise misunderstanding might arise, data referring to the steel tube will be denoted by an index s, like η_s.

For the combination steel-plastic primarily a total value of the bluntness is obtained (such data will be denoted by an index t). The question is how to obtain the damping of the plastic alone (index p) from total and steel tube values.

The damping b_t of a composite structure is obtained by integrating both resistance and elasticity over all volume elements dv:[5]

$$b_t=2\pi f\int a^2\eta dv/\int a^2 E dv, \tag{8}$$

where a=amplitude of strain. This equation could be solved rigorously, if required; an approximate solution is obtained in substituting an average squared amplitude $\overline{a^2}$ for the variable a^2 values, in which case (8) yields

$$b_t=2\pi f\int \eta dv/\int E dv$$

or

$$b_t=2\pi f\frac{\eta_s v_s+\eta_p v_p}{E_s v_s+E_p v_p}, \tag{9}$$

[4] S. Timoshenko, *Vibration Problems in Engineering* (Van Nostrand Co., New York, 1937), p. 343.

[5] A. L. Kimball, *Vibration Prevention in Engineering* (Wiley, New York, 1932), p. 120.

where v_s and v_p are the respective volumes for a given length of the tube. If

$$E_s v_s \gg E_p v_p,$$

a condition which will hold with most plastics, (9) can be written as

$$\eta_p = \frac{v_s}{v_p}\left(\frac{E_s b_t}{2\pi f} - \eta_s\right) \tag{10}$$

from which η_p of the plastic can be computed. As to θ_p, its knowledge would require E_p, which, however, is not given by the above method.

3. Apparatus

Some details of our apparatus, in principle that of Förster, are shown in Fig. 1. Two headphones H, built into iron boxes B, were used as mechanical vibrators. Shielded leads connected the vibrators to the generator G and the amplifier A. The latter, a three-stage set with a step-up transformer at the input, operated a copper-oxide type milliammeter as indicator. The boxes B were attached to heavy blocks and supported by pieces of rubber, in order to minimize mechanical disturbances.

Short pieces of copper wire W, 1 mm in diameter, were cemented to the membranes M of the headphones. The connection between specimen and vibrators should be as loose as possible, in order to minimize a dissipation of energy, making the internal loss appear too high. The sensitivity of the amplifier, of course, sets a limit to the looseness of the coupling. A sling S of copper wire gauge 40 served as coupling; it had a shape, shown in Fig. 2, to touch the specimen at two

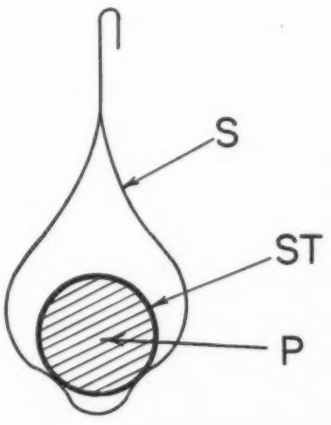

Fig. 2. Shape of sling, holding steel tube.

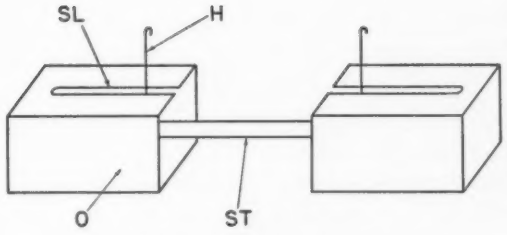

Fig. 3. Diagram of oven.

points only. The specimen is indicated as the steel tube ST filled with the plastic P. Since the amplitude of vibrations diminished with increasing order of the harmonics, it was sometimes necessary for the sling S, shown in Fig. 2, to be replaced by a circular one, tightly surrounding the tube ST.

The specimen has to be supported at the nodes, in order to minimize dissipation of energy. The distance of the nodes from the ends is somewhat less than $\frac{1}{4}$ of the length for the fundamental, $\frac{1}{6}$, $\frac{1}{8}$, $\frac{1}{10}$ . . . of the length for the successive harmonics.

The steel tube used had an outer diameter of 0.8 cm and a wall thickness of 0.06 cm. Three different lengths of 40, 30 and 23 cm were selected.

In cases where the specimen had to be tested at higher temperatures, an electric oven (see Fig. 3), consisting of two halves O was pushed over the tube ST. Two slits SL at the top accommodated the slings H. The temperature was measured by means of a thermometer, a previous calibration allowing for the difference of temperature inside and outside the steel tube.

As was shown in the previous section, measurements on plastics require the knowledge of η_s. The results of this determination are shown in Table I. The first column indicates the length of the tube used, the second the order of the natural vibration, the third the experimentally observed frequencies and the fourth the bluntness, the last two data being read by the setting of a precision condenser of the generator. The fifth column gives the calculated specific loss, and the sixth the equivalent viscosity, as computed from Eq. (5). A value according to the literature of 2.0×10^{12} abs. for E_s was taken; Eq. (6b) with $\rho=7.8$ yielding, as was expected, the same figure.

The specific loss θ is seen to be approximately constant over the whole frequency range. The

same was found by W. Jackson and the author[6] in an earlier publication, also by A. J. Ockleston.[7] These authors, as already Kimball, have noted a certain variation of the specific loss with the amplitude of the strain. Although this effect, too, could be investigated with the apparatus described, it has not been considered in the course of the present paper.

In Fig. 4, the values of θ are plotted against $\log f$, and it can be seen that it slowly decreases with increasing frequency. The data for η_s at different frequencies will be required in using Eq. (10) in connection with plastics.

4. Measurements

The following results can be divided into two groups, those on glass and polystyrene on the one hand, paraffin wax on the other. It is intended later to continue the research by taking the internal friction of several technical synthetic plastics both at room and higher temperatures.

The first group of data aims at checking the method itself. Since with materials obeying condition (7) it is possible to carry out both combined measurements with the steel tube and single ones with the plastic alone, both sets ought to yield the same friction data, if the combined method works satisfactorily. It will be seen that the agreement, indeed, is fairly good with both glass and polystyrene.

The paraffin wax measurements represent a set of data of which a direct check was not any more possible.

a. Glass

Preliminary tests indicated that it is not possible just to place a glass rod (or tube) inside the steel tube. The damping, especially for the harmonics, becomes unreasonably high. This is not surprising, since the method is based on the assumption that both materials vibrate as one unit; in other words, the amplitude of the inner wall of the steel tube should be the same as the amplitude of the outer surface of the plastic. If this is not the case, the external surface friction, which is quite high, comes into play and spoils the result.

Table I. *Internal friction of steel tube.*

l in cm	Order of vibration	f	b_s	θ_s	η_s (abs. units)
40	fundamental	290	0.26×10^{-3}	1.6×10^{-3}	280×10^{3}
40	1st harm.	797	0.15	0.95	60
40	2nd harm.	1550	0.20	1.2	41
30	fundamental	522	0.15	0.95	92
30	1st harm.	1428	0.17	1.1	38
30	2nd harm.	2770	0.11	0.70	13
23	fundamental	889	0.18	1.1	65
23	1st harm.	2415	0.12	0.75	16
23	2nd harm.	4625	0.15	0.95	10

[6] A. Gemant and W. Jackson, Phil. Mag. **23**, 960 (1937).
[7] A. J. Ockleston, Phil. Mag. **26**, 705 (1938).

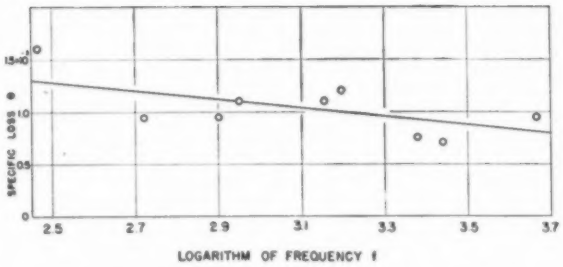

Fig. 4. Specific loss of steel as function of frequency.

In order to overcome this difficulty, a glass tube fitting tightly into the steel tube was selected, and the thin interspace left lubricated with a small amount of heavy paraffin oil. Thus external friction was eliminated, while the added viscous loss was certainly small. The ideal arrangement is, of course, to pour or mold the plastic directly in the steel tube, but this was not feasible with glass.

The combination thus obtained vibrated as a whole, as could be seen from the natural frequencies. Whereas the fundamental for the steel alone is given by Eq. (6a), that for the combination, if it vibrates as a unit, is, in first approximation, given by the same equation, in replacing E/ρ by

$$(E_s v_s + E_p v_p)/(\rho_s v_s + \rho_p v_p).$$

Here v_s (steel volume of the 40-cm tube) $=5.2$ cc, $v_p=7.0$ cc, $E_p=0.7\times10^{12}$ and $\rho_p=2.5$. In computing the frequency ratio of the combination ($d_i=0.48$ cm) to that of the steel tube, the figure 0.89 is obtained, whereas the experimentally observed ratio was 0.94, which is a fair agreement, considering the large increase (about 50 percent) of both mass and elasticity.

Table II gives the results referring to the steel-glass combination. The 40-cm tube was used. Column 1 gives the order of vibration, column 2 the frequency, and 3 the bluntness observed.

Next η_s is listed for the frequency in question, according to the data given in Section 3. η_p was computed from Eq. (9), since the second term in the denominator could not be neglected. The last data are the specific loss figures for glass after Eqs. (4) and (5).

In order to check the last figures, the same glass tube was tested for itself. Table III gives the results. Column 1 contains the order of vibration, 2 the frequency and 3 the bluntness. The last column gives the specific loss. The sets in both tables show a slight decrease with increasing frequency, in agreement with data of Wegel and Walther,[8] and they also agree with each other to show that the figures, as obtained from measurements with the steel tube and using Eq. (9), are reliable. The difference is perhaps due to the losses in the lubricating layer.

b. Polystyrene

This test was carried out on a solid cylinder, made of polystyrene, tightly fitting into a steel tube, the boundary lubricated with heavy liquid paraffin. For more accurate measurements it is recommended to fill the tube with the styrene monomer and polymerize it in the tube, thus avoiding any third material. Also it should be mentioned that the lubricant, if used at all, must be of sufficiently high viscosity; low viscosity ones are liable to introduce increased losses because of turbulence.

The polystyrene rod had a length of 30.5 cm, a diameter of 0.95 cm, density 1.20. The steel tube was different from those of the foregoing sections: $l=30.6$ cm, $d_0=1.12$ cm, $d_i=0.99$ cm, $v_p/v_s=3.5$.

The results are summarized in Table IV. Only the fundamental was used. The first horizontal row refers to the steel tube alone, the second to the polystyrene rod. E was computed from (6), giving 45×10^9. The third row gives the data on the combined test, η_s being computed on the basis $\theta_s=$const., and η_p calculated from Eq. (10), valid for this case with sufficient accuracy. The data for θ_p in the second and third row agree fairly well.

It should be noted that the agreement both for glass and polystyrene is fair, although θ_p for polystyrene is about 30 times larger than that for glass, shown in the previous section. Both are appreciably higher than θ for steel ($\sim1\times10^{-3}$), an essential requirement of the method. The damping of the holder, i.e., the steel tube, must be as low as feasible, since the method is a differential one.

c. Paraffin wax

Measurements on paraffin wax were carried out by pouring the material into the steel tubes where they were allowed to solidify. No lubricant is required in this case. The material was a high melting product (m.p. about 70°C). The choice of paraffin wax is certainly not the best possible in that the temperature range of softening is rather narrow, a circumstance impairing the accuracy of the data. Synthetic resins with an extended softening range will be better suited for the method.

TABLE II. *Steel-glass combination.*

ORDER OF VIBRATION	f	b_i	η_s	η_p	θ_p
fundamental	273	0.55×10^{-3}	300×10^3	490×10^3	7.4×10^{-3}
1st harm.	753	0.39	64	130	5.7
2nd harm.	1465	0.40	43	63	5.2

TABLE III. *Data for glass tube.*

ORDER OF VIBRATION	f	b_p	θ_p
fundamental	233	0.93×10^{-3}	5.8×10^{-3}
1st harmonic	643	0.91	5.7
2nd harmonic	1262	0.76	4.8

TABLE IV. *Data on polystyrene.*

SPECIMEN	f	b	η_s	η_p	θ_p
Steel tube	720	0.16×10^{-3}	70×10^3		
Polystyrene	175	20.		820×10^3	0.13
Polystyrene +steel	540	2.2	95	325	0.155

TABLE V. *Data on paraffin wax at room temperature.*

l IN CM	ORDER OF VIBRATION	f	b_i	η_s	η_p	θ_p
40	fundamental	262	0.43×10^{-3}	330×10^3	70×10^3	0.14
40	1st harm.	724	0.35	67	30	0.17
40	2nd harm.	1404	0.40	45	17	0.17
30	fundamental	458	0.57	105	105	0.38
30	1st harm.	1252	0.40	43	20	0.20
30	2nd harm.	2428	0.46	15	16	0.31
23	fundamental	772	0.48	75	45	0.28
23	1st harm.	2127	0.80	26	34	0.56
23	2nd harm.	4050	0.75	20	14	0.45

[8] R. L. Wegel and H. Walther, Physics 6, 141 (1935).

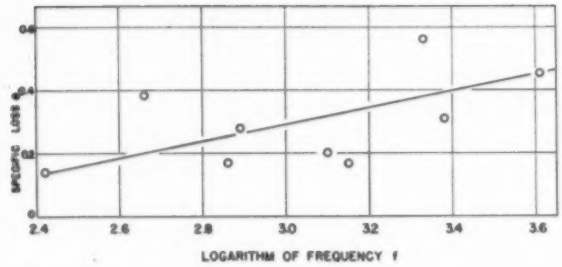

FIG. 5. Specific loss of paraffin wax as function of frequency.

First room temperature data are given in Table V, carried out with the three tubes described in Section 3. θ_p is computed by using $E_p = 5 \times 10^9$ (see below), and plotted in Fig. 5. It slowly increases with increasing frequency.

One single datum obtained from paraffin wax alone should be mentioned, although its determination was near the limitations set by the method. A 22-cm long paraffin cylinder of 1.2 cm diameter was used, having a natural frequency of 165. E_p was calculated to 5×10^9 (with $\rho = 0.9$). The bluntness was found to be 30×10^{-3}, giving $\theta_p = 0.19$ in fair agreement with the low frequency range of θ_p shown in the last column of Table V.

Next the results obtained at higher temperatures are given. The procedure consisted in carefully raising the temperature of the oven shown in Fig. 3 up to a point corresponding to a paraffin temperature of about 65°C which was about 5 degrees below melting. Then the oven was allowed to cool slowly, and the damping determined at frequent intervals. It was found decreasing rapidly from around 62°C to 54°, and then remaining practically constant up to room temperature.

Because of this narrow temperature range the curves obtained cannot be considered very accurate. In order to obtain more exact data with paraffin wax, a larger and more elaborate oven had to be used. An oven of the above type, on the other hand, will be completely sufficient for measurements on synthetic plastics, possessing a large softening range.

The results are shown in Fig. 6. The data of η_p^* (the significance of the index * will be explained below) were computed from Eq. (10), but no data of θ_p could be obtained, owing to the uncertainty regarding E_p at those temperatures. Four curves at four different frequencies are presented. The one for $f = 260$ refers to the fundamental of the 40-cm tube filled with paraffin, those for $f = 461$ and 1264 refer to the fundamental and first harmonic of the 30-cm tube, and the last for $f = 778$ to the fundamental of the 23-cm tube.

It is shown in the theory[3] that the damping is determined by the equivalent viscosity η of the solid friction alone, as long as condition (7) holds, that is, for temperatures appreciably below the softening point. With increasing temperature the plasticity constant, η_0, will decrease and the damping will increase. The experimental quantity as defined by Eq. (5) is now determined by the solid friction, elasticity and plasticity *together*, and will be denoted by η^* in contradistinction to η of the solid friction. Since, with increasing temperature, η^* is more and more dependent on the plasticity constant η_0, it should gradually become independent of the frequency.

This conclusion is verified in a semiquantitative way by Fig. 6. Whereas around 50°C η_p^* decreases pronouncedly with increasing frequency, around 55°C it becomes independent of the frequency, and at still higher temperatures it even increases with increasing frequency.

The final aim of tests of the type described in this section is the following. Simultaneously with measurements on the damping the plasticity as a function of temperature will have to be measured by means of a stationary process. The two sets of data will allow the pure solid friction (expressed either by η or θ) to be determined as a function of

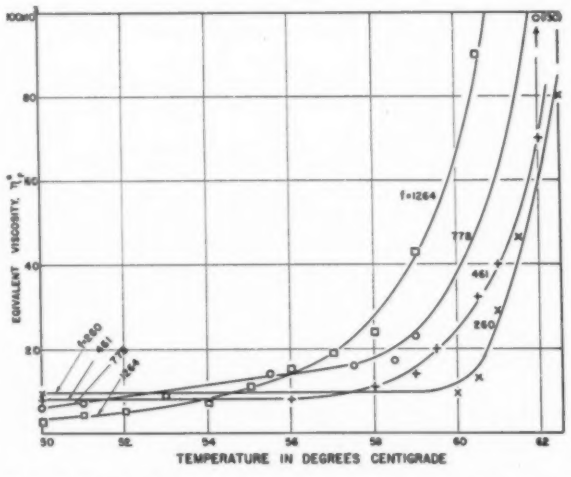

FIG. 6. Equivalent viscosity of paraffin wax as function of temperature for different frequencies.

temperature. Such information will be very valuable, in order to know more about the physical processes underlying solid friction, and to evaluate dielectric properties of synthetic plastics.[9]

The above method was developed for the purpose of carrying out such measurements on damping, which, in their turn, will allow a determination of solid friction in a wide range of temperature. It is felt that synthetic plastics will lend themselves readily for a research of this type.

Summary

(1) A method to measure the vibrational damping of plastic materials is described. It should be useful (a) from the standpoint of technical applications of plastics, and (b) in order to evaluate the solid friction constant as a function of temperature, information likely to increase our understanding of the physical mechanism of solid friction.

(2) The principle of the method, based on that of Förster for metals, together with the theory of the computation of the damping factors, and some constructional details of the apparatus used are presented.

(3) Three materials were tested: glass, polystyrene and paraffin wax. The first two were investigated at room temperature, and the purpose of obtaining these data was chiefly to check the efficiency of the method. Data on paraffin wax were obtained both at room and elevated temperatures up to the softening range. The general trend of the temperature curves is in agreement with theoretical expectations.

(4) It is intended to continue the research with technical plastics within a wide range of temperature.

[9] J. M. Davies and W. F. Busse, "Dielectric Properties of Plasticized Polyvinyl Chloride," 99th Meeting Am. Chem. Soc., Cincinnati, April, 1940.

The Optical Properties of Colloidal Suspensions in Relation to the Measurement of Particle-Size Frequency

E. G. Richardson

King's College, Newcastle upon Tyne, England

(Received May 6, 1940)

I. The Extinction of Light by Colloidal Suspensions

SINCE the object of this research was to develop an apparatus in which the light transmitted through a polydisperse suspension of opaque particles during sedimentation is used to derive the size-frequency curve for the solid in question, a preliminary investigation had to be made of the manner in which the light extinction varies with particle diameter and concentration. The range of size in which the author is particularly interested in the present work is that from 1 to 0.1 micron, since the majority of pigments and clays have most of their particles lying within this range.

It is evident that, with a sufficiently low concentration of large grains, the amount of light cut off by the suspension will be proportional to the total surface area of the particles. With white light the author has verified that this law holds down to diameters of 10 microns and for concentrations below 0.1 percent by volume. This was done by using monodisperse suspensions of the spores of certain fungi or of pollen grains in a liquid of equal specific gravity. With the smaller particles which form the subject of this article it is no longer safe to use white light since the amount of light intercepted is likely to be a function of the wave-length as well as of the granularity. At the other end of the scale of diameter, where the dispersion of the light is a scattering effect, Rayleigh's law that the extinction coefficient is proportional to the sixth power of the diameter directly, and the fourth power of the wave-length of the light inversely, is known to hold when the diameter of the particles is small compared with the wave-length. Thus, both for the large and the small particles a

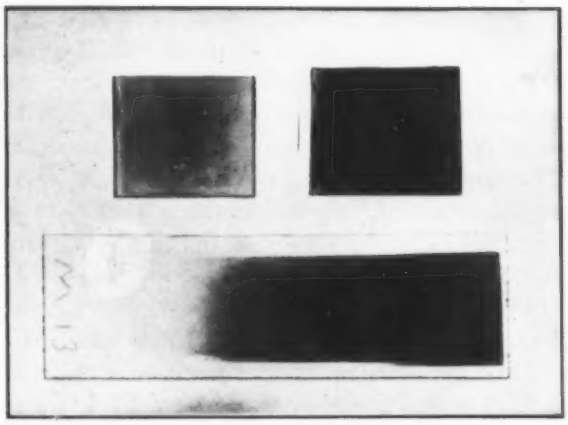

FIG. 1.

valid law exists connecting extinction and granularity which can be used for this purpose (with a monochromatic source) and in fact colloidal solutions with particles ranging *up* to 0.1 micron have been examined in infra-red radiation in order to make a gross estimation of their mean particle size,[1] but in the analysis of pigments it would be impossible to secure a source with a wave-length in the infra-red sufficiently large to bring the system entirely within the Rayleigh territory. It might have been possible, by using an x-ray beam to satisfy the conditions for the "shadow" effect to apply to these fine particles, but with a view to simplicity of apparatus, it was decided to use an ultraviolet source and to investigate the absorption of this radiation in fractionated suspensions of more or less uniform granules over the range concerned. The mercury line 0.365μ was chosen as source.

The only previous practical investigation of the optical properties of this range of sols which has come to the author's notice is contained in the work of Cheveneau and Audubert[2] two decades ago on fractionated series of particles of gum arabic and mastic in the range 10 to 1 micron with monochromatic sources of 0.644 and 0.498μ. They claimed a general law for these sols of the type $\alpha = KNd/\lambda^n$ for the extinction coefficient in which N represents the number of particles of diameter d in one ml and K is a factor which depends only on the nature of the two phases. A detailed examination of their results does not, however, bear out the contention of a direct proportionality between concentration on the one hand and diameter on the other, and the extinction coefficient. The particles in the sols which they examined were (unlike those in clays and most pigments) transparent.

On the theoretical side Jobst[3] has calculated the extinction coefficient for suspensions of uniform granularity in which the wave-length of the light is comparable with the size of the grains. The relevant parameter is $2\pi d/\lambda$. For values of this factor greater than unity, the Rayleigh law is followed. As the factor increases there comes a departure from this law and after reaching a maximum at a moderate value of d/λ the absorption (for a specific total surface area of grains) approaches asymptotically the steady value corresponding to the "shadow" effect that we have already noted for the larger grains (cf. lower line of Fig. 2). Jobst performs the complete calculation only for conducting particles (metal sols), but gives also some data for partially conducting particles, as for sols in which the refractive indices of the disperse and continuous media bear a stated ratio to each other. In any case his conception of "conductivity" is purely a theoretical figment which represents the validity of neglecting certain terms in the mathematical expansions.

For the calibration of the particle-size meter, titanium oxide is used since it is readily obtained as an opaque powder with the bulk of its particles lying between 3 and 0.1 microns, in which form it is used in the rayon and paper industries. Moreover, small quantities of it can be accurately estimated by a colorimetric method which, in turn, lends itself to photoelectric processes. Some of this titanium oxide, as prepared in the form of a paste by Messrs. Courtauld's, was fractionated in a high speed centrifuge in the familiar Perrin technique so as to give specimens graded in steps of 0.1 micron for the coarser grades and 0.05 micron for the finer grades in the range 1.5 to 0.1 micron in diameter. Each of them was placed in turn with a suitable dilution of water in one compartment of a horizontal cell with quartz

[1] D. L. Gamble and C. E. Barnett, Ind. Eng. Chem. **9**, 310 (1937).

[2] C. Cheveneau and R. Audubert, Ann. de physique **13**, 134 (1920).

[3] G. Jobst, Ann. d. Physik **76**, 863 (1925).

base. The other compartment contained pure water to an equal depth. This cell and a narrow angle flint glass optical wedge lay in a shallow box whose bottom contained a Chance's glass filter and whose top carried a dark slide holding the photographic plate. About one foot below was the mercury lamp provided with a shutter. A lens was not used since a dummy exposure with water alone in the cell had shown uniformity of illumination over the relevant portion of the field of view. The lamp was of the linear source type, set parallel to the edge of the prismatic wedge. Figure 1 shows a typical plate obtained in the calibration series. The plates, after development, were passed through a microphotometer and the mean density of exposure above the sections of the cell containing the clear water and the suspension, respectively, matched with two positions over the wedge, after the method originally used by Fabry[4] for measuring optical absorption coefficients.

The optical wedge had been calibrated beforehand to verify that the optical density varied directly as the distance from a datum line near the refracting edge; consequently, if I_1 is the light transmitted by a section distant x_1 from this line and I_2 that by a section distant x_2, $\log I_2/I_1 = x_2 - x_1$. Further, if I_1 is also equal to the light which gets through the portion of the cell containing the suspension, while I_2 is equal to that passing through the clear portion we shall have $I_1 = I_0\epsilon^{-\alpha_1 x}$ and $I_2 = I_0\epsilon^{-\alpha_2 x}$ where I_0 is the incident light and x the optical thickness of the cell. Then the extinction coefficient due to the solid in suspension alone is $\alpha_2 - \alpha_1 = (\log I_2/I_1)/x_1$ and is therefore represented in terms of the distances along the wedge of the two matched positions.

The next step was to estimate the titanium oxide. This was done by evaporating the contents of the cell to dryness, boiling with concentrated sulphuric acid and diluting the titanium sulphate so obtained to a volume of 100 ml in a graduated flask, following the method used by Martin.[5] Each solution was then titrated into a six-percent hydrogen peroxide solution in such proportions that each mixture reached the same orange-yellow color. This test was assured photoelectrically by observing the absorption spectrum of the mixed solution and using a source of light in conjunction with a filter which transmitted the same band of light as the solution and then interposing each solution in turn between the filter and a photoelectric cell. In this way the relative masses of titanium oxide in the test cell were calculated, and from these masses again, dividing by the mean diameter in the particle-size range comprised by each, the relative total surfaces were calculated. Then from the wedge measurements we derived the extinction coefficients corresponding to the same surface areas for the corresponding particle groups. In the case when the light cut off is a linear function of the total surface area, these pairs of data would be in direct proportionality.

Some results for sulphur, clay and zinc oxide were also obtained. These are probably less accurate than the titanium oxide values since the masses were estimated directly by evaporating to dryness and weighing larger quantities of the suspensions from which representative volumes were drawn off for the optical measurements.

The results are shown in Fig. 2 in such a way that the departure from the area effect as the mean particle size in a group decreases is plainly visible. The upper line is drawn through the titanium oxide results while the lower one is the theoretical curve of Jobst. The two lines concur above 0.5 micron. The horizontal axis of the graph represents what one would expect if extinction were truly proportional to surface area. It may be objected that, since all the data are relative, there is no indication of the level at

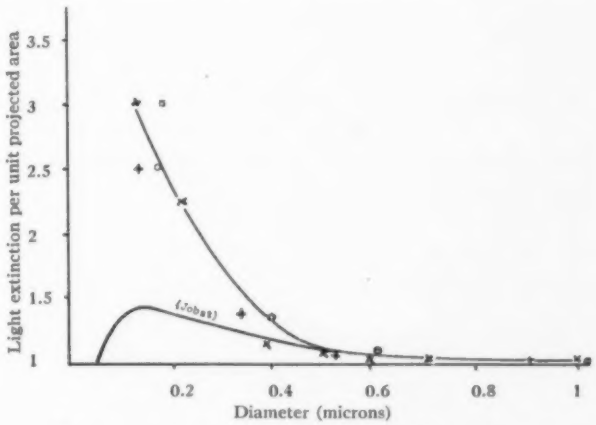

FIG. 2. ×—titanium oxide; ○—sulphur; +—clay.

[4] C. Fabry, Proc. Phys. Soc. **39**, 1 (1926).
[5] S. W. Martin, Ind. Eng. Chem. **11**, 471 (1939).

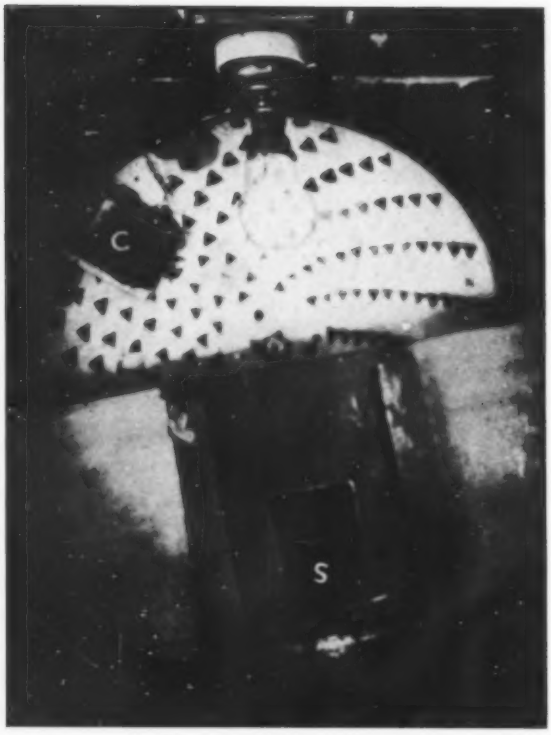

FIG. 3(a).

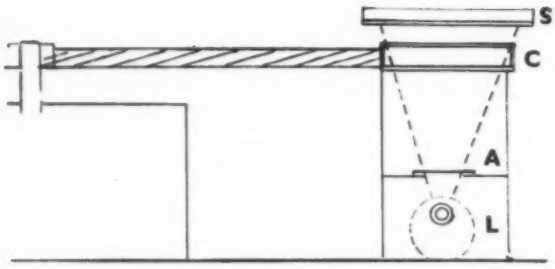

FIG. 3(b).

which this axis is to be drawn. Actually an absolute value of the extinction coefficient was obtained with a counted number of the uniform spores already mentioned and this was compared with the reading for the coarsest grade of each of the other suspensions of like concentration and mean particle size.

II. Applications to the Delineation of Size-Frequency Curves of Fine Suspensions

A few years ago Wagner[6] and the writer[7] independently devised apparatus for obtaining the size-frequency curves—or mechanical analysis, as the soil physicists call it—of specimens in the form of a powder by measurements of the turbidity of a suspension of the powder in a liquid in which it was allowed to settle under gravity. The principle of the apparatus was the same in both cases, though the method of calibration was different. In the writer's instrument, the suspension was contained in a tall glass tank and a thin pencil of light from a "pea lamp" passed athwart the tank at a fixed depth to fall upon a photoelectric cell, the current from which was continuously recorded as the suspension settled. In an alternative form, a wide beam of light passed through the whole tank from one side and cast a shadow of the suspension upon a photographic plate at a certain instant after sedimentation had been allowed to continue for a minute or so. The plate was then analyzed in a microphotometer in the same way as a spectrum photograph is analyzed. As already indicated, it had been shown by using monodisperse systems kept in continuous suspension by stirring, that down to diameters of 2 microns, and with a low concentration, the light cut off is proportional to the total surface area of the solid.

The S-shaped curve resulting from an analysis of a polydisperse system during sedimentation, whether in the form of (1) photoelectric current at a fixed depth but varying time, or (2) observations at a fixed time but varying depth, is then the "summation curve" for the system, whose

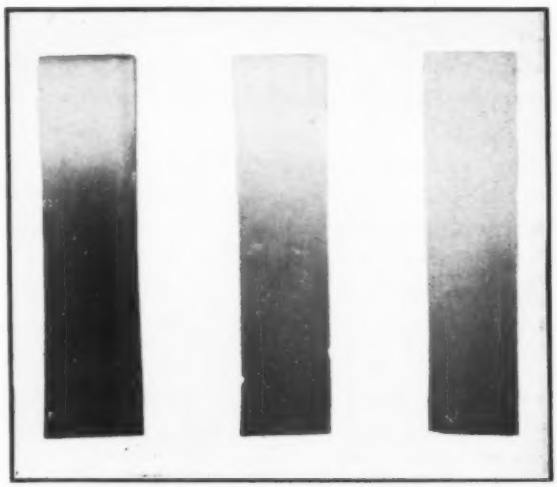

FIG. 4.

[6] L. A. Wagner, Proc. A. S. T. M. **33**, 553 (1933).
[7] E. G. Richardson, J. Agric. Sci. **24**, 459 (1934); also in Phys. Soc. Exhibition Program, Christmas, 1933.

ordinates represent surface areas and whose abscissae can be converted into particle diameters when the Stokes constant for the sedimentation is known. The ordinate of such a curve above any value of the diameter then gives—in relative magnitude—the area of all particles up to and including this size. The "distribution curve" in the form of the surface area of individual particle sizes is then derived in the usual way by replotting the slope of the curve at the size values in question, or by measuring increments in the area of the summation curve between pairs of values of the diameter, if a step-by-step form of analysis is preferred. If we require relative masses instead of surfaces we must multiply each of these slopes or increments by the mean diameter to which each refers before replotting.

Armed with the data of Part I we can now proceed to apply one or the other of these methods to pigments and clays. The second method is preferable and since pigment particles would take an inordinately long time to settle under gravity (with the exception of zinc oxide, which, on account of its high density, may be successfully analyzed under gravity in the lightest brands of petrol) a low speed centrifuge was built, following the accelerated method for mechanical analysis of Svedburg[8] and Marshall.[9] The source was the aforesaid mercury arc (L) and Chance's filter (A). A small cell (C) (6×4×2.5 cm) with quartz sides was built up and fitted into a slot in a wooden disk, which mounted on the vertical axis of an electric motor, formed the centrifuge (Fig. 3). This cell held 50 ml of the suspension which was well shaken up before it was placed in position. The full voltage was then turned on to the motor whose speed under these circumstances

TABLE I. *Particle-size analysis of specimens of titanium oxide in acetone. The figures in brackets are the corrected values, using factors derived from the data of Fig. 2.*

Diam. Micron	0.1	0.2	0.3	0.4	0.5	0.6	0.7	0.8	0.9	1.
No. 5013	3(1)	7(3)	14(8)	18(13)	14(13)	14	12	9	5	4
No. 5014	5(2)	16(7)	28(16)	20(14)	16(15)	8	5	2	–	–
No. 5039	14(5)	14(6)	22(13)	18(13)	14(13)	9	6	3	–	–

[8] T. Svedburg and H. Rinde, J. Am. Chem. Soc. **45**, 350 (1923).
[9] C. E. Marshall, Proc. Roy. Soc. **126**, 427 (1930).

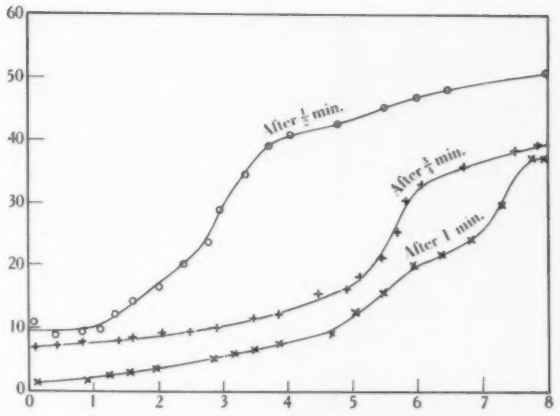

FIG. 5.

rises exponentially so that a correction can be made for the time spent at reduced speed. This speed was checked by a flashing neon lamp and a stroboscopic pattern drawn on the disk. After the lapse of a suitable time (determined by the speed of sedimentation of the average particle) a shutter was operated over the mercury lamp so that an exposure of the photographic plate, P, placed in a frame above the circumference of the disk, was made.

Typical "shadowgraphs" of a suspension at three different epochs during the operation of the centrifuge are shown in Fig. 4. A set of curves derived by analysis of another set of photographs like these when they were passed through the microphotometer are given in Fig. 5. In a gravity field and with particles above 2 microns these would be the actual distribution curves of the specimens in respect to superficial area, but smaller particles in the centrifuge require two corrections, (1) the usual one in centrifuge work which allows for the fact that the acceleration varies a little over the cell (in this case in the ratio 5 to 6 for the extreme diameters), and (2) the optical correction factor derived from Fig. 2.

As a test application of the apparatus, analyses of three specimens of titanium oxide, ground under different milling conditions are shown in Table I, both with and without the optical correction factors. The numbers representing relative masses in the finer grades have in fact to be lowered by amounts equal to the corresponding ordinates of Fig. 2 (upper curve).

Velocity of Compressional Waves in Petroleum Fractions at Atmospheric and Elevated Pressures

ROBERT MATTESON, *Research and Development Department, Standard Oil Company of California, Richmond, California*

AND

C J. VOGT, *University of California, Berkeley, California*

(Received May 27, 1940)

The problem of dynamics of liquid columns, particularly in Diesel engine injection systems, requires a knowledge of the velocity of propagation of compressional waves in the system. Approximate values are generally used in the solution of such problems. In an effort to correlate the physical properties of petroleum oils with the velocity of wave propagation and to relate the characteristics determined at atmospheric pressure with those at higher pressures, tests were conducted in the Physical Laboratories of the Standard Oil Company of California on thirty-seven hydrocarbon oils at atmospheric pressure. Five hydrocarbon oils were investigated in the Mechanical Engineering Laboratories at the University of California at four temperatures ranging from 57°F to 210°F, and pressures ranging from 500 lb. per square inch to 6000 lb. per square inch. In this paper the experimental methods are described and results presented.

VELOCITY OF COMPRESSIONAL WAVES IN PETROLEUM FRACTIONS AT ATMOSPHERIC PRESSURE

THE velocities of compressional waves at atmospheric pressure were measured in 37 petroleum fractions. These stocks ranged from light gas oils to highly viscous lubricating oils and residual stocks. Viscosity indices[1] of the oils used in the tests ranged between −55 and 100+.

Experimental

Wave velocities were calculated from the results of wave-length determinations made by means of a modified Hubbard ultrasonic interferometer[2] used in conjunction with a quartz crystal ultrasonic wave generator operating at 457±1.4 kilocycles. Compressional waves from the vibrating crystal were transmitted through the oil which was held in a thin-walled cup resting on the upper surface of the crystal. The cup was $2\frac{3}{8}$ inches in diameter, sufficiently great so that viscous drag was negligible, and the depth was 2 inches. The bottom of the cup was made of copper 0.001 inch thick. Compressional waves in the oil were reflected from the plane surface, parallel to the crystal surface, of a piston $1\frac{5}{16}$ inches in diameter mounted upon a micrometer screw. The passage of the piston through the nodes of the standing waves in the oil was noted by the deflections of a galvanometer in the generator plate circuit.

In a typical test run the cup was filled approximately to $\frac{3}{4}$ inch depth with the oil under investigation. The cup was electrically grounded, the piston introduced into the oil, and the generator started. Measurements consisted of noting the distance between 10 nodes (5 wave-lengths) over a temperature range from 70° to 105°F for each oil, no attempt being made to control the temperature. The temperature—wave-length data were plotted and from the resulting curves the value for the wave-length at 100°F was read. The velocity at 100°F of the compressional wave was then obtained from the relation

$$\text{velocity} = \text{frequency} \times \text{wave-length}.$$

Specific gravities were obtained by means of A.P.I. hydrometers. Kinematic viscosities were measured at 100°F, and in some cases also at 210°F, using Zeitfuchs[3] type capillary viscometers.

Results

The results of the interferometric measurements are essentially those that would be obtained in a medium of infinite extent since viscous

[1] E. W. Dean, A. D. Bauer and J. U. Berglund (Standard Oil Development Company), "Viscosity index of lubricating oils," Ind. Eng. Chem. **32**, 102 (1940).

[2] J. C. Hubbard and A. L. Loomis, "Compressibilities of liquids by the sonic interferometer," Phys. Rev. **31**, 158 (1928).

[3] E. H. Zeitfuchs, "An accurate kinematic viscosimeter for refinery control laboratories," Proc. Am. Petroleum Inst., Section III, p. 104 (May, 1939).

drag and tube wall expansion are negligible in the type of interferometer used. Table I is a summary of the results obtained at atmospheric pressure.

In Table I are given complete data on specific gravity at 60°F and viscosity at 100°F from which the fractions may be characterized as to chemical type. In addition, the viscosity at 210°F is shown for 12 samples of the oils tested. Kinematic viscosities were converted to Saybolt Universal values according to A.S.T.M. method D446-39.

Figure 1 shows the relationship between velocity, A.P.I. gravity, and kinematic viscosity at 100°F. The curves are based upon the experimental data obtained with the interferometer. The last column in Table I shows percent deviation of the observed velocities from those estimated in Fig. 1 and the agreement is seen to be remarkably close.

TABLE I. *Velocity of compressional waves in petroleum fractions at 100° F and atmospheric pressure.*

Sample Number	Gravity A.P.I.	Specific Gravity 60°F/60°F	Kinematic Viscosity, Centistokes 100°F	210°F	Saybolt Universal Viscosity, Seconds 100°F	210°F	Pressure Wave Velocity Ft./Sec. at 100°F 1 Atmos. Obs.	From Curve	% Diff.
28598	28.3	0.8855	125.2	12.6	578	68.8	4659	4645	+0.3
28599	27.4	.8905	213.2		98.5		4685	4680	+0.1
28600	26.8	.8939	321.4		1485		4728	4700	+0.6
28601	25.9	.8990	532.4	32.5	2460	153.1	4712	4735	−0.5
28602	11.8	.9874	184.4	8.5	852	54.2	4761	4735	+0.6
28603	12.1	.9854	337.8	11.1	1561	63.2	4771	4755	+0.3
28604	12.4	.9833	563.1		2601		4853	4770	+1.7
28606	32.4	.8633	41.1		191		4567	4550	+0.4
28610	23.6	.9123	78.2	7.3	361	50.2	4646	4640	+0.1
28611	22.6	.9182	115.3		533		4675	4665	+0.2
28612	22.2	.9206	201.3		930		4669	4700	0.0
28613	22.4	.9194	376.6	18.0	1740	89.8	4705	4725	−0.4
28614	16.7	.9554	727.9		3363		4771	4770	0.0
28615	16.6	.9548	728.0	18.9	3363	93.4	4761	4770	−0.2
28616	17.6	.9490	154.9	8.9	716	55.5	4715	4705	+0.2
28617	25.8	.8996	525.6		2428		4738	4730	+0.2
28632	15.8	.9606	2112	35.0	9757	164.1	4761	—	—
28769	26.3	.8967	5.44	1.65	43.7		4459	4460	0.0
28770	35.7	.8463	7.71	2.2	51.0	33.5	4420	4405	+0.3
28771	34.3	.8534	3.74		38.3		4334	4340	−0.1
29101	29.4	.8794	2.77	1.10	35.3		4364	4355	+0.2
30989	16.2	.9582	686.6		3172		4757	4765	−0.2
30990	19.7	.9358	49.8		226		4682	4650	+0.7
30991	14.7	.9680	2365		10924		4784	—	—
30992	23.0	.9157	64.2		297		4597	4635	−0.8
30993	29.2	.8806	9.94		58.6		4472	4480	−0.2
31020	38.8	.8309	4.85		41.9		4321	4315	+0.1
31021	36.0	.8448	7.85		51.5		4406	4405	0.0
31022	18.5	.9433	95.0		439		4712	4675	+0.8
31023	31.0	.8708	2.90		35.7		4262	4335	−1.7
31024	32.2	.8644	5.80		44.9		4383	4405	−0.5
31025	30.4	.8740	39.5		183.5		4613	4570	+0.9
31026	24.9	.9047	9.30		56.4		4541	4551	+0.6
31027	19.3	.9383	433.6		2003		4754	4745	+0.2
31028	30.1	.8756	2.50		34.4		4337	4335	0.0
31029	30.4	.8740	20.4		99.2		4508	4530	−0.5
31030	31.2	.8694	9.75		58.0		4469	4470	0.0

Average Arith. Dev. = 0.39%
Average Alg. Dev. = +0.10%

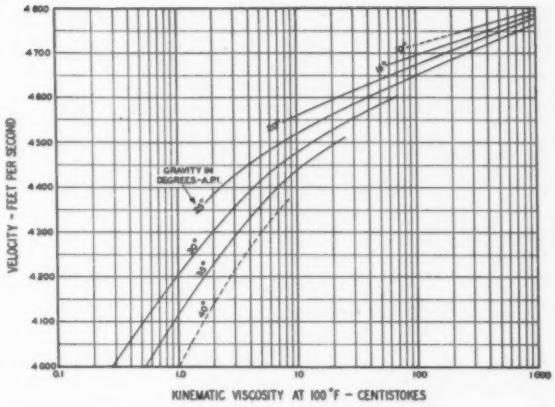

FIG. 1. Velocity of compressional waves in petroleum fractions at 100°F and atmospheric pressure.

The curves in Fig. 1 clearly illustrate that for a given A.P.I. gravity, or specific gravity at 60°F/60°F, the velocity of compressional waves in petroleum fractions increases with kinematic viscosity. In other words, velocity increases with the so-called "paraffinicity." This behavior, it must be remembered, is for oils essentially infinite in extent. For oils in small tubes the viscous drag at the tube walls has the reverse effect, as will be discussed later.

In Fig. 2 are plotted velocity-temperature curves for pure hydrocarbons at atmospheric pressure based upon data from the literature.[4, 5] These curves illustrate the effect of temperature on the velocity of compressional waves in pure hydrocarbons and, at a given temperature, the variation of velocity with chemical type is brought out. For example, the velocities at 73.4°F (23°C) for benzene, cyclohexane, and hexane are

C_6H_6 4320 feet per second
C_6H_{12} 4125 feet per second
C_6H_{14} 3650 feet per second.

At first glance, the behavior of the pure hydrocarbons appears to be the opposite of the petro-

[4] Egbert B. Freyer, J. C. Hubbard and Donald H. Andrews (Johns Hopkins Univ.) "Sonic studies of the physical properties of liquids. I. The sonic interferometer. The velocity of sound in some organic liquids and their compressibilities," J. Am. Chem. Soc. **51**, 759 (1929).

[5] S. Parthasarathy, "Determination of ultrasonic velocity in 52 organic liquids," Proc. Ind. Acad. Sci. **2A**, 497–511 (1935).

leum fractions; the velocity decreases in going from aromatic to paraffinic compounds. This is true, however, only when a series is chosen in which the number of carbon atoms is constant. Selecting a series of pure hydrocarbons of the same specific gravity would show the reverse trends; namely, the velocity increases in going from aromatic to paraffinic compounds. Thus it is seen there is no conflict between the curves of Fig. 1 and Fig. 2.

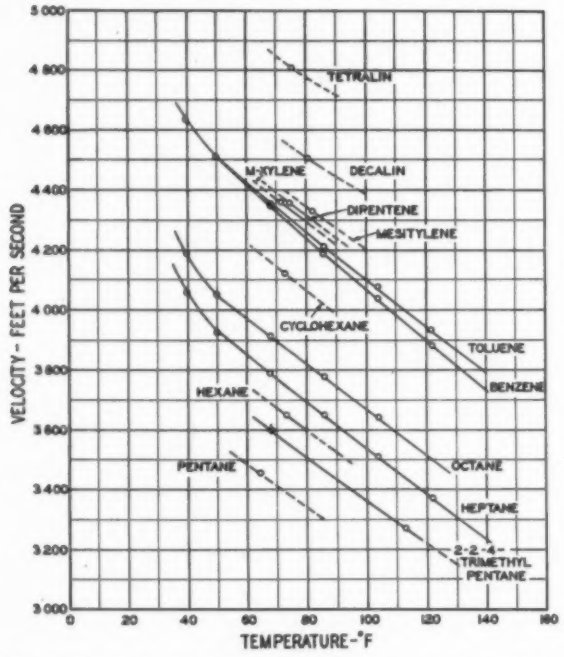

FIG. 2. Velocity of compressional waves in pure hydrocarbons at atmospheric pressure.

VELOCITY OF COMPRESSIONAL WAVES IN PETROLEUM FRACTIONS AT ELEVATED PRESSURES

The velocity of propagation of compressional waves at various pressures and temperatures was measured in a closed system. Five petroleum fractions designated as *V*-2, *V*-3, *V*-7, *V*-11, and *V*-12 were investigated. These oils were from the same stock as those indicated respectively in Table I as 31021, 31022, 31026, 31029, and 31030 and at time of use exhibited the viscosities and gravities at atmospheric pressure as given in Table II.

Experimental equipment

The equipment used in these investigations is shown diagrammatically in Fig. 3. A seamless steel tube (1), approximately 25 feet long having an internal diameter of 0.180 inch and outside diameter of 0.3125 inch was supported in a 2.5-inch iron pipe (2) which served as a heating or cooling jacket. Steel diaphragms (3) 0.625 inch in diameter and 0.026 inch thick were mounted in the seamless steel tube for pressure disturbance indicators. The distance between the two diaphragms was 24.4 feet. A magnetic spray valve[6] (4) mounted at the end of the tube permitted the discharge of a small quantity of the oil in the system, thus setting up the disturbance from which the velocity of wave propagation was determined. The oil to be tested was pumped into the tube past the needle valve (6) and allowed to flow past the bleeder valve (7) until the air in the system was expelled. The desired initial pressure was indicated on a Bourdon type pressure gauge. Temperatures in the water jacket were indicated by mercury thermometers (5). The pick-up unit (8) consisted of a small soft metal armature pivoted at its midpoint and surrounded by a small induction coil. The coil and armature were placed between the poles of a permanent magnet so that the poles were located on either side of the armature. One end of the armature was connected to the diaphragm through a rigid link. Motion of the armature due to sudden changes of pressure at the diaphragm induced a current in the coil. By the use of direct-coupled two-stage amplifiers the output of the coil was amplified sufficiently to give the desired galvanometer deflection in a Westinghouse three-element, galvanometer type oscillograph. The disturbances at the two diaphragms were recorded by separate elements in the oscillograph. The third oscillo-

TABLE II.

Oil	Kinematic Viscosity, Centistokes		Specific Gravity 60°F/60°F	Viscosity Index*
	100°F	210°F		
V-2	7.59	3.10	0.8452	76
V-3	92.0	7.35	0.9509	0
V-7	9.0	2.20	0.9037	36
V-11	19.5	3.82	0.8658	87
V-12	9.25	2.40	0.8713	−38

* Standard Oil Development Company "*Basic Values for Calculating Viscosity Index from Kinematic Viscosities*," Table I, Circular 30.50.

[6] C. J. Vogt and T. A. Rogers, "Operating characteristics of a magnetically actuated fuel injection valve," Automotive Industries **80**, 530–536 (April 22, 1939).

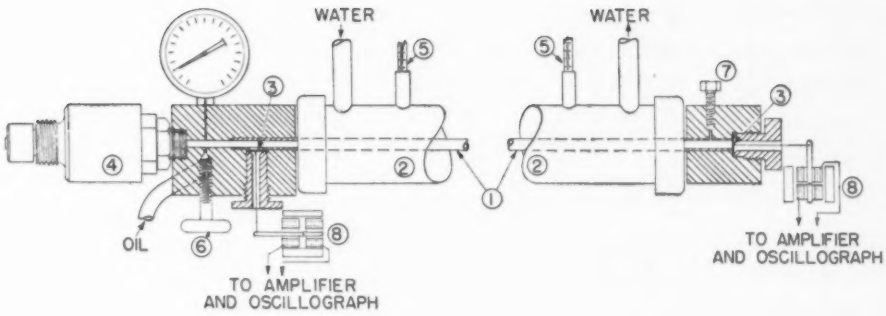

FIG. 3. Diagrammatic sketch of the equipment used in determining the velocity of compressional waves at pressures above atmospheric.

graph element was used to record the timing wave obtained from a 1000-cycle audio-oscillator.

The initial disturbance in the oil was timed with the shutter on the rotating oscillograph drum by allowing the bell-crank which released the shutter to close a switch in the condenser and magnetic spray valve circuit. The condenser capacity used in the tests was sufficient to lift the needle in the magnetic valve and discharge a small quantity of oil. The average pressure drop in the line was less than five pounds per square inch at the higher line pressures.

Test results

A representative oscillogram obtained in the tests is shown in Fig. 4. Trace *A* shows the 1000-cycle timing wave, trace *B* the disturbance at the diaphragm nearest the magnetic valve, and trace *C* the disturbance at the diaphragm at the closed end of the line. The first disturbance on trace *B* indicates a pressure rise due to the needle and armature of the magnetic valve moving into the system. The pressure disturbance due to the discharged oil is indicated on trace B, by point 1, as a sudden pressure drop at the first diaphragm. The arrival of this disturbance at the second diaphragm is indicated by point 3 on trace *C*. The time required for the disturbance to travel the distance of 24.4 feet between the two diaphragms is obtained by dividing the horizontal distance in inches between points 1 and 3 by the distance in inches spanned by ten cycles of the timing wave *A* equivalent to 0.01 second. The time so obtained divided into 24.4 feet, the line length between the two diaphragms, gives the velocity of the disturbance in the oil in feet per second. The disturbance on trace *C* represented by point 2 is due to the acoustic wave traveling through the metal of the seamless steel tube.

FIG. 4. Typical oscillogram of pressure disturbance in the oil column. Trace *A*—timing wave. Traces *B* and *C*—pressure disturbance.

Oscillograms of the type indicated in Fig. 4 were analyzed for the five oils given in Table II. The results of these analyses for four temperatures and various pressures are plotted in Figs. 5 to 9, inclusive.

From these relations it might be concluded that increased viscosity and density due to pressure, increase the velocity of wave propagation, while a decrease in viscosity and density with temperature will reduce the velocity. A cross-plot of all the oils tested failed to show that viscosity and density alone are the deciding factors from which the velocity of propagation in tubes might be predicted. The chemical type of the oil as indicated by the viscosity index shows no correlation with the velocity of propagation at any pressure or temperature where the viscosity of all the oils have the same value.

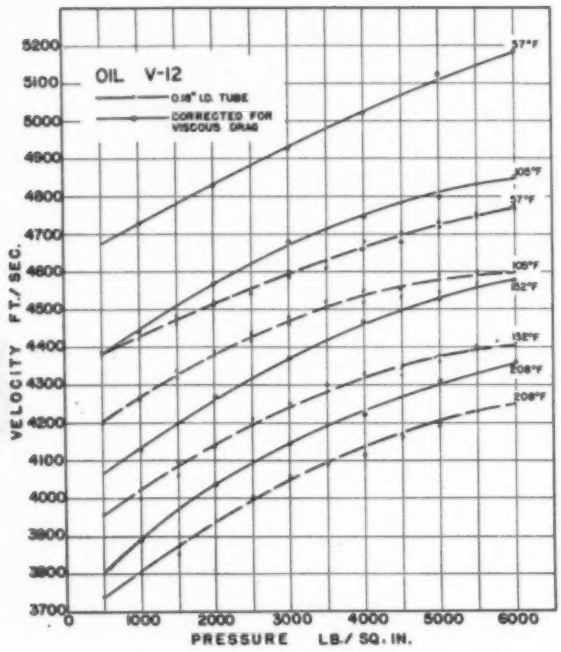

FIG. 5. Velocity of compressional waves in the oil as a function of pressure and temperature.

Viscous Drag

The velocity of wave propagation in tubes of small diameter is greatly reduced due to the viscous drag at, and near, the wall. The effect of viscous drag is to distort the plane wave in an infinite medium to a parabolic velocity distribution in the narrow tube. The magnitude of the attenuation effect may be calculated with the aid of the Helmholtz equation[7]

$$a' = a \Big/ \frac{1}{\left(1+\frac{2}{r}\left(\frac{\eta}{2\rho\omega}\right)^{\frac{1}{2}}\right)^{\frac{1}{2}}}, \qquad (1)$$

where a' = velocity (ft./sec.) of wave propagation corrected for drag at the walls of the tube, a = measured velocity (ft./sec.) of wave propagation in a tube of radius r, r = internal radius (ft.) of the tube, η = absolute viscosity of the oil at test conditions—lb. sec./ft.^{2}, ρ = mass density of the oil at test conditions—lb. sec.^{2}/ft.^{4}, ω = frequency—cycles/sec., $\omega = 2\pi a/2L$, and L = length of tube—ft. The application of Eq. (1) to the test results requires a knowledge of the change of the mass density of the oil and the absolute viscosity with pressure and temperature.

The change in density with temperature is readily obtained from the equation:

$$\text{sp.gr.}_t = \text{sp.gr.}_{60°\text{F}} - K(t°\text{F} - 60°\text{F}), \qquad (2)$$

where "K" varies with the type of stock. An average value of $K = 0.000397$ was used in the present tests, then

$$\text{sp.gr.}_t = \text{sp.gr.}_{60°\text{F}} - 0.000397(t°\text{F} - 60°\text{F}). \quad (2a)$$

The change in mass density for the range of pressures considered is negligible. As an example

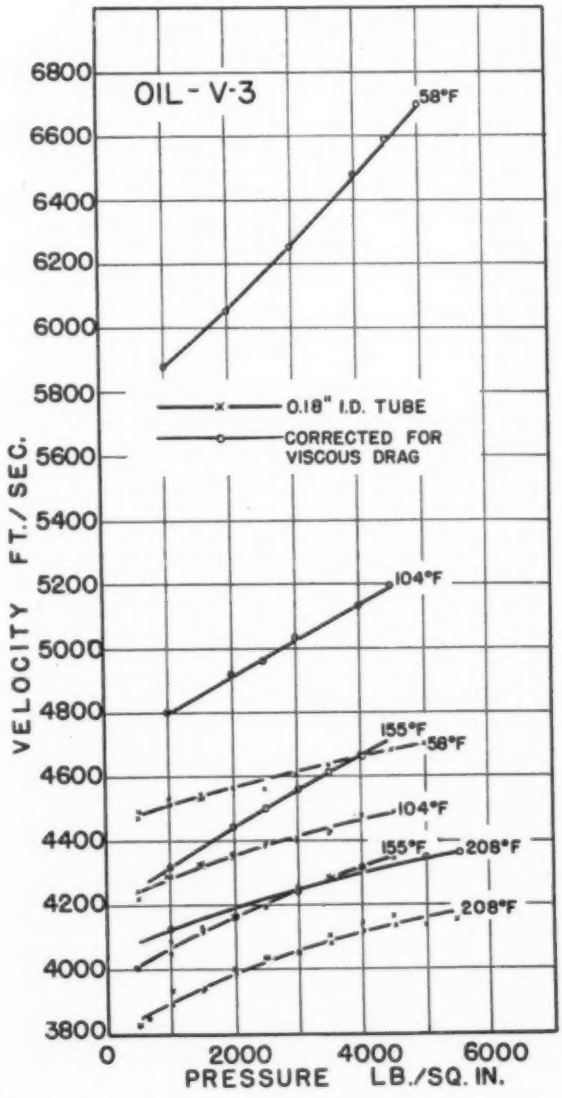

FIG. 6. Velocity of compressional waves in the oil as a function of pressure and temperature.

[7] I. B. Crandall, *Theory of Vibrating Systems and Sound* (D. Van Nostrand Co., 1927).

the correction factor[8] for an oil at a temperature of 212°F and a pressure of 6000 lb./sq.in. is 0.964. The mass density of oil *V*-11 at 60°F is 1.678 lb. sec.^{2}/ft.^{4}, and at 212°F and 6000 lb./sq.in. is 1.618. Where the effect of temperature alone is considered the mass density at 212°F is 1.561 or 3.5 percent less than when both pressure and temperature are considered. Since only the fourth root of this error enters the equation for the modified velocity, the pressure effect can be neglected.

The viscosity of the oil increases exponentially with pressure[9–12] according to the relation

$$\eta_P = \eta_0 e^{\alpha P},$$

where: η_P = absolute viscosity at pressure P—centipoises, η_0 = absolute viscosity at atmospheric

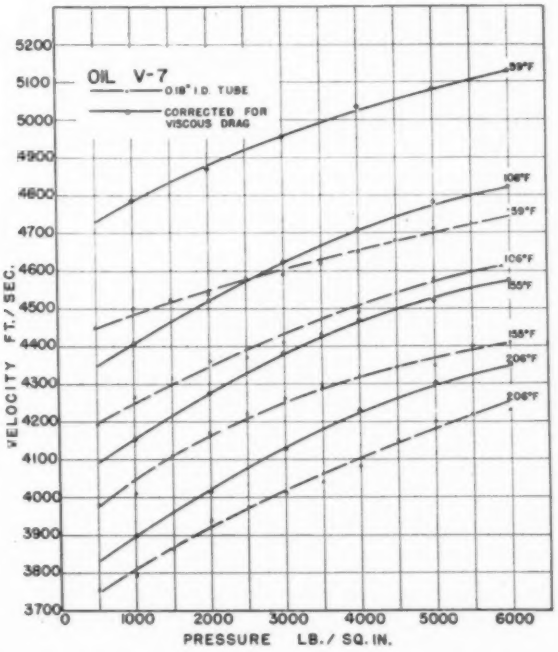

FIG. 7. Velocity of compressional waves in the oil as a function of pressure and temperature.

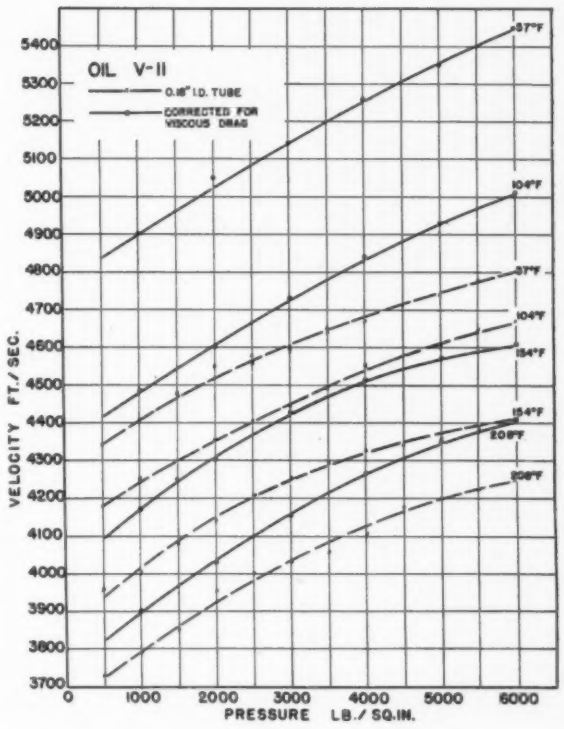

FIG. 8. Velocity of compressional waves in the oil as a function of pressure and temperature.

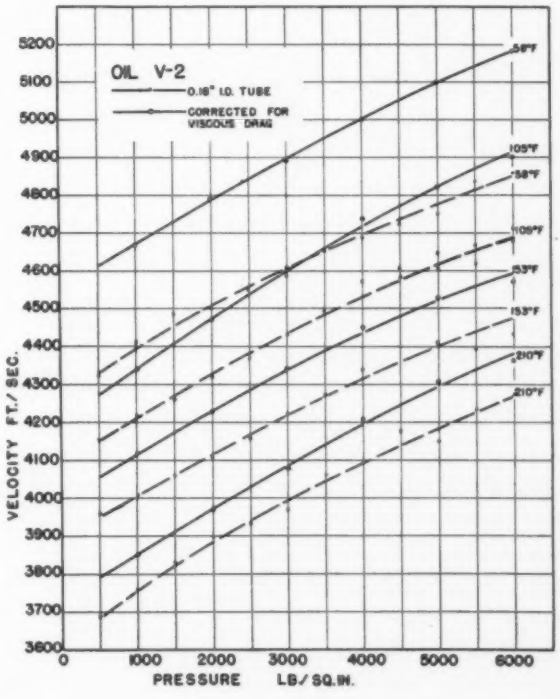

FIG. 9. Velocity of compressional waves in the oil as a function of pressure and temperature.

[8] R. Matteson, "Compressibility and velocity of pressure waves in petroleum oils," J. App. Phys. **9**, 44–49 (1938).
[9] S. Kiesskalt, "Untersuchungen über den Einfluss des Druckes auf die Zähigkeit von Oelen und seine Bedeutung für die Schmiertechnik," Forschungsarbeiten No. 291 (1927).
[10] Y. Suge, "Viscosity of oil under pressure" (in Japanese), Sci. Pap. Inst. Phys. Chem. Research (Tokyo), **11**, 877–894 (1932); **12**, 643–662 (1933).
[11] A. C. Talbott, "Velocity of pressure waves in oil under pressure," Phil. Mag. **19**, 1126–1141 (1935).
[12] J. H. Hyde, "On the viscosities and compressibilities of liquids at high pressures," Proc. Roy. Soc. **A97**, 240–249 (1920).

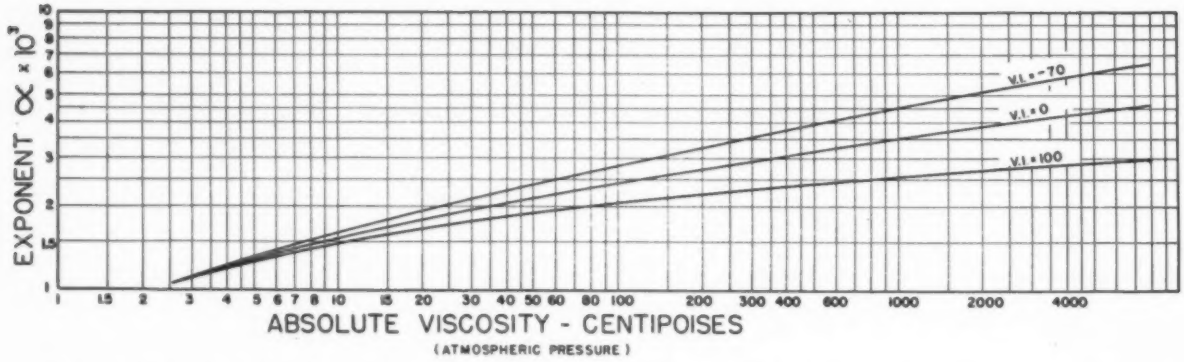
EXPONENT α x 10³
V.I. = -70
V.I. = 0
V.I. = 100
1 1.5 2 3 4 5 6 7 8 10 15 20 30 40 50 60 80 100 200 300 400 600 1000 2000 4000
ABSOLUTE VISCOSITY - CENTIPOISES
(ATMOSPHERIC PRESSURE)

FIG. 10. The relation between the exponent "α" and the viscosity of the oil at atmospheric pressure and operating temperature. $\eta_P = \eta_0 \times e^{\alpha P}$, η_0 = viscosity at atmospheric pressure-centipoises, η_P = viscosity at pressure "P"-centipoises, P = pressure-atmospheres.

pressure—centipoises, e = base of Napierian logarithms = 2.718, α = a constant for a particular oil, and P = pressure-atmospheres.

Equation (2) was applied to the viscosities obtained from the literature and plotted in Fig. 10. The analyses of the available data showed that the exponent "α" is also dependent upon the chemical type of the oil, which may be indicated by the viscosity index. By taking this factor into consideration the three curves (Fig. 10) were obtained, which were used to determine the viscosity of the oils tested at the various pressures.

Experimenters[7] do not fully agree on the validity and limitations of the Helmholtz relation (Eq. 1); however, the velocities corrected for viscous drag and plotted in Figs. 5 to 9 when extrapolated to atmospheric pressure give results which are in good agreement with those in Fig. 1, with the one exception of oil *V*-3 at a temperature of 58°F. The viscosity of oil *V*-3 at 104°F and atmospheric pressure is 74.6 centipoises, while at 58°F and atmospheric pressure it is 530 centipoises. Since the discrepancy in the results is quite abrupt between these two viscosities it is reasonable to assume, until the value is definitely fixed, that the Helmholtz relation is not valid when the term $(\eta/2\rho\omega)^{\frac{1}{2}}$ is greater than 1.5×10^{-3}. This value may be reduced by increasing the value "ω" with a reduction in line length.

The effect of tube wall expansion may further reduce the velocity of wave propagation. The thickness of the walls of the tube used in the experimental investigation was 0.0662 inch which may be considered as relatively rigid in comparison to the bore.[8] Calculations showed that the error involved in the corrected velocity was, in the extreme case, less than 1 percent when tube expansion was neglected.

Summary and conclusions

1. Velocities of compressional waves in 37 petroleum fractions were measured at 100°F and atmospheric pressure. The oils investigated included stocks ranging from light gas oils to highly viscous lubricating and residual oils. The types of stocks used in the investigation ranged from −155 to 100+ viscosity index.

2. Curves are shown from which it is possible to estimate the velocity of compressional waves in petroleum fractions (infinite in extent) at 100°F and atmospheric pressure. The only properties of the stocks that must be known are the A.P.I., or specific, gravity, and the kinematic viscosity at 100°F.

3. Velocity-temperature curves for a number of pure hydrocarbons at atmospheric pressure are shown to illustrate how velocity in pure hydrocarbons varies with chemical composition. These curves apply to a medium infinite in extent.

4. Five of the above-mentioned petroleum fractions were subjected to tests in a seamless steel tube approximately 25 feet long and having an internal diameter of 0.180 inch. Wave velocities in the oils confined in the tube were measured at four temperatures ranging from 57° to 210°F and pressures from 500 to 6000 pounds per square inch.

5. The results of the tests indicate that the velocity of propagation of compressional waves, obtained quite readily at atmospheric pressures, can be reduced to the conditions found in Diesel engine fuel lines by the use of the Helmholtz relation if its limitations are observed. The velocities encountered in the average injection system may vary as much as 25 percent for the normal range of operating conditions and oils used today. When the effects of such disturbances on injection timing are considered it is evident that the result might be the difference between satisfactory and unsatisfactory engine operation. These phenomena are by no means inherent only in the Diesel injection system but are also important in any system in which a liquid is subjected to periodic disturbances.

Acknowledgment

The authors are indebted to Dr. H. R. Wakeham of the Research and Development Department, Standard Oil Company of California, for the interferometer measurements at atmospheric pressures, to Messrs. B. Eastin and C. W. Smith, graduate students at the University of California for the test data at high pressure, and to Mr. F. Ryder for assistance in the design and construction of the amplifiers. It is a pleasure to acknowledge the interest and advice given by Professor L. M. K. Boelter in the analysis of the test data. The writers also wish to express their gratitude to Mr. R. A. Halloran, Manager of the Research and Development Department, Standard Oil Company of California, for permission to use the data obtained at atmospheric pressure.

Electric Oscillations and Surges in Subdivided Windings

REINHOLD RÜDENBERG
Graduate School of Engineering, Harvard University, Cambridge, Massachusetts
(Received May 31, 1940)

1. INTRODUCTION

UNIFORM windings of coils, transformers and electric machines perform differently from smooth lines with respect to traveling waves. The front of impinging steep surges is flattened by the effect of the internal capacitance of the winding and only this flattened part can propagate deep into the winding. The remainder of the incident wave is reflected within the terminal elements back to the incoming line.

Actual windings, however, are always built up of many distinct elements. This is shown in Fig. 1 for a transformer. Here several turns form a layer, several layers form a coil, and a number of coils form the entire winding. As Fig. 2 shows, a corresponding scheme holds for machine windings as well.

Thus there appear two problems with actual windings: first, to consider the effect of a finite number of elements belonging to one group[1,2] as for example, six coils forming the whole winding, or 20 layers forming a complete coil, or 12 turns forming one layer; second, to extend the analysis to the consideration of waves passing from one group to another one with different elements, such as from turns to layers, or from layers to coils.

2. OSCILLATIONS IN A FINITE NUMBER OF ELEMENTS

Denote by e_n and i_n the mean voltage and the mean current in the nth element of a group, by l and c the average self-inductance and ground capacitance per unit length of the wire, and by k the internal capacitance per unit length between any two adjacent elements. Note that l and c

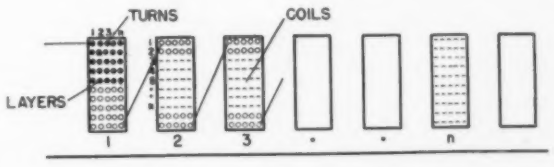

FIG. 1. Transformer winding subdivided into lumped coils, layers and turns.

[1] K. W. Wagner, "Wanderwellen-Schwingungen in Transformatorenwicklungen," Archiv Elektrotech. 6, 301 (1918).
[2] P. L. Bellaschi and A. J. Palermo, "Analysis of transient voltages in networks." A. I. E. E. Tech. Paper 40–5, presented at the Winter Convention, New York, 1940.

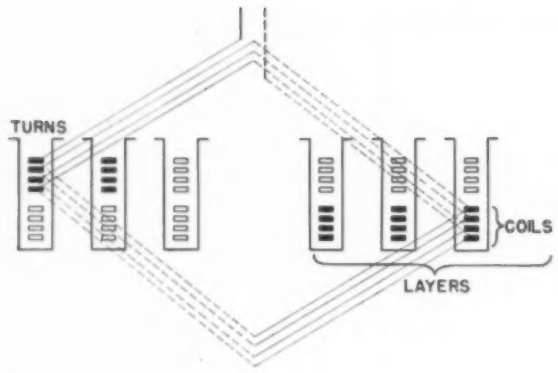

FIG. 2. Machine winding subdivided into lumped layers, coils and turns.

have to be taken as the contribution of each element of length w to the total self-inductance and capacitance of the winding. Then the differential equations for such windings are, as shown in a previous paper,[3]

$$\begin{aligned} -\Delta i_n &= cw\frac{\partial e_n}{\partial t} - kw\frac{\partial \Delta^2 e_n}{\partial t}, \\ -\Delta e_n &= lw\partial i_n/\partial t, \end{aligned} \tag{1}$$

where t is the time, Δ denotes the difference of current or voltage within two adjacent elements, and

$$\Delta^2 e_n = e_{n+1} - 2e_n + e_{n-1} \tag{2}$$

is the second difference between three consecutive elements. The method of solution of these difference-differential equations corresponds in principle to that of chain-filter circuits, though other aspects of the solution are interesting in this paper.

By differentiating the first Eq. (1) with respect to t and by forming the second space difference of the second Eq. (1), we can eliminate the current i and thus obtain for the voltage e_n of the nth element

$$\frac{\Delta^2 e_n}{w^2} - lc\frac{\partial^2 e_n}{\partial t^2} + lk\frac{\partial^2}{\partial t^2}(\Delta^2 e_n) = 0. \tag{3}$$

This is valid for any finite number of winding elements of the same kind.

[3] R. Rüdenberg, "Performance of Travelling Waves in Coils and Windings," A. I. E. E. Tech. Paper 40–102, presented at the Summer Convention, Swampscott, Mass., June, 1940.

We solve this equation first for standing harmonic oscillations with the amplitude E by

$$e_n = E\cdot\epsilon^{j\omega t}\cdot\epsilon^{j\alpha nw}, \tag{4}$$

where ω is the frequency and α the wave density in space. Instead of a continuous coordinate x along the wire, we have introduced within the last term

$$nw = n\cdot\Delta x, \tag{5}$$

which increases in finite steps, if n is an integer denoting the number of the element considered. For a winding consisting of six coils, for example, n increases from 1 to 6.

According to the definition of Eq. (2), the second difference of the coil voltage e_n is

$$\begin{aligned} \Delta^2 e_n &= (\epsilon^{j\alpha w(n+1)} - 2\epsilon^{j\alpha wn} + \epsilon^{j\alpha w(n-1)})E\epsilon^{j\omega t} \\ &= (\epsilon^{j\alpha w} - 2 + \epsilon^{-j\alpha w})e_n = (\epsilon^{j\alpha w/2} - \epsilon^{-j\alpha w/2})^2 e_n \\ &= -4e_n \sin^2(\alpha w/2). \end{aligned} \tag{6}$$

By introducing this expression into Eq. (3) and differentiating, we obtain the characteristic equation

$$-\frac{4}{w^2}\sin^2\left(\alpha\frac{w}{2}\right) + lc\omega^2 + lk\omega^2 4\sin^2\left(\alpha\frac{w}{2}\right) = 0. \tag{7}$$

If we compare the formation of a difference with the differentiation of a harmonic function, we thus obtain, as multiplier, instead of the wave density α, the somewhat more complicated function

$$\frac{2}{w}\sin\left(\alpha\frac{w}{2}\right).$$

If we change over from the solution (4) for standing waves to that for traveling waves,

$$e_n = E\epsilon^{j\omega(t - z/v)}, \tag{8}$$

we see that the velocity of propagation v along the wire is given simply by

$$v = -\omega/\alpha, \tag{9}$$

which can be computed after solving Eq. (7).

For wave density α and for the frequency ω,

we obtain the solutions of Eq. (7), namely

$$\frac{2}{w}\sin\left(\alpha\frac{w}{2}\right)=\left(\frac{cl\omega^2}{1-kl\omega^2w^2}\right)^{\frac{1}{2}},$$
$$\omega=\frac{(2/w)\sin(\alpha w/2)}{(cl+kl4\sin^2(\alpha w/2))^{\frac{1}{2}}}, \tag{10}$$

which are transcendental in α but nevertheless easy to compute numerically. For increasing ω, α at first increases proportionally. However, since the sine cannot exceed the value 1, the square root of the first Eq. (10) has, with further increasing ω, a definite limit long before its denominator becomes zero. Our solution (4) is valid only up to this definite limit, the frequency at this limit forming a critical frequency ν. Its value is, according to the second Eq. (10), the sine now being 1,

$$\nu=\frac{2/w}{(cl+4kl)^{\frac{1}{2}}}=\frac{1}{w(kl+\frac{1}{4}cl)^{\frac{1}{2}}}. \tag{11}$$

The critical frequency of a finite number of elements is thus determined by the sum of the internal capacitance k and $\frac{1}{4}$ of the ground capacitance c, and is therefore smaller than for an infinite number of elements, where the fraction $c/4$ does not exist.

Even if there is no internal capacitance, there remains a definite critical frequency, namely

$$\text{for } k=0: \qquad \nu_0=2/w(cl)^{\frac{1}{2}}, \tag{12}$$

which is due solely to the lumped arrangement of the winding elements of length w. If, on the other hand, the internal capacitance k is overwhelming, we obtain the extreme value

$$\text{for } k=\infty: \qquad \nu_\infty=1/w(kl)^{\frac{1}{2}}, \tag{13}$$

which coincides with the value for uniform coils. For machine windings with small k the critical frequency is in the neighborhood of ν_0; for transformer windings with large k it approaches ν_∞. The actual critical frequency is given by

$$\nu^2=\frac{1}{1/\nu_0^2+1/\nu_\infty^2} \tag{14}$$

and is always smaller than either ν_0 or ν_∞.

The wave density α_ν in the critical state of the winding follows from

$$\sin\left(\alpha\frac{w}{2}\right)=1 \quad \text{as} \quad \alpha_\nu=\frac{\pi}{w}, \tag{15}$$

and therefore the wave-length becomes, as reciprocal of the density,

$$\lambda_\nu=2\pi/\alpha_\nu=2w. \tag{16}$$

This means that every element having the length w oscillates against its two adjacent elements, forming a half-wave-length of this resonance state, represented by Fig. 3. A finite number of coils, layers or turns thus prevents the wave-length of harmonic oscillations from decreasing towards zero as it would do with infinite subdivision.

The natural frequencies of a winding with open or closed ends are given by the number m of full waves over the total wire length a, so that the wave density becomes

$$\alpha=2\pi/\lambda=2\pi m/a. \tag{17}$$

Inserting this in the second Eq. (10), we derive

$$\omega=\frac{2}{w(cl)^{\frac{1}{2}}}\cdot\frac{1}{\left(\frac{k}{4c}+1/\sin^2\left(\pi\frac{m}{a}w\right)\right)^{\frac{1}{2}}}. \tag{18}$$

If in this equation we increase the number m from its fundamental value $\frac{1}{4}$ to integer multiples of this value, we obtain the entire series of natural frequencies. However, we cannot increase m beyond the value

$$m_\nu=m/2w, \tag{19}$$

because otherwise the argument of the sine in Eq. (18) would exceed $\pi/2$. The number of

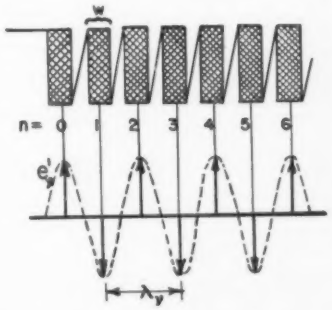

FIG. 3. Critical oscillations of a finite number of lumped elements in a winding.

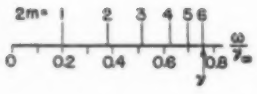

FIG. 4. Spectrum of natural frequencies of a winding consisting of lumped elements.

natural frequencies of every group of elements is therefore limited and, since a/w is identical with the number of elements, we see that there develops only a finite number of natural frequencies equal to twice the number of elements in every group.[1]

A winding, for example, with both ends open, consisting of $a/w=6$ coils, has only six different natural frequencies, the lowest one being given by $m=\frac{1}{2}$, the highest by $m=6/2$, according to Eq. (19). If one end of the winding is grounded, the lowest natural frequency corresponds to $m=\frac{1}{4}$, the highest to $m=11/4$, the number of frequencies remaining 6. Both groups together thus form 12 possible natural frequencies. All higher frequencies of the two groups are cut off by the effect of the lumped elements and the spectrum of frequencies is limited as in Fig. 4. The highest natural frequency of each group either coincides with or is adjacent to the critical frequency, as we see by comparison of Eqs. (18) and (11).

The fundamental frequency is given by $m=\frac{1}{4}$ or $\frac{1}{2}$, and if the number of elements a/w is not too small, the argument of the sine in Eq. (18) for this lowest frequency is a small fraction of $\pi/2$, and can thus be taken instead of the sine itself. In this example there is no substantial difference between the rigorous calculation and the formula for uniform windings.

The wave velocity can be computed by inserting α from Eq. (9) in the first Eq. (10). We obtain

$$\sin\left(\frac{\omega w}{2v}\right)=\frac{\omega w}{2}\frac{1}{\left(\frac{1}{cl}-\frac{k}{c}\omega^2w^2\right)^{\frac{1}{2}}}=\frac{\omega w}{2v_\infty}, \tag{20}$$

where we have supplemented on the right-hand side a term containing the velocity v_∞ for infinite subdivision. For low frequencies ω, the velocity simplifies in any case to

$$v_0=1/(lc)^{\frac{1}{2}}. \tag{21}$$

For larger frequencies, we realize that in addition to the decrease due to internal capacitance, the velocity of propagation is always diminished by the effect of lumped elements. Its variation is represented by Fig. 5. At the critical frequency the argument of the sine in Eq. (20) becomes $\pi/2$ and thus the limiting velocity is

$$v_r=\frac{vw}{\pi}=\frac{2/\pi}{(cl+4kl)^{\frac{1}{2}}}. \tag{22}$$

The critical velocity of waves remains therefore at a finite value which, using the limiting value v_0

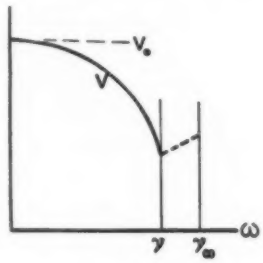

FIG. 5. Change of wave velocity v with frequency, in windings with lumped elements.

for low frequencies, is

$$\text{for } k\leqq c: \quad v_r=2v_0/\pi,$$
$$\text{for } k\geqq c: \quad v_r=\frac{v_0}{\pi}\left(\frac{c}{k}\right)^{\frac{1}{2}}. \tag{23}$$

This remaining velocity corresponds to the fact that in the critical state there are well-formed waves on the winding.

The terminal current of the winding, containing the wire current as well as the internal capacitance current, is determined in a previous article[3] as

$$i_0=cw\sum\frac{\partial e_n}{\partial t}. \tag{24}$$

For a finite number of elements summation is the inverse operation of formation of the difference. This puts a sine expression into the denominator and so we obtain from the voltage in Eq. (4)

$$i_0=\frac{c}{\frac{2}{w}\sin\left(\alpha\frac{w}{2}\right)}E\epsilon^{j\omega t}\epsilon^{jan\omega}, \tag{25}$$

which is valid only for $n=0$. With this the surge impedance becomes, using Eq. (4),

$$Z=\frac{e_0}{i_0}=\frac{2}{w}\frac{\sin(\alpha w/2)}{c\omega}=\left(\frac{l/c}{1-kl\omega^2w^2}\right)^{\frac{1}{2}}$$
$$=\frac{Z_0}{(1-(\omega/v_\infty)^2)^{\frac{1}{2}}}. \tag{26}$$

We have inserted here the first Eq. (10) and see that the surge impedance is independent of the subdivision and increases hyperbolically with ω from an initial value Z_0 which is identical with the surge impedance commonly used. The variation is shown in Fig. 6.

3. Supercritical Phenomena in Subdivided Windings

If the frequency ω exceeds the critical frequency ν, the determining sine in Eq. (10) becomes larger than 1. This is possible only for a complex argument of the sine and we extend this therefore to $\alpha+j\delta$. We can then develop the sine into

$$\sin(\alpha+j\delta)\frac{w}{2}=\sin\left(\alpha\frac{w}{2}\right)\cdot\cosh\left(\delta\frac{w}{2}\right)+j\cos\left(\alpha\frac{w}{2}\right)\cdot\sinh\left(\delta\frac{w}{2}\right). \quad (27)$$

The real part of this is determined by the square root in the first Eq. (10), while the imaginary part must vanish. As δ certainly remains finite, this second condition gives

$$\cos(\alpha w/2)=0 \quad \text{or} \quad \alpha w=\pi. \quad (28)$$

The sine in the first term of the right-hand side of Eq. (27) is therefore equal to 1 and thus there remains the condition

$$\cosh\left(\delta\frac{w}{2}\right)=\frac{w}{2}\left(\frac{c l\omega^2}{1-k l\omega^2 w^2}\right)^{\frac{1}{2}} \quad (29)$$

from which δ can be computed. Every value between 1 and ∞ for the expression on the right-hand side of Eq. (29) gives a definite value of δ. The corresponding variation of ω is from $\omega=\nu$, according to Eq. (11), to $\omega=\nu_\infty$, according to Eq. (13).

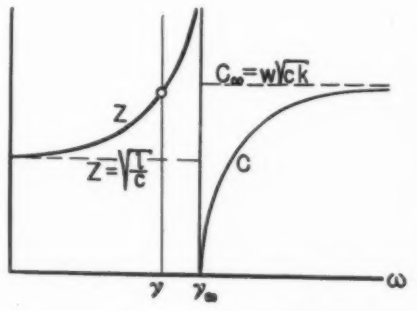

Fig. 6. Change of surge impedance Z and terminal capacitance C with frequency, in windings with lumped elements.

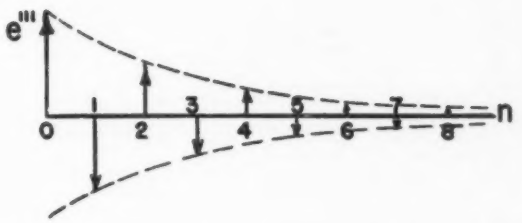

Fig. 7. Standing oscillations in a winding with lumped elements, for the intercritical range of frequencies.

By the complex argument in Eq. (27) the shape of the harmonic wave within the winding, as given by Eq. (4), is altered. We now obtain for the spatial factor, if we use for α the expression (28),

$$\epsilon^{j(\alpha+j\delta)n w}=\epsilon^{jn\pi}\cdot\epsilon^{-\delta n w}, \quad (30)$$

and since the first term on the right-hand side for various integers n is alternately $+1$ and -1 the voltage distribution becomes

$$e_n'''=E\epsilon^{j\omega t}\cdot(-1)^n\cdot\epsilon^{-\delta n w}. \quad (31)$$

This distribution is represented in Fig. 7 and consists of a standing attenuated alternating voltage along the elements of the winding. For the critical frequency ν, the damping factor δ is zero, according to Eq. (29), and the distribution then coincides with that of Fig. 3. For higher frequencies, δ increases and for the frequency ν_∞, becomes infinite, so that only the first coil takes up any voltage. As the voltages of adjacent coils are of opposite sign to each other, the winding is in a kind of resonance at frequencies between ν and ν_∞, and an excitation by any frequency ω within this range appears particularly dangerous.

The ratio of terminal voltage to current within this range, ν and ν_∞, always remains real and still follows Eq. (26). The surge impedance within this range, however, is large and rapidly approaches infinity, according to Fig. 6, indicating an actual state of resonance.

We may conceive of the standing alternating distribution in Fig. 7 as produced by traveling waves, although this conception would not be useful here. The velocity of the necessary pair

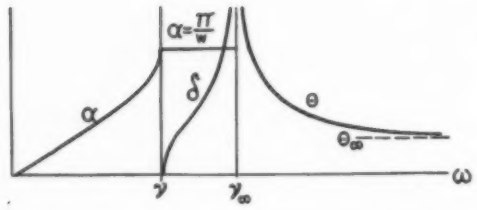

FIG. 8. Wave density α and attenuations δ and θ for subcritical, intercritical and supercritical frequencies.

of exponentially decreasing or increasing traveling waves would then be given by Eqs. (9) and (28) as

$$v=\omega w/\pi, \tag{32}$$

which is represented as a dotted line in Fig. 5 and closely joins the end of the previous curve for v, as seen by Eq. (22).

For exciting frequencies exceeding ν_∞, the square root in the first Eq. (10) becomes imaginary. Thus the argument of the sine is also imaginary, and we now write $j\theta$ instead of α. By expressing

$$\sin\left(j\theta\frac{w}{2}\right)=j\sinh\left(\theta\frac{w}{2}\right), \tag{33}$$

our characteristic equation appears in the real form

$$\sinh\left(\theta\frac{w}{2}\right)=\frac{w}{2}\left(\frac{cl\omega^2}{kl\omega^2w^2-1}\right)^{\frac{1}{2}}. \tag{34}$$

The voltage distribution of Eq. (4) now changes to

$$e_n''=E\cdot\epsilon^{j\omega t}\cdot\epsilon^{-\theta nw}, \tag{35}$$

which represents a uniformly attenuated standing voltage distribution. The space constant of this exponential curve is given by the inverse value of θ. For every value of ω between ν_∞ and ∞ the square root of Eq. (34) has a real value, decreasing from ∞, and therefore θ can always be computed numerically.

For the frequency ν_∞ at the lower limit of the range, the value of θ becomes ∞ and therefore the space constant X is zero. For higher frequencies, the right-hand side of Eq. (34) rapidly approaches an asymptotic value, the space constant of which is given by

$$\sinh\left(\frac{w}{2X_\infty}\right)=\frac{1}{2}\left(\frac{c}{k}\right)^{\frac{1}{2}}. \tag{36}$$

For overwhelming internal capacitance k this value (36) is very small and therefore the space constant becomes, to a good approximation,

$$X_\infty=w(k/c)^{\frac{1}{2}}, \tag{37}$$

coinciding with the expression for uniform windings. For small k/c, we may develop the sine of Eq. (36) into an exponential function and derive in approximation

$$X_\infty=\frac{w}{2\log_\epsilon(c/k)^{\frac{1}{2}}}. \tag{38}$$

Thus the space constant still decreases with k, but more slowly than in a continuous winding.

Our formulation (26) for the ratio of terminal voltage and current remains valid even for frequencies above ν_∞, because the transcendental function has disappeared. However, the square root becomes imaginary for this upper range of frequencies and therefore the winding acts under this condition as pure capacitance. We therefore invert Eq. (26), giving

$$\frac{i_0}{e_0}=j\omega w\left(ck\left[1-\left(\frac{\nu_\infty}{\omega}\right)^2\right]\right)^{\frac{1}{2}}=j\omega C, \tag{39}$$

which agrees completely with the expression for uniform windings. Neither the surge impedance for subcritical frequencies nor the apparent capacitance for supercritical frequencies is altered by the subdivision of the winding into elements. The capacitance approaches rapidly a maximum value shown in Fig. 6, which expresses quite generally the terminal capacitance at the higher frequencies for every kind of winding.

If we survey the whole range of frequencies between 0 and ∞, we see that there are now two different critical frequencies, namely ν and ν_∞, which determine the behavior of the winding. We may transform the characteristic Eqs. (10),

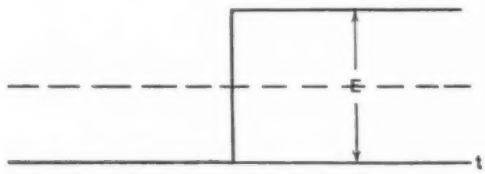

FIG. 9. Rectangular wave front impinging on a winding.

(29) and (34) into the unified relation

$$\sin\left(\alpha\frac{w}{2}\right)=\cosh\left(\delta\frac{w}{2}\right)=j\sinh\left(\theta\frac{w}{2}\right)=\frac{\omega/\nu_0}{(1-(\omega/\nu_\infty)^2)^{\frac{1}{2}}},\quad(40)$$

where the right-hand side is condensed by introducing the two critical frequencies ν_0 and ν_∞ from Eqs. (12) and (13), the former being critical only for subdivided windings without internal capacitance; the latter being critical in the general case. Figure 8 then shows the variation with frequency of the wave density α and of the attenuations δ and θ. The first term of Eq. (40) is valid so long as the value of its right-hand side is less than 1. This is the subcritical range, the waves of which penetrate into the winding and travel undistorted over its extension. The second term is valid for values of the right-hand side greater than 1 but still finite. This occurs for frequencies between ν and ν_∞, these two critical values separating the whole region of frequency into three parts. The waves in this middle range do not travel through the winding; they form rather an alternating standing distribution over the end turns or end coils which is spatially the more attenuated the higher the frequency. The third term in Eq. (40) refers to supercritical frequencies higher than ν_∞ which render the right-hand side imaginary. In this range, too, no oscillation can penetrate through the winding.

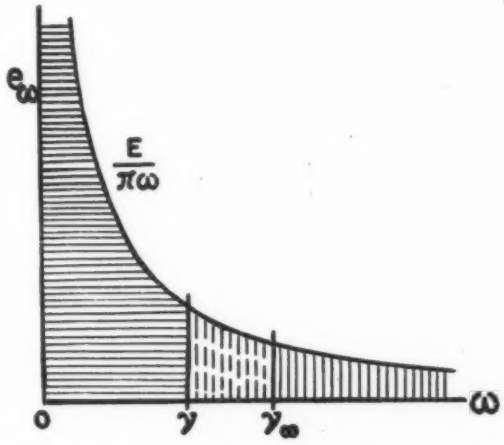

FIG. 10. Three frequency regions in the spectral distribution of harmonic amplitudes of a rectangular front wave.

It forms a spatially attenuated standing voltage distribution which is, however, now uniformly decreasing along the terminal elements. This nonalternating distribution results from the internal capacitance, while the former alternating distribution is due to the finite subdivision of the winding into distinctive elements.

4. Flattening of Traveling Waves

If an incident wave consists of a sudden rectangular jump, as in Fig. 9, the voltage can

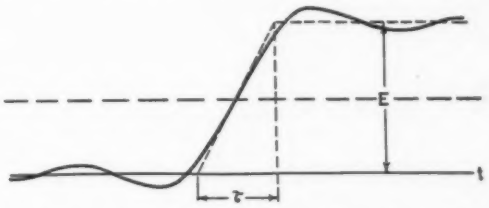

FIG. 11. Subcritical wave front with finite time τ of ascent.

be represented by the Fourier integral

$$e=\frac{E}{2}+\frac{E}{\pi}\int_0^\infty\frac{\sin\omega t}{\omega}d\omega,\quad(41)$$

the spectral distribution of which is given by Fig. 10. Since the reaction of the winding is different for the three regions of frequency indicated in Fig. 10, we split the integral into three parts

$$\int_0^\infty\frac{\sin\omega t}{\omega}d\omega=\int_0^\nu\frac{\sin\omega t}{\omega}d\omega+\int_\nu^{\nu_\infty}\frac{\sin\omega t}{\omega}d\omega+\int_{\nu_\infty}^\infty\frac{\sin\omega t}{\omega}d\omega.\quad(42)$$

Only the voltage formed by subcritical waves and thus corresponding to the first integral can penetrate undisturbed through the winding.[3] This "sine-integral" function

$$Si(\nu t)=\int_0^\nu\frac{\sin\omega t}{\omega}d\omega\quad(43)$$

is shown graphically[4] in Fig. 11, depending on time, and represents physically a traveling wave with a flat front.

[4] E. Jahnke and F. Emde, *Tables of Functions with Formulae and Curves* (Leipzig and Berlin, 3rd ed., 1938), p. 78.

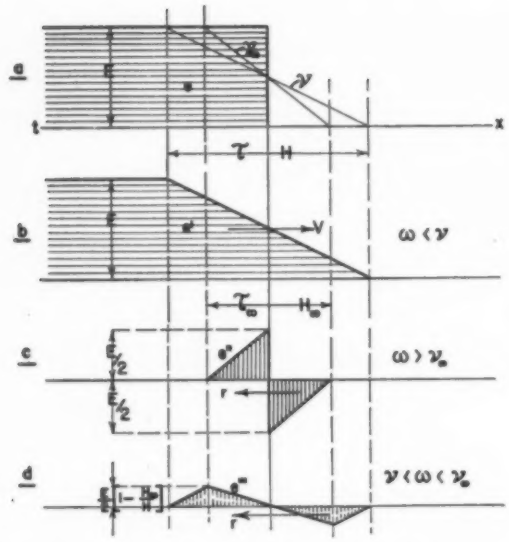

FIG. 12. Subdivision of a rectangular front wave into a subcritical, a supercritical, and an intercritical part, in a simplified form.

The sine-integral, which actually forms a gradual ascent with some oscillations on either side, can be represented in a simplified form by the broken straight lines which are dotted in Fig. 11. The time of ascent is fixed by the upper limit of the integral and is

$$\tau=\pi/\nu=\pi w(kl+\tfrac{1}{4}cl)^{\frac{1}{2}}, \qquad (44)$$

thus being determined wholly by the critical frequency.

The voltages corresponding to the second and third integral on the right-hand side of Eq. (42) can be similarly represented graphically, either by the rigorous curve or by approximate straight lines. So we see that the three regions of the spectral distribution of Fig. 10 produce three voltage distributions which perform differently within the winding. Figure 12 shows the incident impact in space, split into these three components: first, the subcritical part e' with frequencies below ν, forming a flat-fronted traveling wave throughout the winding, as in Fig. 12b; second, the supercritical part e'' with frequencies above ν_∞, containing the incident discontinuous jump, and some adjacent steep parts of the wave, cut from the original front, as in Fig. 12c. This part, consisting of rapid oscillations only, will be reflected upon the incident line, exciting uniformly attenuated voltages in the terminal elements of the winding. Finally, a third or intercritical part is formed of the frequencies between ν and ν_∞, corresponding to the middle integral on the right-hand side of Eq. (42) and forming the remainder of the three former shapes of voltage. This last part, shown in Fig. 12d, is also reflected to the line, exciting alternate voltages within the terminal elements of the winding.

If we use the rigorous sine-integral and exponential curves in time and space, rather than the approximate straight lines of Fig. 12, and superpose all voltage components, we obtain the complete wave shapes of Fig. 13 along the winding for several consecutive times following the arrival of the jump wave. There appears instantaneously an attenuated voltage distribution over the terminal elements and from this there emerges, first slowly and then progressively faster, the smooth traveling wave with its oscillating forerunners.[5]

Instead of expressing the ascent of the subcritical traveling wave in time by Eq. (44), we may determine the length of its front in space as in Fig. 12b. Since the wave propagates substantially with the velocity v_0 of Eq. (21), its head length is, with use of Eq. (11),

$$H=v_0\tau=\pi\frac{v_0}{\nu}=\pi w\left(\frac{k}{c}+\frac{1}{4}\right)^{\frac{1}{2}}. \qquad (45)$$

Because of the subdivision of the winding, the front of this penetrating wave is lengthened, as the term $\frac{1}{4}$ under the square root disappears for uniform windings.

The length H_∞, giving the slope of the super-

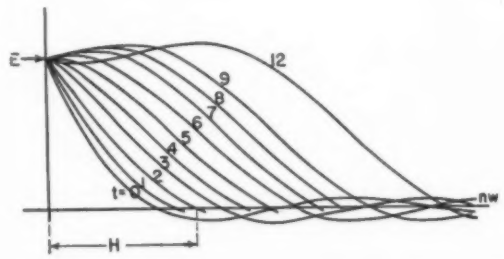

FIG. 13. Change of the voltage along the terminal elements of a winding.

[5] H. Einhorn, "Modellversuche zur Ermittlung der Sprungwellenbeanspruchung von Transformatorenwicklungen," Elektrotech. und Maschinenbau 52, 309 (1934).

critical wave e'' in Fig. 12c, is correspondingly

$$H_\infty = v_0 \tau_\infty = \pi \frac{v_0}{\nu_\infty} = \pi w \left(\frac{k}{c}\right)^{\frac{1}{2}}. \qquad (46)$$

For windings with high internal capacitance k, as in transformers, the difference of the two head lengths is insignificant. Then the intermediate voltage e''' represented in Fig. 12d is very small and only the voltages e' and e'' play a part. However, for small internal capacitance, as in most machine windings, the head length H has a limiting value

$$H_{\min} = \pi w/2 = 1.57 w, \qquad (47)$$

which cannot be lessened in any case. Thus we see that the subdivision of a winding into distinct elements, whether coils or layers or turns, always causes a minimum flattening of rectangular waves which impinge upon its terminals.

5. Straining of the Insulation

The subcritical voltage e' of Fig. 12b proceeds through the entire winding and stresses the internal insulation between adjacent turns, layers or coils by the steepness of its front. The maximum internal stress ϵ' is given by the difference of the voltage over a length w of an element near the center of the front, as shown in Fig. 14. This is expressed by the sine-integral of Eq. (41) and (43) as

$$\epsilon' = \frac{E}{\pi}\left[Si\left(+\frac{\nu t}{2}\right) - Si\left(-\frac{\nu t}{2}\right)\right] = \frac{2}{\pi} ESi\left(\frac{\nu t}{2}\right). \qquad (48)$$

The time interval t corresponding to a wire length w is w/v_0 and therefore the argument in

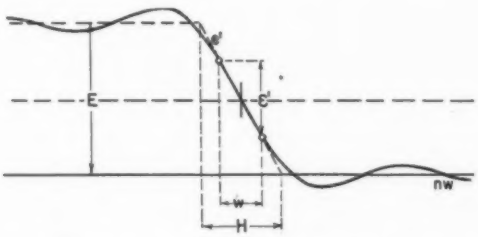

Fig. 14. Voltage to ground e' and internal voltage ϵ' at an interior element.

Eq. (48) becomes, using Eqs. (11) and (21),

$$\frac{\nu t}{2} = \frac{\nu w}{2 v_0} = \frac{1}{(4k/c+1)^{\frac{1}{2}}}. \qquad (49)$$

Thus the maximum internal stress is

$$\epsilon' = \frac{2}{\pi} ESi\left(\frac{1}{(4k/c+1)^{\frac{1}{2}}}\right) \leqq \frac{E/\pi}{(k/c+\frac{1}{4})^{\frac{1}{2}}}. \qquad (50)$$

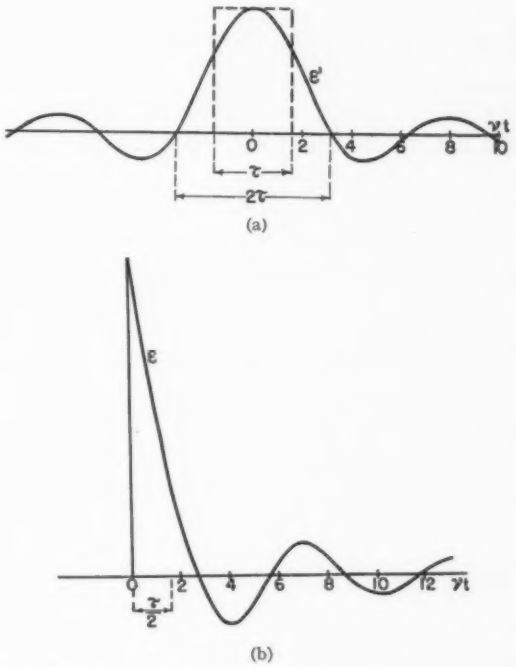

Fig. 15. Change in time of internal stress after arrival of a rectangular wave, (a) over interior elements, (b) over the terminal elements.

On the right-hand side of this equation an approximate value is added, since for small arguments the sine-integral is equal to the argument. Even at the maximum value of the argument which is 1 for $k=0$, the error of this approximation is smaller than 5 percent.

Since w/H is for the most part a relatively small fraction, the internal strain may be computed alternatively by the derivative of the sine-integral, which forms a curve with the shape $\sin(\nu t)/\nu t$, shown in Fig. 15a and giving the entire change of the stress ϵ' against time. As this curve passes through zero for $\nu t' = \pm\pi$, we see that the entire time of exposure of the internal insulation to the excess voltage is

$$t = 2t' = 2\pi/\nu = 2\tau. \qquad (51)$$

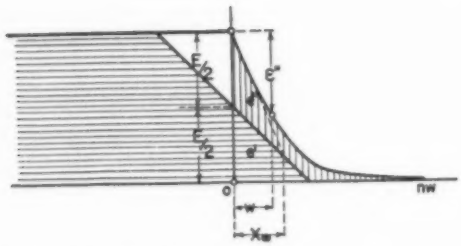

FIG. 16. Additional voltage to ground e'' and internal voltage at a terminal element.

For the most dangerous part of this stress, with a maximum according to Eq. (50), we may take, however, an effective duration of about τ, as indicated in Fig. 15a, which is always a very small fraction of a second.

The terminal elements of the winding are exposed, in addition to this, to the strain of the standing exponential distributions caused by the voltages e'' and e'''. The first one has, according to Fig. 12c, a positive maximum $E/2$ at the moment of incidence of the rectangular wave and decreases into the winding as in Fig. 16, substantially according to the asymptotic space constant X_∞ derived from Eq. (36). This gives over the wire length w a difference of voltage[6]

$$\epsilon''=\frac{E}{2}(1-\epsilon^{-w/X_\infty})=\frac{E}{2}(1-\epsilon^{-2\sinh^{-1}(c/4k)^{\frac{1}{2}}}). \quad (52)$$

If we replace the sinh-function by a logarithm, this value can be expressed algebraically as

$$\epsilon''=E\left(\frac{c}{4k}\right)^{\frac{1}{2}}\left[\left(1+\frac{c}{4k}\right)^{\frac{1}{2}}-\left(\frac{c}{4k}\right)^{\frac{1}{2}}\right] \leqq\frac{E}{2}\left(\frac{c}{k}\right)^{\frac{1}{2}}. \quad (53)$$

On the right-hand side an approximate value is given which is valid, however, only for very large k/c, of the order of 100 and more.

We see from Fig. 12c and d that the duration of the combined positive excess voltages e'' and e''' with simplified triangular shapes is $\tau/2$. The internal insulation is thus exposed to the danger due to the additional terminal stresses $\epsilon=\epsilon'+\epsilon''+\epsilon'''$ only over a period less than $\tau/2$, which is favorable with respect to the time lag of breakdown. Figure 15b shows the change in time, for small w/H, of the internal terminal stress ϵ after arrival of a rectangular wave, as composed of the stress ϵ' of Fig. 15a and the rigorous time variation of the stress ϵ'' corresponding to Fig. 12c.

Many measurements, published in the extended literature on this subject,[7,8] show a change of voltage in time which follows closely the shapes of Fig. 15a and b, for interior as well as terminal turns or coils.

The intermediate voltage e''' produces only very little additional stress at the time of arrival of the incident jump wave since e''' passes through zero just then, as seen in Fig. 12d. The amplitude of this voltage, as given by a simple geometric consideration of the straight-line diagrams in Fig. 12, has the value

$$e'''=\frac{E}{2}\left(1-\frac{H_\infty}{H}\right)=\frac{E}{2}\left(1-\frac{1}{(1+c/4k)^{\frac{1}{2}}}\right). \quad (54)$$

This is for a ratio $k/c=10$ merely 1 percent and even for $k/c=1$ only 10 percent. Since this positive amplitude, according to Fig. 12d, appears at the terminal of the winding somewhat later than the incident jump, namely when the voltage e'' is diminishing towards zero, it is justified to neglect the internal stress ϵ''' for any finite value of k/c.

However, in the extreme case of $k=0$ the two voltages e'' and e''' reverse their roles. Now H_∞ becomes zero according to Eq. (46) and therefore e'' of Fig. 12c vanishes completely. On the other hand, e''' of Fig. 12d expands from both sides and now contains the entire jump in its center, as e'' formerly did. The positive amplitude of e''' in this case is $E/2$, according to Eq. (54). Figure 7 shows that the stress ϵ''' between the terminal coils, due to the intercritical alternating voltage e''', is always given by the sum of adjacent voltages. This yields for $k=0$, using Eq. (54),

$$\epsilon_{max}'''=2e'''=E. \quad (55)$$

This is the highest possible supplementary stress between terminal elements, and is in addition

[6] R. Rüdenberg, "Die Spannungsverteilung an Kettenisolatoren," Elektrotech. Zeits. **35**, 412 (1914).

[7] F. D. Fielder and E. Beck, "Effects of lightning voltages on rotating machines and methods of protecting against them," Trans. A. I. E. E. **49**, 1577 (1930).

[8] R. Elsner, "Zur Theorie des schwingungsfreien Drehstromtransformators," Wissenschaftliche Veröffentlichungen aus den Siemens-Werken **18**, 1 (1939).

to the stress ϵ' from Eq. (50) which is uniformly experienced by all elements, and is nearly $2E/\pi$ for $k=0$.

The total internal voltage between adjacent terminal elements for any k thus is composed of the sum of ϵ' in Eq. (50) and ϵ'' in Eq. (53) or, for $k=0$, ϵ''' in Eqs. (54) and (55). A numerical computation shows that we can combine all these expressions in a form similar to Eq. (50), and so the maximum internal terminal stress becomes, to good approximation,

$$\epsilon=\left(\frac{1}{\pi}+\frac{1}{2}\right)\frac{E}{(k/c+\frac{1}{4})^{\frac{1}{2}}}=\frac{0.818}{(k/c+\frac{1}{4})^{\frac{1}{2}}}E, \quad (56)$$

which is valid for every value of k. The maximum possible stress for $k=0$ has the finite value

$$\epsilon_{max}=2(1/\pi+\tfrac{1}{2})E=1.64E, \quad (57)$$

which never can be surpassed.

If we compare the results of our computations with those obtained for uniform windings, we see that we may take into consideration the effect of the finite subdivision merely by adding $c/4$ to the value of the internal capacitance k, thus obtaining an apparent or effective capacitance

$$k_c=k+c/4. \quad (58)$$

This gives the correct boundary values for $k=0$ and forms a transition to the simpler formulae for large values of k. We see that the use of this effective capacitance k_c is valid for the critical frequency ν in Eq. (11), for the head length H in Eq. (45), and for the voltage stresses ϵ according to Eqs. (50) and (56), but is not valid for surge impedance Z and terminal capacitance C which are, according to Eqs. (26) and (39), independent

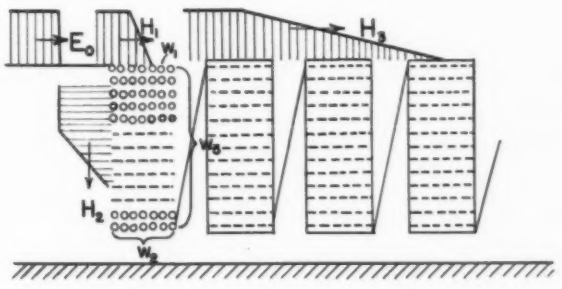

FIG. 17. Threefold consecutive flattening of a steep front wave traveling through turns, layers and coils of a winding.

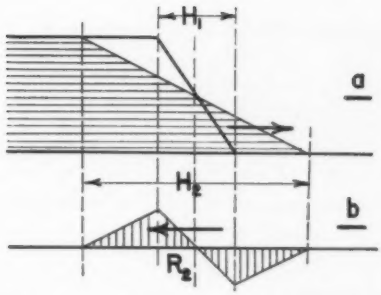

FIG. 18. Transformation of a finite wave front into a flatter one at a transition point.

of the finite subdivision of the winding into lumped elements.

6. Interaction of Coils, Layers and Turns

We will now survey the performance of a complete winding built up of a group of coils, each one consisting of a number of layers, each layer containing many turns. A steep jump wave may arrive at the terminal, as in Fig. 17, and impinge at first upon the turns of the first layer. The layers with the turn length w_1 have a definite, fairly high critical frequency

$$\nu_1=1/w_1(lk_1)^{\frac{1}{2}}, \quad (59)$$

where l is the average self-inductance per unit length of the entire winding and k_1 is the turn capacitance, also per unit length, between every two turns of the layer, including $\frac{1}{4}$ of the ground capacitance as in Eq. (58). As we have seen previously, the steep front of the wave, corresponding to Eq. (43), is converted to a head of the length

$$H_1=\pi v/\nu_1=\pi v w_1(lk_1)^{\frac{1}{2}}=\pi w_1(k_1/c)^{\frac{1}{2}}, \quad (60)$$

which travels over the first layer. Even if the turn capacitance k_1 is only of the order of the average winding capacitance c to ground, the head length comprises several turn lengths on account of the factor π in Eq. (60), and in general the head length is considerably larger.

If this wave front travels from the first to the second and to further layers, as shown in Fig. 17, it cannot retain its relatively short head length, for the layers of a coil have a lower critical frequency

$$\nu_2=1/w_2(lk_2)^{\frac{1}{2}}, \quad (61)$$

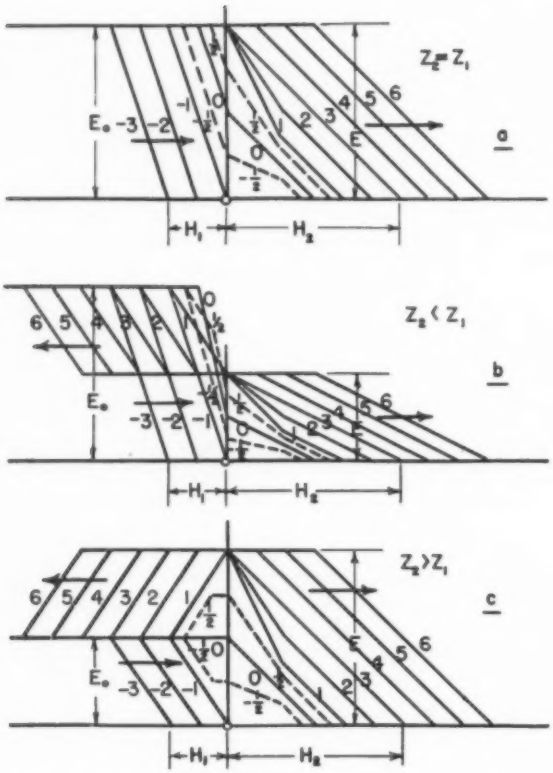

FIG. 19. Refraction and reflection of a finite wave front at transition points with various surge impedances.

where w_2 is now the wire length of the layers which form the elements of the coil, k_2 being the capacitance per unit length between every two layers, including $c/4$. The head length over the layers is therefore

$$H_2 = \pi v/\nu_2 = \pi v w_2 (lk_2)^{\frac{1}{2}} = \pi w_2 (k_2/c)^{\frac{1}{2}}. \quad (62)$$

Because this is a multiple of the wire length w_2 of a layer, it is in all practical cases larger than the first head length H_1, determined by Eq. (60). The transformation of H_1 into H_2 is shown in detail in Fig. 18, using again for this representation the approximate straight-line-front shape. As only the flatter wave H_2 can penetrate into the deeper layers of the first coil, the difference of the shapes, H_1 and H_2, shown in Fig. 18b as R_2, is reflected within the first few layers and causes in these an additional standing distribution of voltage. Since the frequencies of the wave R_2, however, are lower than the critical frequency ν_1 of the turns, the attenuated standing distribution across the layers may consist of traveling waves over the turns forming those layers.

The wave now runs with its new front length H_2 over the whole first coil, and then penetrates into the second and later into the third and further coils. But these coils have altogether a critical frequency

$$\nu_3 = 1/w_3 (lk_3)^{\frac{1}{2}}, \quad (63)$$

which is still lower, because w_3 is the wire length of every complete coil, while k_3 means the internal capacitance between adjacent coils, including again $c/4$. The front is thus distributed over the head length

$$H_3 = \pi v/\nu_3 = \pi v w_3 (lk_3)^{\frac{1}{2}} = \pi w_3 (k_3/c)^{\frac{1}{2}} \quad (64)$$

as shown in Fig. 17. The transformation of the wave front into this new head H_3 follows the same scheme as in Fig. 18. The reflected wave R_3 causes a standing voltage distribution over the first few coils, in addition to the wave front H_3 traveling over these coils. Here, correspondingly, the wave R_3 may be formed by traveling waves within each one of the first coils, as the frequencies of R_3 are smaller than ν_2. The average of these waves traveling to and fro across the layers of each coil forms the attenuated standing distribution over the coils.

So we see that in actual transformer or machine windings which consist of the three elements: turns, layers and coils, each having different wire length and different internal capacitance, an original incident steep-front wave is flattened out in three steps, the head lengths being in the proportion

$$H_1 : H_2 : H_3 = w_1 (k_1)^{\frac{1}{2}} : w_2 (k_2)^{\frac{1}{2}} : w_3 (k_3)^{\frac{1}{2}}. \quad (65)$$

Since the maximum internal stress between adjacent elements is determined by the quotient of their wire length and their respective head lengths, we can compare the internal stress between turns, layers and coils by the proportion

$$\epsilon_1 : \epsilon_2 : \epsilon_3 = \frac{1}{(k_1)^{\frac{1}{2}}} : \frac{1}{(k_2)^{\frac{1}{2}}} : \frac{1}{(k_3)^{\frac{1}{2}}}. \quad (66)$$

Thus it is evident that the voltage between adjacent elements is lower the larger the square root of the effective internal capacitances per

unit length between the elements, while all other characteristics of the design do not matter at all. Usually the internal specific turn capacitance k_1 is much larger than the capacitance k_2 between layers and this is again larger than the specific coil capacitance k_3. By favorable designing of the geometric shape within the cross section of the whole winding, it appears possible to equalize substantially these stresses in their effect on the internal insulation.[9]

At the transition between turns and layers, or layers and coils, the surge impedance Z, according to Eq. (26), may be different for the turns, the layers and the coils, caused by different critical frequencies of these respective groups, so that refraction may occur. Figure 19 shows the conversion of a flat wave front with a head length H_1 into a front with a head length H_2 three times as large as H_1, under three different assumptions as to the relative surge impedances on both sides of the transition point. Step by step the transmitted and reflected waves, together with the standing exponential distributions, are superposed, for simplicity, however, with the approximate straight-line diagrams. Figure 19a shows that for uniform surge impedances the steep incident front is transformed to the flat penetrating front without the occurrence of any reflected wave on the first line. The voltage difference R_2 of Fig. 18b causes only an additional steep terminal distribution in the second line, but

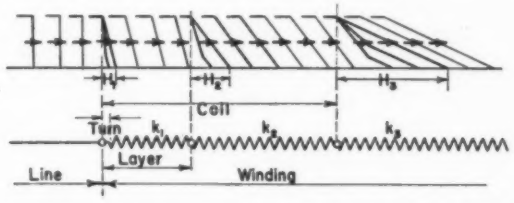

FIG. 20. Three conversions of a steep front wave throughout a complete winding.

even this is now gradually built up, as we see by comparing Fig. 19a with the instantaneous development in the rigorous Fig. 13. For uniform surge impedance Z the maximum value E of the penetrating wave equals E_0 of the incident wave.

If we assume in Fig. 19b a decrease in the surge impedance from Z_1 to Z_2, the graphical construction leads to the result that the converted wave in the second line is refracted into a smaller value, while its general shape remains exactly the same as just explained in Fig. 19a. Simultaneously, there now appears a reflected wave reducing the voltage on the first line, the front of the reflected wave having the same head length as the original incident wave. The surge impedances in Fig. 19b are chosen as 3 : 1 so that the penetrating wave E becomes just one-half of the incident wave E_0.

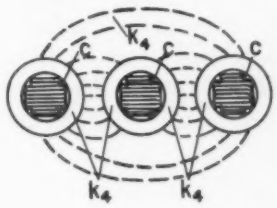

FIG. 21. Three-phase transformer with phase to phase capacitance.

In Fig. 19c the surge impedance Z_2 is chosen large in comparison to Z_1, so that the penetrating wave becomes doubled in amplitude compared with the incident wave. The converted wave, in its traveling parts as well as in its standing part, shows again the same distribution as in the previous cases, and we see that the general shape of the penetrating voltage therefore is independent of the ratio of the surge impedances. The reflected wave on the first line is now positive and increases the voltage beyond the value E_0.

As a whole, we see from Fig. 19 that the transition point between turns, layers or coils acts on the incoming line exactly like an ordinary junction, with either uniform or changing surge impedance. The reflected wave always retains the same shape as the incident one. On the outgoing line, however, simultaneously with the refraction to lower or higher values, the wave front is not only converted into a greater head length but the difference between the incident and the penetrating wave front causes a transient voltage distribution near the transition points, the steepness or space constant of which is somewhere between the head lengths of the incident and the penetrating waves.

As a result of these considerations, Fig. 20 shows the three conversions of the wave front as it travels over the whole winding. The interturn capacitance causes the first flattening within the first layer; the internal capacitance between

[9] W. Reiche, "Messungen über die Spannungsverteilung auf Transformatorwicklungen unter dem Einfluss von Sprungwellen," Archiv f. Elektrotech. **15**, 216 (1925–26).

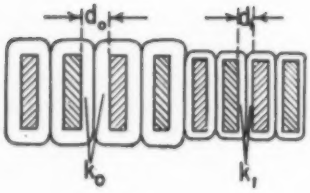

FIG. 22. Extra insulation of protective terminal turns.

layers causes the second flattening during the travel over the first coil; and the coil-to-coil capacitance causes the third flattening during the propagation over the whole winding.

If instead of an individual single-phase winding we have a three-phase winding with connections in star, zigzag or delta and with phase-to-phase capacitance k_4 between the phases, as shown in Fig. 21 for a transformer, then there is one more transition point within the complete course of the traveling waves. Finally, if protective coils with increased insulation, and thereby decreased internal capacitance k_0, are used near the terminals, as in Fig. 22, then the winding is subdivided still further into one more group of elements near its ends, and we have one additional transition point, making five in all.

It may be useful at this point to consider the quantitative advantage of extra insulation of such protective elements, be they turns, layers or coils. We can extend our law of voltage stresses from Eq. (66) to any element of different insulation; for example, to the highly insulated terminal turns of Fig. 22. Instead of ordinary insulation with a thickness d_1, these turns may be covered with material of the same kind but greater thickness d_0. Thereby the internal capacitances between adjacent turns are diminished nearly inversely as the thicknesses,

$$k_0/k_1 = d_1/d_0. \tag{67}$$

The voltage gradient in this insulation, as the quotient of voltage and distance, is

$$\frac{\epsilon_0}{d_0} : \frac{\epsilon_1}{d_1} = \frac{1/(k_0)^{\frac{1}{2}}}{d_0} : \frac{1/(k_1)^{\frac{1}{2}}}{d_1} = \frac{1}{(d_0)^{\frac{1}{2}}} : \frac{1}{(d_1)^{\frac{1}{2}}}, \tag{68}$$

and thus we see that the gradient decreases as the square root of the insulation thickness. If we provide for a protective extra insulation of the terminal layers or terminal coils, the same rule holds, and we see that in general we have to use four times as much individual insulation if we are to reduce the internal surge stress by one-half. This square root law of Eqs. (66) and (68), which governs the internal surge insulation of windings, causes many more difficulties in design than the linear law of the steady state insulation.

7. Natural Oscillations of Composite Windings

If for any wave which penetrates the winding the surge impedance remains constant during its propagation through the entire wire length, there are reflection points only at the ends of the total winding. The spectrum of natural frequencies is then given directly by our previous considerations, leading to Fig. 4. In windings consisting of coils, layers and turns, however, each part has its own critical frequency, according to Eqs. (59), (61) and (63), which is represented on the axis of abscissae in Fig. 23. Then the surge impedance Z of every group, according to Fig. 6, increases as we approach its critical frequency and therefore the surge impedance Z_3 of the whole winding increases, as shown in Fig. 23, faster than Z_2 of the first coil, and this increases faster than Z_1 of the first layer of the first coil. We see from Fig. 23, in which the small difference between ν and ν_x is not considered for reasons of simplicity, that only the initial value Z_0 for very low frequencies is uniformly distributed over the winding, corresponding to the fact that l and c in Eq. (26) are average values throughout the entire wire length. But for any higher frequency, for example ω in Fig. 23, the surge impedance of the first layer is relatively small, that of the first coil is much larger, while that of the whole winding appears as infinite.

Thus for waves of higher frequency we have to reckon with a considerable increase of the surge

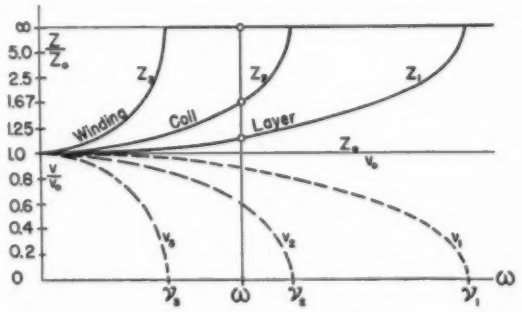

FIG. 23. Change of surge impedance with frequency for the various winding elements.

impedance at each of the transition points and, therefore, there develops, as in Fig. 19c, not only by refraction an increased voltage of the penetrating wave fronts but in addition a considerable reflection occurs and a partial wave travels back to the terminal. Each group of elements, layers and coils as well as the whole winding, is therefore excited in its own natural oscillations, and therefore such composite transformer or machine windings will have three series

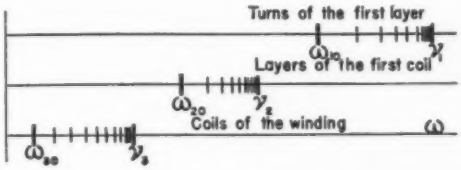

FIG. 24. Three series spectra of natural frequencies with finite upper limits for a complete winding consisting of turns, layers and coils.

of natural frequencies as represented by Fig. 24. Thus we see that in addition to the natural frequencies ω_3 of the entire winding, there develop at the transition points two series of more rapid local oscillations, of which ω_2 occurs within the first coils and ω_1 within the first layers adjacent to the terminal. If we consider three-phase windings with protective coils, there may be developed five such series, forming a fairly complex total spectrum of frequencies. Such local oscillations have often been observed experimentally.[8,10]

While the maximum frequencies ν of the spectral series in Fig. 24 are given by Eqs. (59), (61) and (63), the fundamentals are

$$\omega_{10}=2\pi m_1\frac{v_1}{w_2};\quad \omega_{20}=2\pi m_2\frac{v_2}{w_3};\quad \omega_{30}=2\pi m_3\frac{v_3}{a}, \tag{69}$$

where w_2, w_3 and a are the related wire lengths of the groups and v_1, v_2 and v_3 the traveling velocity of their waves, as shown by the dotted lines in Fig. 23, these velocities being smaller than the limiting velocity v_0 of Eq. (21). The smallest numbers m of wave-lengths along the wire lengths, corresponding to ω_{10} and ω_{20}, are in general equal to $\frac{1}{4}$, as the first layer and the first coil usually have an equivalent closed end at the terminal and

[10] T. E. Allibone, D. B. McKenzie and F. R. Perry, "The effects of impulse voltages on transformer windings," J. I. E. E. **18**, 128 (1937).

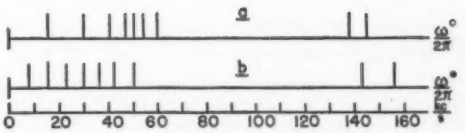

FIG. 25. Measured resonance frequencies of a power transformer with one end of the winding fed, the other end insulated or grounded.

an equivalent open end towards the remainder of the winding.

If under special conditions ω_{10} or ω_{20}, or even the lower harmonics of the corresponding series, are so small that there is no considerable difference of their surge impedance Z at both sides of the transition points, as in Fig. 19a, these oscillations may appear only as very weak if excited by switching processes or by resonance.

Let us compare the highest frequency ν of one group of elements with the lowest possible frequency ω_0 of the following group. For example, the ratio of the lowest natural frequency ω_{20} of the layers to the highest limit ν_3 of the frequencies of the coils is, according to Eqs. (63) and (69),

$$\frac{\omega_{20}}{\nu_3}=2\pi m_2 v_2(lk_3)^{\frac{1}{2}}\cong\frac{\pi}{2}\left(\frac{k_3}{c}\right)^{\frac{1}{2}}. \tag{70}$$

The last approximate expression on the right-hand side is obtained by taking $m_2=\frac{1}{4}$ and the velocity v_2 as the limiting value of Eq. (21). Since in most transformer windings the capacitive ratio k_3/c for the coils is much larger than 1, and for the layers as well, we must expect substantial gaps between the spectra of the various groups, as is indicated in Fig. 24. For machine windings, however, with k_3 approaching $c/4$, these gaps may vanish so that a more continuous spectrum is formed.

Some measurements of the natural frequencies were conducted on a three-phase transformer bank of 50 mva, having pancake windings. The high voltage windings of the three single-phase transformers were connected in open delta in order to extend the spectrum to values as low as possible. Alternately both ends of the open delta were insulated or one end was insulated and one end grounded. The low voltage windings were always short-circuited and grounded. The 19-kv H. V. winding was excited by a high frequency source of variable frequency and resonance was

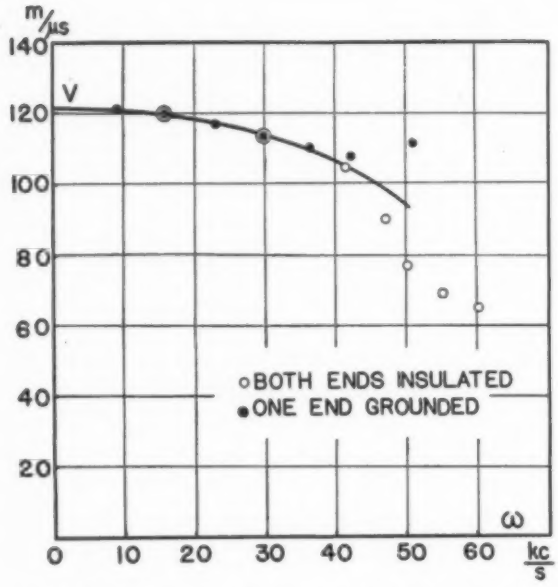

FIG. 26. Measured wave velocity in the winding of a power transformer depending on the frequency of excitation.

indicated, by means of a cathode-ray tube, by phase coincidence of voltage and current. The spectrum in Fig. 25a shows the resonance frequencies observed with both ends of the open delta insulated, in Fig. 25b those with one end grounded. We note in both examples the wide gap between the spectrum of the first and the second range, due to the subdivision into coils and layers. The experimental observations at the end of the first group were somewhat uncertain and the second group could not be followed further because of the frequency limit of the oscillator.

If we correlate consecutive numbers m to the measured frequencies of the first range, we can compute the wave velocity for every natural frequency by using Eqs. (9) and (17), since the length of the winding is known as $a = 3810$ m. In Fig. 26 this wave velocity is plotted against frequency and we see that it is constant for lower frequencies, starting with a value of 122 $m/\mu s$, and that it decreases more rapidly for higher frequencies. The velocity curve may reach the ω-axis at a critical frequency of about 80–90 kc/s. So we find experimentally the same shape of curve which we have derived analytically in Fig. 5. With a closed oil transformer the coordination of a number "m" to a definite frequency is certain only for the lower resonance points which are well determined. At the higher natural frequencies, however, the dispersion of the points represents the uncertainties due to observation as well as to correlation.

Thus we see that some very significant results of our theoretical considerations, namely, decrease of wave velocity with frequency, finite boundary of the spectrum of natural frequencies, and separation of the entire spectrum into series of different ranges, are experimentally verified for an actual transformer.

SUMMARY

Lumped subdivision of windings into distinct elements as coils, layers or turns causes a critical frequency of its own, lower than that due to internal capacitance. Within the intermediate range of both critical frequencies, attenuated standing waves appear within the winding.

Propagation of steep waves through successive turns, layers and coils effects a flattening of the front in several steps. Simultaneously local oscillations within the layers or turns may be excited by reflections at the transition points of the groups of elements.

The head length of the propagating wave and the internal stress of the insulation are favorably influenced by subdivision into elements, particularly in case of small internal capacitance. The change in time of the internal voltage is derived both for interior and terminal elements. Formulae are given for the computation of the internal stresses between turns, layers and coils as well as between extra-insulated terminal elements.

Some significant results of the analysis are verified by experiments with a power transformer.

LIST OF SPECIAL SYMBOLS

a = winding length
c = ground capacitance per unit length
d = thickness of insulation
k = internal capacitance per unit length
l = self-inductance per unit length
m = number of waves
n = number of element
r = reflected wave
v = wave velocity
w = wire length of element
H = head length
X = space constant
α = wave density
β = attenuation factor
δ = attenuation factor
ϵ = internal voltage
θ = attenuation factor
λ = wave-length
ν = critical frequency
τ = time of ascent

The Dielectric Properties of the Rutile Form of TiO_2*

L. J. Berberich and M. E. Bell
Westinghouse Research Laboratories, East Pittsburgh, Pennsylvania
(Received June 13, 1940)

Three specimens of rutile were prepared and the dielectric properties studied over a range of frequency and temperature. A dielectric constant of approximately 100 was found which remained substantially constant through the highest radiofrequencies, falling off only in the infra-red region. The dielectric losses are low, particularly at the higher frequencies. The dielectric constant decreases with increasing temperature, having an average temperature coefficient of -8.2×10^{-4}/°C. An exponential relationship between conductivity and the reciprocal of the absolute temperature holds for rutile in the higher temperature region. Mixtures of rutile powder with other dielectric materials obey a logarithmic mixture formula. Two mechanisms which have been proposed to explain the high dielectric constant of rutile are discussed. A simple mechanism based on the Clausius-Mosotti equation is described.

I. Introduction

MOST of the known solid dielectrics have dielectric constants ranging from 1 to 10. There are, however, a few inorganic solids which have dielectric constants between 15 and 30. Certain lead compounds such as lead oxide, lead borate and lead carbonate as well as certain oxides, such as tin dioxide and zirconium dioxide belong to this class. The departure of the dielectric constants of these materials from the Maxwell relation, $\epsilon=n^2$ (the dielectric constant equals the square of the refractive index) is considerable in some cases. This is explained on the basis that, in addition to electronic polarization, atomic polarization, which arises out of the displacement of ions, contributes to the total polarization. Most of these substances are characterized by a positive temperature coefficient of dielectric constant.

There are liquids, such as liquid HCN whose dielectric constants are greater than 100. Their behavior can be explained on the basis of the Debye theory which postulates the existence of permanent dipoles and their orientation with the field. A consequence of this theory is a negative temperature coefficient of dielectric constant. Rochelle salt ($KOOCCHOHCHOHCOONa\cdot\cdot 4H_2O$) is a very unusual solid in that it has exhibited dielectric constants of 20,000 and higher. Although the theory is somewhat unsatisfactory, it is believed that the water of crystallization plays a role in producing the high dielectric constant. Fowler[1] has explained that such behavior is possible in certain crystals through a cooperative rotational effect in the solid state.

Rutile, one of the three crystalline modifications of TiO_2, has the unusually high dielectric constant of over 100. It differs from most inorganic solids, not only in having a high dielectric constant, but also in that it is characterized by a negative temperature coefficient of dielectric constant. The usual mechanisms which explain the dielectric constant of most materials do not appear to explain the high dielectric constant of rutile. It is not possible, on the basis of its crystal structure, to postulate a permanent dipole moment or molecular rotation in the solid state. A few scattered investigations have been made on this interesting material. Most of these, however, covered only a narrow frequency range. Moreover, most of the results reported in the literature are of questionable reliability because of unknown purity of the specimens. Several attempts at explaining the cause of the high dielectric constant have also been made, but there is considerable disagreement. After a discussion of the general characteristics of rutile, this paper will be concerned with (1) the presentation of the results of a thorough investigation of

* This paper besides being presented at the Columbus meeting of the American Physical Society, December, 1939, was a part of a symposium on Electrical Insulation sponsored by the Subcommittee on Chemistry of the Conference on Electrical Insulation of the National Research Council, at the Cincinnati meeting of the American Chemical Society, April, 1940.

[1] R. H. Fowler, "A theory of the rotations of molecules in solids and the dielectric constant of solids and liquids," Proc. Roy. Soc. **A149**, 1 (1935).

the dielectric properties of rutile of known purity and (2) with the discussion of the dielectric constant mechanism in the light of present theories.

II. General Characteristics of Rutile

The fact that the dielectric constant of rutile is high has been known since 1902, when it was measured by Schmidt.[2] He found a dielectric constant of 173 parallel to the principal crystal axis and 89 perpendicular to this axis. This corresponds to a mean dielectric constant of 114 for randomly oriented crystals.* This value is in rough agreement with values found for a sintered rutile body as will be seen later.

TiO_2 occurs in nature in three crystalline forms; namely, rutile, brookite and anatase. In Table I some properties of rutile may be compared with those of the other forms of TiO_2. It is observed from Table I that the refractive indices are high and in the same order as the dielectric constants for the three crystalline forms, but very much too low to satisfy Maxwell's relation. The several refractive indices given for each crystalline form refer to different crystal axes, the highest value always referring to the principal axis. Rutile has the highest dielectric constant of the three crystal forms. It is also the most dense and the highest temperature form of TiO_2. The other forms must be heated above 820°C[3] to be converted into rutile.

Table I. *Physical properties of the three crystalline modifications of* TiO_2.

Properties	Rutile	Brookite	Anatase
Crystal structure	Tetragonal	Rhombic	Tetragonal
Density g/cc	4.25	4.11	3.87
Refractive index	2.903	2.741	2.554
	2.616	2.586	2.493
		2.583	
Mean dielectric constant	114	78	31
Coefficient of expansion/°C	$7.1\text{–}9.2\times10^{-6}$	$14.5\text{–}22\times10^{-6}$	$4.7\text{–}8.2\times10^{-6}$
Melting point °C	1800–1900	—	—

Rutile has a di-tetragonal, bi-pyramidal crystal structure (body-centered) which is illustrated in schematic fashion in Fig. 1(a). The elementary lattice is represented which shows that the two oxygens and the titanium form a linear molecule. No permanent dipole moment is therefore indicated. Fig. 1(b) is a scale drawing of the diagonal plane $WXYZ$ of Fig. 1(a) which shows the oxygen atoms in their relation to the titanium atoms in a crystal of twice unit dimensions. By examining the central titanium atom it will be observed that each titanium atom is surrounded by six oxygen atoms, four of which are shown. The other two are located, one below and one above the plane of the paper. The unit dimensions of the crystal as given by Vegard,[4] which appear to be more self-consistent than those reported by Wyckoff[5] are $a=4.65$A and $c=2.99$A. The radii of the titanium and oxygen atoms according to Vegard[4] are 1.31A and 0.67A, respectively.

So far as we know, no electrical use was made of rutile prior to 1925 when a German patent[6] appeared covering its use as a high frequency capacitor dielectric. Since then, a number of patents have appeared in this country and abroad covering its use as a dielectric in mixtures with other ceramic materials such as ZrO_2, MgO, SiO_2, ThO_2, CdO, etc., as well as with a considerable number of organic materials. Capacitors for radiofrequency application embodying rutile in a ceramic mixture have been manufactured for some time both here and abroad.

III. Experimental Results and Discussion

1. Preparation and descriptions of test specimens

In order to obtain satisfactory dielectric measurements and to interpret the results properly, particular care must be given to the preparation of samples and application of electrodes. The rutile used in making the specimens was the purest commercial grade available. The analysis

[2] W. Schmidt, "Determination of dielectric constants of crystals by means of electric waves," Ann. d. Physik (14) **9**, 919 (1902); *ibid.* **11**, 114 (1903).

* The mean dielectric constant of randomly oriented crystals is determined by adding twice the polarizability corresponding to a dielectric constant of 89 to that corresponding to a dielectric constant of 173, and then computing the dielectric constant corresponding to one-third of this sum. In rutile there are two axes parallel to which the dielectric constant is 89 and hence the value of polarizability corresponding to this dielectric constant has to be taken twice in computing the mean dielectric constant. The polarizability is computed by means of the Clausius-Mosotti relation, $P=(\epsilon-1)/(\epsilon+2)$. The validity of this relation in the case of rutile, however, has not been definitely established.

[3] G. F. Huettig and K. Kostehen, "Transition from anatase to rutile as influenced by the presence of HCl gas," Kolloid Zeits. **89**, 202–8 (1939).

[4] L. Vegard, "Results of crystal analysis," Phil. Mag. [7] **1**, 1151–1193 (1926).

[5] R. W. G. Wyckoff, *Structure of Crystals* (Chemical Catalog Company, 1931).

[6] German Patent No. 545,402.

of the 325 mesh powder having a specific gravity of 4.23 shows the following:

TiO_2	98.2%
ZrO_2	0.1
SiO_2	0.8
CaO	0.6
Al_2O_3	0.15
MgO	0.05

Traces of other impurities.

The test specimens were made by mixing approximately 15 percent by weight of water with the rutile powder and then molding into disks in a hydraulic press at a pressure of several tons per square inch. The strength of the disks, which were 4″ in diameter and $\frac{1}{4}$″ in thickness, was ample for the handling required previous to firing. Since the rutile has a melting point in the neighborhood of 1800°C a high firing temperature was necessary to obtain a dense disk in a short firing cycle. Some sintering takes place at temperatures as low as 1300°C. A long time, however, is required to obtain a dense disk at this temperature. In this work three specimens were fired in an oxidizing atmosphere in the following manner:

Specimen No. 1, composed entirely of rutile, was held for 2 hr. at a maximum temperature of 1675°C. Definite crystal formation was indicated by the appearance of bright scintillating spots on the surface which could be observed with the unaided eye. The specific gravity of this specimen was found to be 4.06 and the porosity was zero.

Specimen No. 2, composed of 95 percent rutile and 5 percent by weight of ceramic material having a relatively low dielectric constant, was held at a maximum temperature of 1330°C for 6 hr. No crystal formation was evident on the surface. The specific gravity of this specimen was found to be 3.89 and the porosity was 0.98 percent by volume.

Specimen No. 3, composed entirely of rutile, was held at a maximum temperature of 1330°C for 6 hr. No crystal formation was evident on the surface. The specific gravity of this specimen was found to be 3.97 and the porosity was 0.06 percent by volume.

In the firing operation, extreme care had to be exercised that an oxidizing atmosphere was maintained about the specimens in the furnace. The white TiO_2 is relatively easily reduced to the black suboxide TiO. This reduction has been found to take place at temperatures as low as 600°C. The original 4″ diameter of the specimens was decreased 5 to 7 percent by shrinkage in firing. Electrodes $2\frac{1}{2}$″ in diameter were formed on the surface by applying a special platinic chloride paint and reducing to platinum. In order to assure good adhesion of the platinum film, the specimens were given a final firing for several hours at 900°C. The resistance of the thin platinum film was too high, however, to permit accurate measurements. For the conductivity measurements, disks of palladium placed on the platinum coating were found satisfactory up to 600°C. For power factor and dielectric constant measurements, which were carried to only 125°C, a lead film sprayed on the platinum reduced the lateral resistance sufficiently.

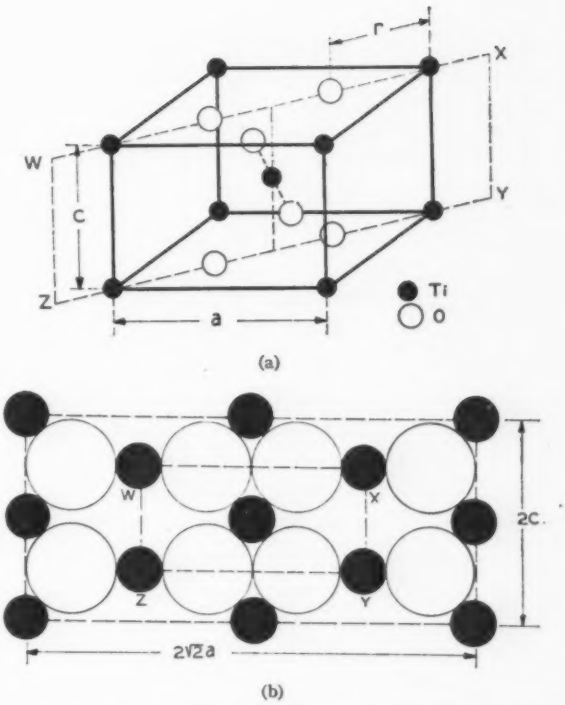

FIG. 1. Crystal structure of rutile. (L. Vegard.) (a)—Schematic diagram. (b)—Scale diagram of section in plane *WXYZ*.

The porosity was measured by determining the water absorbed after immersion in water for 96 hr. and boiling the water every 24 hr. This gave a measure of those pores which are connected to the surface. Specimen No. 1 showed no porosity in this test, yet the specific gravity of the powder from which the disk was made was 4.23 and the specific gravity of the fired disk

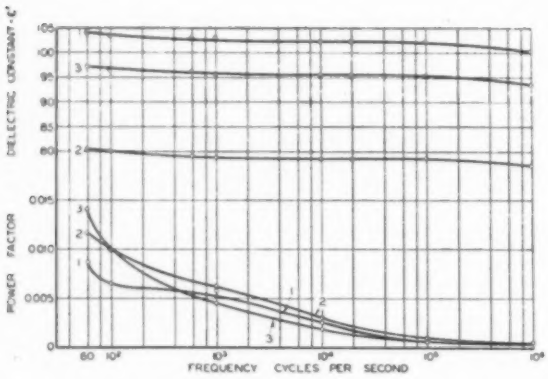

FIG. 2. Power factor and dielectric constant *vs.* frequency at 30°C for rutile specimen Nos. 1, 2 and 3.

was only 4.06. It is indicated, therefore, that there must be some volume porosity which is not measured by the test used.

2. Methods of measurement

The dielectric constant and power factor* of the three specimens were measured over a range of frequency from 60 to 10^6 cycles per second, and also over a temperature range from 30 to 125°C at frequencies from 60 to 20,000 cycles per second. For the low frequency measurements a General Radio Type 716-A capacitance bridge was used which was modified to cover a range of frequency. For the high frequency measurements the ordinary resonant substitution method served the purpose. Since no guard rings could be used conveniently on the specimens, an edge correction had to be estimated. This correction amounted to approximately 7 percent of the dielectric constant and was made according to the method of Scott and Curtis.[7]

3. Power factor and dielectric constant *vs.* frequency

The results of the power factor and dielectric constant measurements as a function of the frequency for the three specimens are shown in Fig. 2. It will be observed that not only is the dielectric constant high but the decrease is slight over the whole frequency range. Specimen No. 1 has the highest dielectric constant because it has the highest density and the lowest impurity content. No. 3, which contains rutile of the same composition as that in No. 1, has a somewhat lower dielectric constant since it has a lower density. The data for No. 2 show a marked lowering in dielectric constant as a result of the addition of 5 percent of a low dielectric constant ceramic material. This specimen also has an appreciable porosity, thus, a small percentage of impurities can bring about a marked reduction in dielectric constant.

The power factor of all specimens decreases gradually as the frequency increases to 0.0005 at 10^6 cycles. Considering the high dielectric constant, this is a surprisingly low value. The higher power factor at the lower frequencies may be attributed to oscillation of ions or an interfacial polarization of the Maxwell-Wagner type.[8] It is, however, not certain that this behavior in the case of rutile can be ascribed to either mechanism. The Maxwell-Wagner mechanism has been invoked frequently to explain high losses at low frequencies, mainly because no other mechanism seemed plausible.

Figure 3 shows that the high dielectric constant of rutile persists even at 10^{12} cycles per second. It gives the infra-red reflection data for rutile and thallium chloride, a material of similar dielectric properties, in comparison with those for potassium chloride as obtained by Liebisch and Rubens.[9] The infra-red data for rutile and TlCl differ from those for KCl, especially in the asymptotic values at the long wave-lengths. The refractive index can be com-

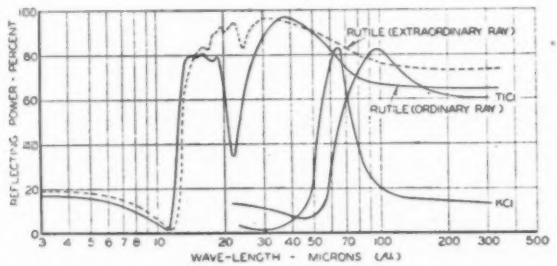

FIG. 3. Behavior of rutile, TlCl and KCl in the infra-red (Liebisch and Rubens).

* Power factor is reported instead of loss factor because the former is more familiar to engineers. If loss factor is desired, it is merely necessary to multiply the dielectric constant by the power factor, since for these low power factors sin δ is approximately equal to tan δ.

[7] A. H. Scott and H. L. Curtis, "Edge correction in the determination of dielectric constant," J. Research Nat. Bur. Stand. **22**, 747–775 (1939).

[8] J. B. Whitehead, *Lectures on Dielectric Theory and Insulation* (McGraw Hill Book Co., 1927), p. 92.

[9] T. Liebisch, and H. Rubens, "Ueber the Optischen Eigenschaften einiger Kristalle im longwelligen Ultraroten Spektrum," Preuss. Akad. Wiss. Berlin Ber. **8**, 211–20 (1921).

puted from the reflection data by the use of the equation, $R=[(n-1)/(n+2)]^2$ which is valid in the frequency region where the absorption is small. The results of this computation together with that for the dielectric constant ($\epsilon=n^2$) is made in Table II.

Table II shows that there is very little diminution in dielectric constant between 10^{12} cycles (300μ) and radiofrequencies for rutile and KCl. There is, however, some diminution for TlCl, probably because at 300μ the reflection coefficient curve had not yet flattened out to its final value. Figure 3 shows also that the reflecting power of KCl goes through a sharp maximum and falls to a low value on either side of the peak, which is characteristic of many materials. This is to be contrasted with the broad maxima for rutile and thallium chloride which level off to high values of reflection coefficient at longer wave-lengths.

4. Power factor and dielectric constant *vs.* temperature

Figures 4, 5 and 6 show the temperature dependence of dielectric constant and power factor for the three rutile specimens. At 10,000 cycles the temperature coefficient of dielectric constant is negative over the temperature range investigated. At 60 cycles, however, the dielectric constant has a minimum after which it rises sharply. The rise in dielectric constant at this frequency is accompanied by a sharp rise in power factor. At the higher frequencies, however, the rise in dielectric constant is absent and the power factor rise is much smaller over the range of temperature investigated. Such behavior has been ascribed by various investigators to oscillation of ions which might be released thermally. It is believed that at higher frequencies these ions can no longer follow the field and therefore cannot contribute to the power factor and dielectric constant. Nothing is known regarding the possible nature of these ions in rutile. It is usually thought that they originate in impurities. The three specimens all show the same general behavior with respect to temperature and frequency.

TABLE II. *Dielectric constant and refractive index data for rutile,* TlCl *and* KCl.

	Coefficient of Reflection ($\lambda=300\mu$)	Refractive Index		Dielectric Constant	
		Visible D-Line	Infrared from Reflection Coef.	Computed from Refl. Coef.	Meas. at Radio Freq.
Rutile crystal					
Extraordinary ray	0.733	2.903	13.0	169	173
Ordinary ray	0.644	2.616	9.2	83.8	89
Thallium chloride	0.567	2.25	7.1	50.4	31.9
Potassium chloride	0.140	1.490	2.2	4.84	4.68

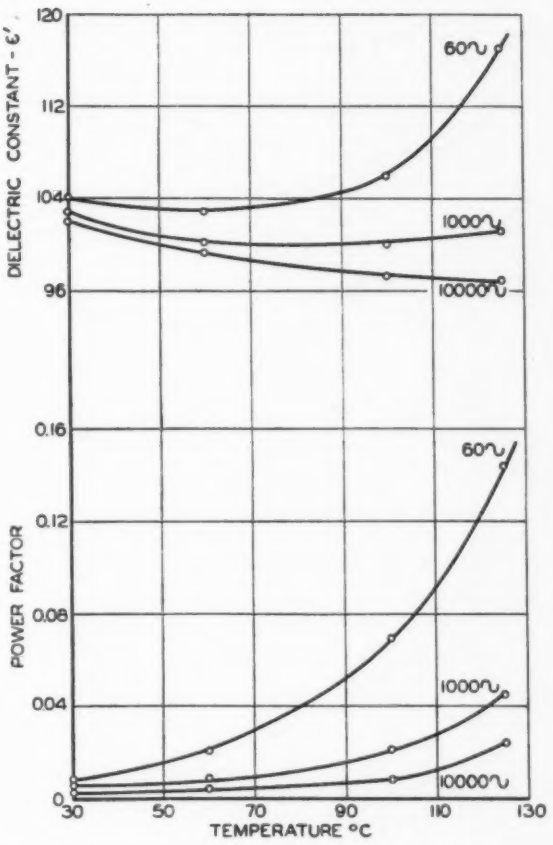

FIG. 4. Power factor and dielectric constant *vs.* temperature for specimen No. 1.

Figure 7 gives additional data obtained from various sources, on the temperature dependence of the dielectric constant, all determined for frequencies at or above 10,000 cycles. Attention is called to the data obtained by Schusterius[10]

[10] C. Schusterius, "Ueber einige Untersuchungen der Temperaturabhaengkiet der dielectrischen Eigenschaften von Titanoxyd and Zinnoxyd," Zeits. f. tech. Physik **16**, 640–2 (1935).

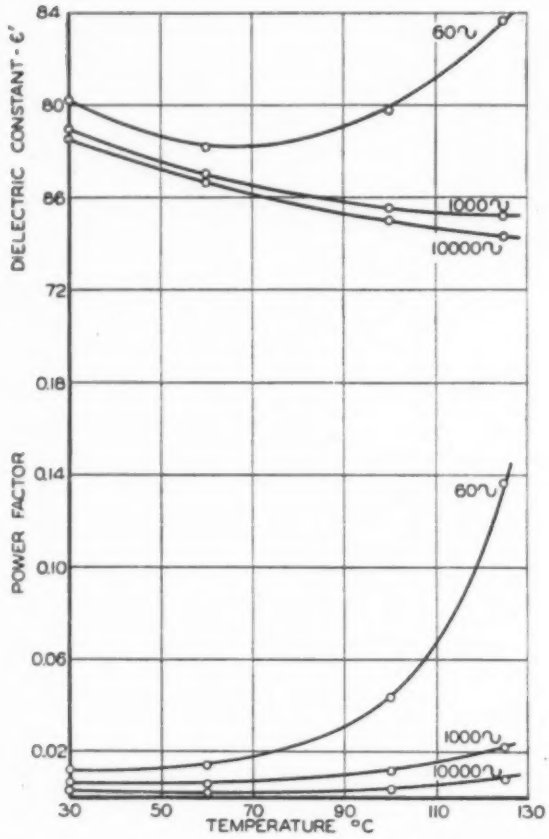

FIG. 5. Power factor and dielectric constant *vs.* temperature for specimen No. 2.

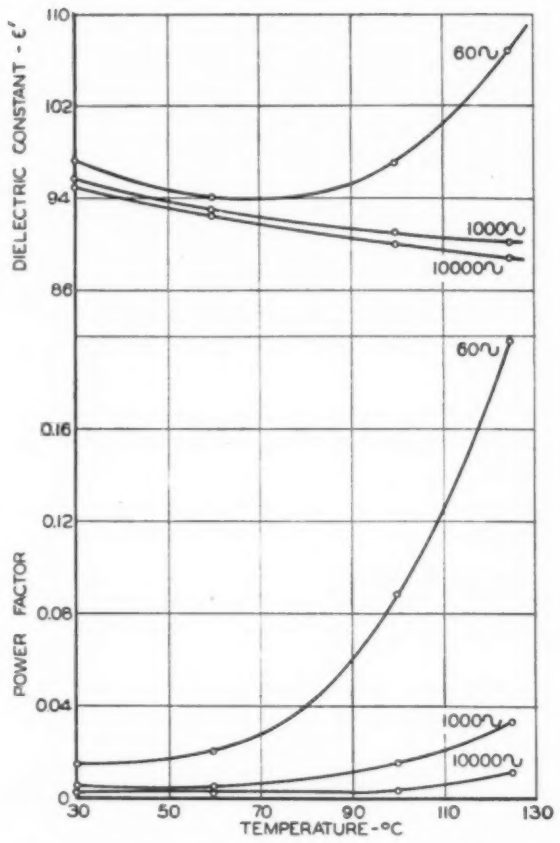

FIG. 6. Power factor and dielectric constant *vs.* temperature for specimen No. 3.

(curve 1) and by the writers (curve 6). Both show a negative temperature coefficient over the range investigated. Curve 1 shows less curvature than curve 6 because the former was measured at higher frequencies. Eucken and Büchner[11] obtained data on natural crystals determined at 0.5×10^6 and 3×10^6 cycles per second which show pronounced minima at temperatures below 20°C (curves 2, 3, 4 and 5). It will be observed that the minima for the higher frequency occur at the higher temperatures. The high frequencies and low temperatures at which these minima occur appear to eliminate the hypothesis that this behavior is caused by oscillation of ions. An alternative explanation has been suggested by Schusterius[10] who also found minima at low temperatures and high frequencies when his specimens were partially reduced. He attributed this behavior to the fact that when TiO_2 is partially reduced it becomes an electronic semiconductor. It is difficult, however, to see on the basis of the electronic semiconduction theory, that increasing frequency can cause a shift of the minima to higher temperatures. It is possible that Eucken and Büchner's crystals may have been somewhat reduced or contained considerable percentages of impurities since most natural crystals are dark in color, but the mechanism by which these enter into the production of the minima shown in Fig. 7 remains in question.

5. Resistivity and conductivity data

The resistivity and conductivity data for the three rutile specimens is given in Fig. 8. The one curve shows the logarithm of the resistivity plotted against the temperature in degrees centigrade and the other shows the logarithm of the conductivity plotted against the reciprocal of the absolute temperature. The resistivities of the three specimens do not differ appreciably from each other except at low temperatures. The

[11] A. Eucken and A. Büchner, "Die Dielektrizitaetskonstante swach polarer Kristalle und ihre Temperaturabhaengigkeit," Zeits. f. physik. Chemie **B27** 321–49 (1934).

logarithm of the conductivity, when plotted against $1/T$, approximates a straight line in the high temperature range and down to 125°C. Below 125°C the conductivity is influenced strongly by the time. The long time or constant values were plotted. As is the case with most solid dielectrics, the lower the temperature the greater is the difference between the first measurable conductivity (20 sec. after application of voltage in this case) and the final conductivity. At room temperature approximately one hour was required to reach a constant value of conductivity, but at 125°C the effect of time is small. The dashed portions of the curves indicate the region where the conductivity is affected by time.

Since the conductivity curve is straight in the high temperature region it can be represented by the equation,

$$\sigma = Ae^{-B/T} \quad \text{or} \quad \ln \sigma = \ln A - B/T,$$

where σ is the conductivity, A and B are constants and T the absolute temperature. In solid salts the conductivity has been shown to be electrolytic and an equation of the same form

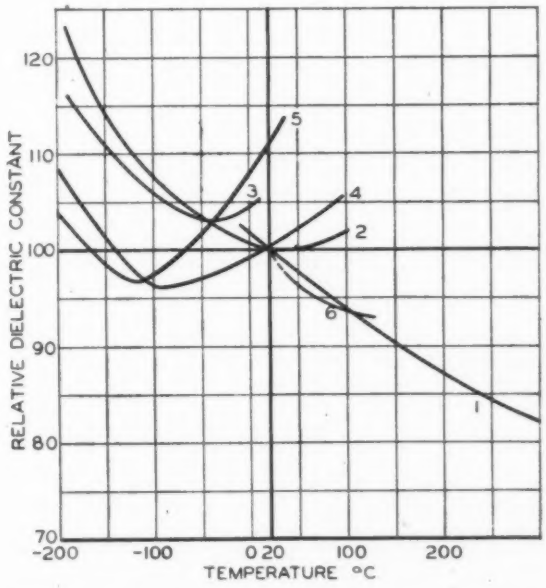

FIG. 7. Data from various sources on temperature coefficient of dielectric constant. 1—Fired rutile disk. $f = (0.2 \text{ to } 3.3) \times 10^6 \sim$ (Schusterius); 2—Single rutile crystals $\perp$ to axis $f = 3 \times 10^6 \sim$; 3—Single rutile crystals $\perp$ to axis $f = .5 \times 10^6 \sim$; 4—Single rutile crystals $\parallel$ to axis $f = 3 \times 10^6 \sim$; 5—Single rutile crystals $\parallel$ to axis $f = .5 \times 10^6 \sim$; (curves 2–5 incl. Eucken and Büchner); 6—Fired rutile disk $f = 10{,}000 \sim$ (specimen No. 1).

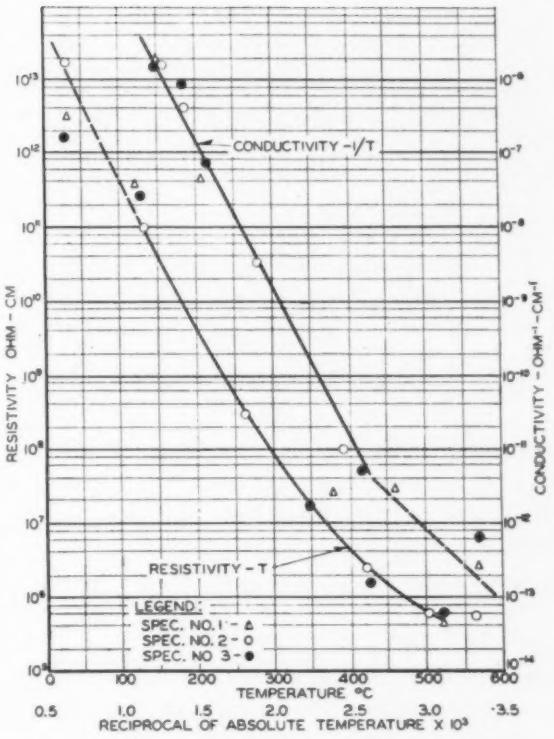

FIG. 8. Temperature variation of resistivity and conductivity for three rutile specimens.

applies in certain temperature regions.[12] This equation is identical with van't Hoff's relation expressing chemical reactivity with temperature when the constant B is set equal to the ratio of the activation energy Q and the universal gas constant R.

IV. Behavior of Rutile in Mixtures

When it is desired to use rutile powder in admixture with other dielectrics, the question arises—What will be the dielectric constant of the mixture? One might expect that a mixture formula derived from the Clausius-Mosotti relation[13] to be applicable. This mixture formula takes the form:

$$P = X_1P_1 + X_2P_2 \quad \text{or} \quad \frac{\epsilon-1}{\epsilon+2} = X_1\frac{\epsilon_1-1}{\epsilon_1+2} + X_2\frac{\epsilon_2-1}{\epsilon_2+2}$$

in which P and ϵ are the polarizability and dielectric constant of the mixture, respectively; X_1 and X_2 are the volume percentages, P_1 and P_2

[12] W. Seith, "Die Ionenleitfaehigkeit in festen Salzen," Zeits. f. Elektrochem. **42**, 635–54 (1936).

[13] P. Debye, *Polar Molecules* (Chemical Catalog Co., 1929).

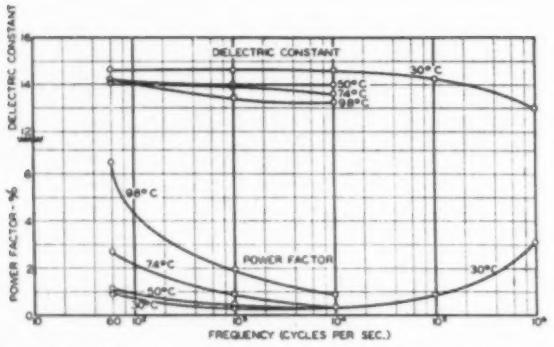

FIG. 9. Dielectric properties of mixture −64 percent chlorinated diphenyl and 36 percent rutile by volume.

the polarizabilities, and ϵ_1 and ϵ_2 the dielectric constants of the two components in the mixture. We have found, however, that too small a dielectric constant is always obtained for rutile mixtures when computed by means of this formula.

Many mixture formulae have been proposed, none of which are of universal application. Lichtenecker[14] has discussed the dielectric constant of mixtures and suggested a number of formulae. It might be well to examine a few of these of which the following general expression is the basis:

$$\epsilon^K = X_1\epsilon_1^K + X_2\epsilon_2^K,$$

where K is a constant for a given binary mixture, its value depending on the form and distribution of the two components and the other symbols are the same as before. K can have any value from $+1$ to -1. For $K=1$ the equation holds for the parallel disposition of components or

$$\epsilon = X_1\epsilon_1 + X_2\epsilon_2.$$

For $K=-1$ the equation holds for the series disposition of components or

$$1/\epsilon = X_1/\epsilon_1 + X_2/\epsilon_2.$$

Büchner[15] found that the series formula above holds very well for the two-component material consisting of paper impregnated with a liquid dielectric. As K approaches zero, Lichtenecker and Rother[16] have shown that the general expression takes the form of the logarithmic mixture formula which is

$$\log \epsilon = X_1 \log \epsilon_1 + X_2 \log \epsilon_2.$$

It was found that the logarithmic formula holds approximately for rutile powder mixed with other ceramic powders and even organic resins and liquids. An example of the properties of a mixture is given in Fig. 9, which shows the dielectric properties over ranges of frequency and temperature for rutile powder mixed with chlorinated diphenyl, the latter being a polar liquid having a dielectric constant of 4.5. Even though the mixture contains 36 percent by volume of rutile its dielectric constant is about 14.5 at low frequencies and room temperature. The value computed by use of the logarithmic mixture formula is 15.4. Similar agreement was obtained with mixtures of rutile powder and shellac or polystyrene. The dielectric constant of the rutile-chlorinated diphenyl mixture decreases at the higher frequencies. This occurs because a dispersion region for the polar chlorinated diphenyl is being approached. Here the effective dielectric constant of chlorinated diphenyl is less than 4.5.

While our work was in progress, some data on rutile mixtures were published by Büchner.[15] These data are reproduced in Fig. 10 because a wider range of mixtures was covered than in our work. The straight lines on a semilog plot give further confirmation that dielectric constant of such mixtures can be computed by means of the logarithmic mixture formula. The coincidence of the curves for the polystyrene-TiO_2 and kaolin-TiO_2 mixtures is entirely fortuitous. These data show strikingly that the dielectric constant of a rutile mixture is far from linear with the volume percent of rutile in the mixture.

V. Possible Mechanisms for High Dielectric Constant of Rutile

Two mechanisms have been proposed to explain the behavior of inorganic materials having

TABLE III. *Density, dielectric constant and molar polarizabilities of the three forms of* TiO_2.

	Rutile	Brookite	Anatase
Density (g/cc)	4.25	4.11	3.87
Dielectric constant	114	78	31
Molar polarizability (cc)	18.2	18.7	18.8

[14] K. Lichtenecker, "Die Dielektrizitaetskonstante natuerlicher und kuenstlicher Mischkoerper," Physik. Zeits. **27**, 115–158 (1926).

[15] A. Büchner, "Das Mischkoerperproblem in der Kondensatorentechnik," Wiss. Veröff. a. d. Siemens-Werken **18**, 204–216 (1939).

[16] K. Lichtenecker and K. Rother, "Die Herleitung der logarithmischen Mischungsgesetzes aus allgemeinen Prinzipien der stationaeren Stroeming," Physik. Zeits. **32**, 255–260 (1931).

high dielectric constants. Assuming that the Clausius-Mosotti equation gives the correct relation between dielectric constant and polarizability, Frank[17] has attempted to show that a high dielectric constant arises when the electronic and atomic polarizabilities are simultaneously large. Eucken and Büchner[11] on the other hand, make use of an equation derived by Born[18] to explain the high dielectric constant on the basis of an unusually high atomic polarizability only. The Born equation depends upon a linear relationship between the dielectric constant and the polarizability. The greatest disagreement between the linear relationship used by Born and the Clausius-Mosotti equation may be expected when the dielectric constant is large. These two attempts to explain the high dielectric constants of materials not exhibiting polar rotation have, therefore, been based on contradictory equations.

Elaborating first on Frank's mechanism, which is based on the Clausius-Mosotti equation,

$$p = p_e + p_a = (\epsilon - 1)/(\epsilon + 2),$$

where p is the total volume polarizability consisting of the electronic polarizability p_e and the atomic polarizability p_a and ϵ is the dielectric constant, it is seen that the dielectric constant will be large when the sum of p_a and p_e approaches unity. The magnitude of the electronic polarizability is governed by the number of atoms or ions in a given space and by the ease of distortion of the electron shells. In rutile, the electronic polarizability is large because, as Frank shows, the ratio of the mean electronic polarizability per atom to the mean atomic volume is high.

TABLE IV. *Dielectric constants and polarizabilities for a number of materials.*

MATERIAL	ϵ	p	ϵ_0	p_e	p_a
Rutile	114	0.974	7.42	0.681	0.293
Brookite	78	0.963	6.97	0.667	0.296
TlCl	47	0.939	5.05	0.574	0.365
$PbCl_2$	33.5	0.915	4.94	0.568	0.347
Anatase	31	0.909	6.33	0.640	0.269
PbO	26	0.893	6.62	0.652	0.241
SnO_2	24	0.885	4.11	0.509	0.376
$HgCl_2$	14	0.813	3.43	0.447	0.366
AgCl	12.3	0.790	4.28	0.522	0.268
LiCl	11.1	0.769	2.76	0.369	0.400
LiF	9.3	0.735	1.94	0.238	0.497
MgO	8.2	0.706	3.01	0.401	0.305
NaF	6	0.625	1.76	0.202	0.423
NaCl	5.6	0.605	2.38	0.315	0.290
RbCl	5.2	0.583	2.23	0.291	0.292
KCl	4.8	0.557	2.22	0.289	0.268

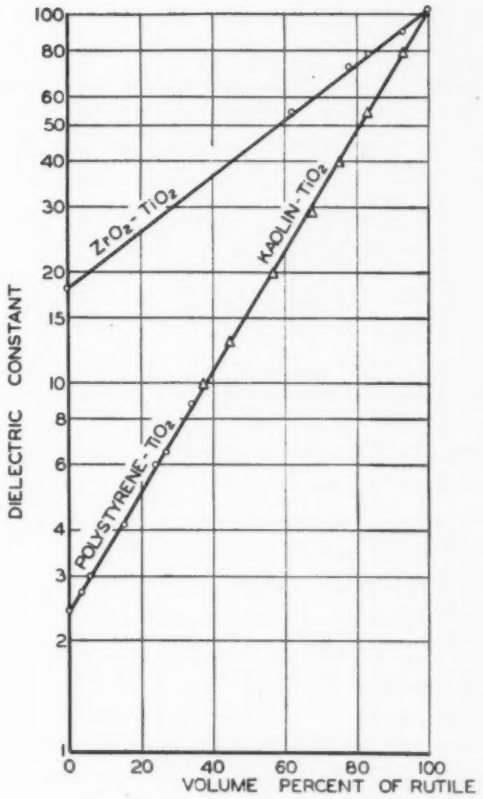

FIG. 10. Dielectric constant of rutile mixture as a function of rutile content (Büchner).

The atomic polarizability arises out of the motion of the positive ions with respect to the negative ions. The ease with which this can take place is supposed to depend chiefly on the ease of distortion of the anions. The magnitude of the atomic polarizability therefore depends principally on the charge on the cations and the polarizability of the anions. According to Frank, the atomic polarizability for rutile should be high because of the quadruply charged cations and the easily distortable anions. It is found, however, that some materials such as LiF, $PbCl_2$ and MgO selected from a group listed in Table IV, have a higher atomic polarizability than rutile, although they have a smaller number of charges on the cations and some have less polarizable anions. All of these materials have considerably lower dielectric constants than

[17] F. C. Frank, "On high dielectric constants," Trans. Faraday Soc. **33**, 513–23 (1937).

[18] M. Born and M. Göppert-Mayer, "Dynamic lattice theory of crystals," *Handbuch der Physik*, second edition, Vol. 24/2 (1933), p. 646.

rutile. This indicates that Frank's criteria for high atomic polarizability are not true in general.

Frank also pointed out that the differences in dielectric constant among the three forms of TiO_2 are very nearly accounted for by the differences in densities. To show this, he computed the molar polarizabilities by means of the Clausius-Mosotti relation in the molar form, or

$$P_m = \frac{\epsilon - 1}{\epsilon + 2} \cdot \frac{M}{\rho},$$

where P_m is the total molar polarizability, M the molecular weight and ρ the density. The results of this computation are shown in Table III. The molar polarizability is approximately constant in going from rutile to anatase while the dielectric constant decreases markedly and the density only moderately. Although density differences approximately account for differences in dielectric constant among the allotropic forms of TiO_2, the dielectric constant of materials of different chemical composition cannot be predicted either on the basis of density alone or on the basis of differences in molar volume M/ρ. Taking SnO_2 for example, it is found that the density is 6.95, compared with 4.25 for rutile, yet the dielectric constant of the former is only 24. This shows that the polarizability per gram or the value of $(\epsilon-1)/(\epsilon+2)\rho$* is not constant for all materials. In spite of its low dielectric constant, SnO_2 also has a higher molar polarizability (19.2 cc) than rutile (18.2).

This discussion, therefore, indicates that the dielectric constant cannot be predicted on the basis of (1) the magnitude of the ratio of the electronic polarizability per atom to the atomic volume; (2) the magnitude of the charge on the cation and the ease of distortion of the anion, and (3) the density. It would appear that Frank's mechanism for the high dielectric constant of rutile is inadequate.

A better understanding of the mechanism for the high dielectric constant of rutile can be obtained by examining Table IV. In this table a number of inorganic materials are arranged in the order of decreasing dielectric constants. The third column gives the total volume polarizability, calculated by means of the Clausius-Mosotti relation, the fourth gives the high frequency dielectric constant or that part of the total dielectric constant contributed by the electronic polarizability, the fifth column gives the electronic polarizability calculated from the value of ϵ_0 given in the fourth column, and the sixth column gives the atomic polarizability found by subtracting the electronic part from the total. In the case of isotropic materials the high frequency dielectric constant, ϵ_0, was obtained by squaring the refractive index for the sodium D line. For anisotropic materials the square of the appropriate mean refractive index was used.

Rutile has the highest electronic polarizability of all the materials listed. On the other hand, a number of materials have a higher atomic polarizability. Therefore, the high dielectric constant is attributable to the high electronic polarizability rather than to any unusual atomic polarizability. This conclusion is at variance with the suggestion made by Frank that, although the electronic and atomic polarizabilities separately are incapable of giving values of p approaching 1 and hence high values of ϵ, they can do so together when both are high.

Because of the nature of the Clausius-Mosotti equation which may be written in the form,

$$\epsilon = \frac{3}{1-p} - 2,$$

a small change in p produces a large change in ϵ when p is near unity. On this basis the large difference between the dielectric constant of rutile and that of other materials does not appear so unreasonable. Rutile has a polarizability of 0.974 while SnO_2, for example, has a polarizability of 0.885; the corresponding dielectric constants are 114 and 24, respectively. Thus, the difference between rutile and SnO_2 appears insignificant when viewed from the standpoint of the volume polarizability.

The negative temperature coefficient of the dielectric constant of rutile can be made plausible by a consideration of the mechanisms contributing to the temperature dependence as discussed by Bretscher.[19] In the first place, a

* This has been called the specific polarizability which is usually found to be independent of temperature for any one material.

[19] E. Bretscher, "The temperature variation of the dielectric constant of ionic crystals," Trans. Faraday Soc. 30, 684–7 (1934).

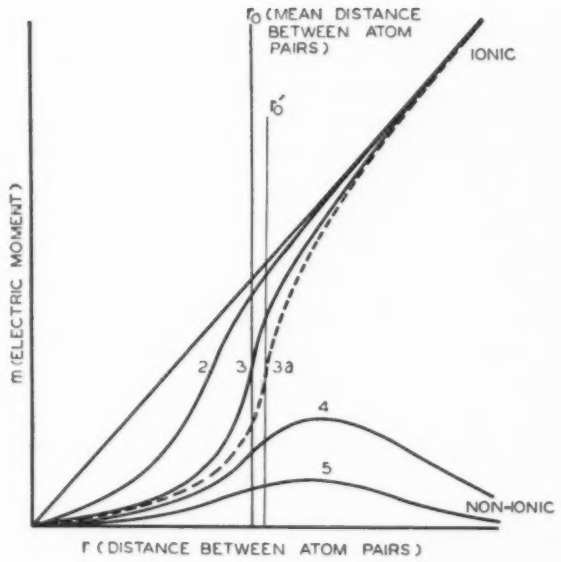

FIG. 11. Dependence of induced moment on internuclear distance (Eucken and Büchner).

decrease in density with increasing temperature tends to decrease the dielectric constant and affects both the electronic and atomic parts of the total polarizability. A second contribution to the temperature coefficient based on the decrease in interatomic forces with thermal expansion tends to increase the dielectric constant with temperature. This latter mechanism operates only on the atomic polarizability. Since the electronic polarizability is considerably larger than the atomic polarizability, the density effect should predominate and should result in an over-all temperature coefficient which is negative.

Let us now consider the mechanism proposed by Eucken and Büchner. They computed the dielectric constants of a number of materials including rutile using an equation derived by Born[18] for the dielectric constant of an ionic crystal. This equation takes the following form:

$$\epsilon = \epsilon_0 + (ne)^2 Nq\rho/\pi\nu^2 M_1 M_2,$$

where ϵ_0 is the dielectric constant corresponding to the square of the refractive index extrapolated to the frequency for which the dielectric constant is to be computed, n is the valence, e is the charge on the electron, N is Avogadro's number, q is a constant equal to 1 for diatomic molecules, 2 for triatomic molecules, etc., ρ is the density, ν the characteristic frequency of infra-red vibrations of the lattice (ν^2 is proportional to the force between two ions) and M_1 and M_2 are the atomic weights of the ions. This equation resulted in too small values for the alkali halides and much too small values for rutile, TlCl and TlBr.

Eucken and Büchner suggested that the Born equation is in error and that the cause of the error is the term ne which is a measure of the effective charge on the ions. The earlier theoretical work of Kirkwood[20] and the experimental work of Bartholomé[21] on hydrogen halides indicates that the effective charge on the ions varies with the distance between ions. Using this idea, Eucken and Büchner constructed the series of curves shown in Fig. 11. If r is the interatomic distance, ne the effective charge and if ne is independent of r, then the electric moment m per molecule and the first derivative of m with respect to r are, respectively,

$$m = (ne)r$$
$$dm/dr = ne = \text{constant}.$$

If, however, ne is dependent upon r, then dm/dr can no longer be equated to ne, but becomes

$$dm/dr = ne + d(ne)/dr.$$

This indicates the rate of change of moment with respect to interatomic distance is no longer constant and equal to the effective charge, but larger by a term depending upon the rate of change of the effective charge with interatomic distance. If it is true that ne is dependent upon the interatomic distance then the term ne in the Born equation should be replaced with dm/dr. By means of the curves of Fig. 11 giving the variation of m with respect to r, Eucken and Büchner attempt to show that dm/dr is larger than ne and that therefore substitution of ne by dm/dr should result in higher dielectric constants.

The various curves of Fig. 11 are for various types of binding ranging from the purely ionic to the non-ionic or homopolar. Curve 1 is for purely ionic crystals with point charges, a condition which even the alkali halides cannot meet. It is seen that dm/dr or the slope of curve 1 is equal to ne. Curve 2 is supposed to represent conditions for the alkali halides and curves 4 and 5 for

[20] J. G. Kirkwood, "Quantum-mechanical calculation of the constants of some polar molecules," Physik. Zeits. **33**, 259–265 (1932).

[21] E. Bartholomé, "On the character of binding in the halogen hydrides on the basis of absolute intensity measurements of the infra-red vibration bands," Zeits. f. physik. Chemie **B23**, 131 (1933).

materials possessing largely homopolar binding. Curve 3*a* is presumed to represent the case of the borderline between ionic and non-ionic binding. Eucken and Büchner present some chemical evidence which is, however, not very convincing, that rutile possesses a type of binding which lies near the borderline, but slightly on the ionic side. Curve 3 is, therefore, supposed to represent conditions for rutile. They make the further assumption that the inflection point of curve 3 comes at or near a value of r equal to the value of the mean interatomic distance r_0. If this is granted, then the value of dm/dr is considerably larger than ne at the inflection point and therefore a high dielectric constant should be expected.

Eucken and Büchner also explain the negative temperature coefficient of rutile on the basis of curve 3. When the temperature is raised the crystal expands so that at a certain elevated temperature the mean distance between atoms is greater than r_0 or r_0'. At r_0', curve 3 has a lower value of dm/dr than at r_0 and hence an increase in temperature would be expected to result in a lower dielectric constant.

This mechanism appears to explain the dielectric properties of rutile in a qualitative way. It rests, however, on the questionable basis of the Born equation which assumes additivity of the electronic and atomic parts of the dielectric constant, rather than additivity of the polarizabilities calculated from the more generally accepted Clausius-Mosotti equation. Since the differences among the refractive indices of different materials are at most not very large, gross differences among dielectric constants must be explained by large differences in the atomic part of the dielectric constant. This is in direct contradiction to the mechanism based on the Clausius-Mosotti equation. Furthermore, the variation of effective charge with change in interatomic distance, which plays a large role in this mechanism, has not been proved. This explanation of the high dielectric constant therefore, does not appear to be well founded.

On the other hand, if the correctness of the Clausius-Mosotti equation is assumed, the rapidly varying nature of the function connecting dielectric constant and polarizability for values of polarizability near unity, is itself sufficient to account for large differences in dielectric constants. On the basis of this picture, therefore, the high dielectric constant of rutile is attributable to a slightly high index of refraction coupled with a normal atomic polarizability which produces an over-all polarizability nearer unity than for most other materials. The validity of the Clausius-Mosotti equation is difficult to establish. Some support for it, however, is found in the fact that when a mean dielectric constant for randomly oriented crystals is computed by means of this equation from the values corresponding to the different crystal axes, a value nearer the measured value results than when the simple average dielectric constant is computed.

VI. Summary

Power factor and dielectric constant data over a range of frequency and temperature are presented for three specimens of rutile. The preparation of the specimens is described. The data show that the rutile form of TiO_2 combines a dielectric constant in the neighborhood of 100 with low dielectric losses over a wide frequency range. At the higher frequencies a negative temperature coefficient of dielectric constant is found. The dielectric constants of mixtures of rutile with other dielectric materials are shown to follow a logarithmic mixture formula. Two different mechanisms for the high dielectric constant, one proposed by Frank and the other by Eucken and Büchner, are discussed. Evidence is presented that a mechanism based on the Clausius-Mosotti equation offers a plausible expianation for the high dielectric constant. This indicates that a high refractive index coupled with a normal atomic polarizability is sufficient to account for a high dielectric constant. The validity of the Clausius-Mosotti equation for rutile, however, is not conclusively established.

VII. Acknowledgment

We wish to express our appreciation to Drs. C. F. Hill and E. U. Condon of the Westinghouse Research Laboratories for their interest and helpful suggestions. We are also indebted to the Stupakoff Laboratories, Inc., of Pittsburgh, Pennsylvania, for firing the rutile disks and to the Titanium Alloy Manufacturing Company of Niagara Falls, New York, for making available the rutile powder.

Contributors to This Issue

C. G. Cruzan

C. G. Cruzan received the B.S. and M.S. degrees from the Oklahoma Agricultural and Mechanical College in 1934 and 1938, respectively. He was at one time associated with the engineering staff of the Fort Supply Dam, and he taught in high school for three years. Mr. Cruzan is now Professor of Physics in the Junior College of Woodward, Oklahoma.

R. B. Block

Raymond B. Block is an Assistant Aeronautical Engineer in the Experimental Engineering Section at Wright Field, Dayton, Ohio. He was graduated from the Massachusetts Institute of Technology in 1927 and later took advanced work in physics and mathematics at the Johns Hopkins University and at the George Washington University.

M. E. Bell

Maurice E. Bell received his Ph.D. degree in 1937 from the Massachusetts Institute of Technology, where he held a teaching fellowship for the years 1934–35 and 1936–37. In 1935–36 he was Redfield Proctor Travelling Fellow at Trinity College, Cambridge, England. Since 1937 he has been employed with the Westinghouse Electric and Manufacturing Company.

R. Rüdenberg

Reinhold Rüdenberg took his doctor's degree at the Institute of Technology in Hannover, Germany. He was at one time assistant in mechanics at Göttingen University. Dr. Rüdenberg did electrical engineering work at Siemens Schuckertwerke and was, simultaneously, honorary professor at the Institute of Technology, Charlottenburg. After a period of consulting engineering with the General Electric Company, Ltd., London, he became Gordon McKay Professor of Electrical Engineering at Harvard University.

C. J. Vogt

Carl J. Vogt received his B.S. and M.S. degrees from the University of California. From 1926 to 1928 he was associated with the Research and Development Department of the Standard Oil Company of California. In 1928 he joined the faculty of the University of California, where he now holds the position of Associate Professor of Mechanical Engineering.

L. J. Berberich

Robert Matteson's biography appeared in the *Journal of Applied Physics* on page 36, Vol. 9, No. 1, 1938.

Andrew Gemant is a consultant and research engineer with the Detroit Edison Company, Detroit, Michigan. A biographical sketch and picture of Dr. Gemant appeared in the *Journal of Applied Physics*, page 704, Vol. 9, No. 11, 1938, at which time he was associated with the University of Wisconsin.

Leo J. Berberich received his Dr. Eng. degree in 1931 from the Johns Hopkins University. After having been connected with the laboratories of the National Bureau of Standards and the Socony-Vacuum Oil Company, Inc., he is now a research engineer in electrical insulation at the Westinghouse Research Laboratories.

M. H. Pakkala

M. H. Pakkala obtained a B.S. degree at Montana State College in 1929. At Oxford University, England, he received a B.A. degree in 1931 and completed his examinations toward a B.Sc. degree in 1932. During 1936 and 1937 he studied at Harvard and Massachusetts Institute of Technology. Since 1937 he has been employed by the United States Steel Corporation and the Carnegie-Illinois Steel Corporation.

R. Hultgren

H. A. Miley

H. A. Miley holds a Ph.D. degree in physics from the University of Colorado and a Ph.D. degree in metallurgy from Cambridge University, England, where he was a Carnegie research scholar. He is now a member of the physics staff at the Oklahoma Agricultural and Mechanical College.

Ralph Hultgren, Assistant Professor of Metallurgy at Harvard University, received his Ph.D. degree in physical chemistry at California Institute of Technology in 1933 and was appointed National Research Fellow at the Massachusetts Institute of Technology. In 1935 he joined the staff of the Harvard Engineering School.

Here and There

Cover Photograph

The cover photograph, taken in the laboratories of the American Optical Company, shows a physicist preparing a report of control measurements made on absorption glasses. Every melt must be approved by the laboratory before the raw glasses are released for fabrication into lenses. The tests include determination of the index of refraction, ultraviolet absorption, visual color, visual transmission, total energy transmission, and, when necessary, dispersion, coefficient of expansion, chemical durability, stability against color changes in ultraviolet and sun light, and softening point. Absorption glasses are made up into ophthalmic, sun glass, and protection lenses, the latter being used by welders, furnace and foundry men.

★

University of Pennsylvania Bicentennial Conference

A Bicentennial Conference held September 16 to 20 on the campus of the University of Pennsylvania in Philadelphia formed part of a Bicentennial Week program commemorating the 200th anniversary of the origin of that University. The list of speakers for the Conference included more than 200 American and European scholars and leaders in various fields of science and thought. The sessions on the subject of nuclear physics included the following speakers: Enrico Fermi, Ph.D., Professor of Physics, Columbia University; Gregory Breit, Ph.D., Professor of Physics, University of Wisconsin; I. I. Rabi, Ph.D., Professor of Physics, Columbia University; Eugene Paul Wigner, Dr. Ing., Thomas D. Jones Professor of Mathematical Physics, Princeton University; J. Robert Oppenheimer, Ph.D., Professor of Physics, University of California; and John Hasbrouck Van Vleck, Ph.D., Sc.D., Professor of Mathematical Physics and Tutor in the Department of Physics, Harvard University.

★

Conference on Nuclear Physics at Indiana University

To celebrate the opening of the new physics building, Swain Hall, a Conference on Nuclear Physics will be held at Indiana University, Bloomington, Indiana, on Friday and Saturday, October 25 and 26, according to an announcement made by the Physics Department there. The program will be devoted to the discussion of current problems in Nuclear Physics. Special lectures will be given by Professor H. A. Bethe, Cornell University; Professor G. Breit, University of Wisconsin; Professor L. A. DuBridge, University of Rochester; and Professor I. I. Rabi, Columbia University. Visitors will have the opportunity of inspecting the new Physics Laboratories, the Indiana University cyclotron, and the researches on nuclear physics in progress in the department.

Symposium on Physics of Rubber

A Symposium on the Physics of Rubber, sponsored by the Ohio Section of the American Physical Society, will be held October 11 and 12 in Akron, Ohio, according to the announcement made by Dr. H. P. Knauss, chairman of the program committee. The tentative program is as follows:

Friday afternoon: Tours through factories or research laboratories, and the Guggenheim Institute.
Friday evening: Dinner at the University Cafeteria. Address: **Physical Methods for Investigating the Structure of Molecules,** by PROFESSOR P. DEBYE, *Cornell University.*
Saturday morning:
1. **Physics in the Manufacture and Use of Rubber,** by JAMES W. SCHADE, *Director of Research, B. F. Goodrich Company, Akron, Ohio.*
2. **Thermal Problems in Rubber Manufacture,** by STUART H. HAHN, *B. F. Goodrich Company, Akron, Ohio.*
3. **The Optical Properties of Rubber,** by DR. LAWRENCE A. WOOD, *National Bureau of Standards.*
4. **Dielectric Constant and Power Factor of Koroseal at Radio Frequencies,** by DR. O. R. FOUTS, *University of Akron.*
5. **An X-Ray Study of the Proportion of Crystalline and Amorphous Components in Stretched Rubber,** by DR. J. E. FIELD, *Goodyear Tire and Rubber Company, Akron, Ohio.*
6. **Infra-red Spectra of Rubber,** by DR. W. C. SEARS, *B. F. Goodrich Company, Akron, Ohio.*
7. **Some Applications of the Kinetic Theory of Rubber Elasticity,** by DR. H. MARK, *Brooklyn Polytechnic Institute, New York.*

Luncheon, University Cafeteria.

★

RCA Fellowship

A fellowship for the investigation of biological problems with the electron microscope recently developed in the RCA research laboratories has been established in the National Research Council through funds provided by the RCA Manufacturing Company.

With the electron microscope it is possible to see minute objects that are 20 to 50 times smaller than can be seen with the finest optical microscope. Further research with this new scientific tool is expected to reveal new data on the structure of viruses, bacteria and other micro-organisms, and tissue cells.

In considering candidates, the National Research Council will give preference to "versatile young men of United States citizenship, who have sound training in micro-biology, a doctor's degree (Ph.D. or M.D.), and a record of original work." The RCA Fellowship is for the year 1940–41 and will carry a stipendium of $3000. The work will be carried on at the research laboratory of RCA at Camden, New Jersey.

★

Institute of Meteorology

Establishment of an Institute of Meteorology at the University of Chicago at which Army, Navy and Air Corps students as well as weather bureau and lay personnel will be trained, has been announced by President Robert M. Hutchins. Creation of the Institute was made possible by an anonymous doner who has made funds available permitting founding of a long-range comprehensive program. The Institute will be headed by Dr. C. G. Rossby, originator of the "Rossby diagrams" and a leading exponent in this country of the air mass theory.

Necrology

Sir Oliver Lodge, who was from 1881 to 1900 Professor of Physics and Mathematics at University College, Liverpool, and from 1900 to 1919 Principal of Birmingham University, died on August 22 at the age of eighty-nine years, *Science* reports.

★

NRC Conference on Electrical Insulation

The Conference on Electrical Insulation of the National Research Council, Division of Engineering and Industrial Research, will hold a three-day meeting in Washington, D. C., beginning October 31. The meeting will be held at the headquarters of the National Research Council in the building of the National Academy of Sciences.

As in other years there will be numerous reports on current investigations covering different aspects of dielectric problems which should prove interesting and stimulating to workers in this field. Anyone interested and not on the mailing list of the Conference may obtain a program for the meeting by writing the Secretary of the Conference, Thorstein Larsen, Consolidated Edison Company, 55 Johnson Street, Brooklyn, New York.

★

Calendar of Meetings

October

2– 4	American Oil Chemists' Society, Chicago, Illinois
2– 5	Electrochemical Society, Ottawa, Canada
3– 5	Optical Society of America, Rochester, New York
7–11	National Safety Council, Chicago, Illinois
18–19	Society of Rheology, New York, New York
18–19	American Association of Textile Chemists and Colorists, New York, New York
21–25	American Society for Metals, Cleveland, Ohio
21–26	American Welding Society, Cleveland, Ohio
28–30	National Academy of Science, Philadelphia, Pennsylvania
28–Nov. 2	Conference on Applied Nuclear Physics, Cambridge, Massachusetts

November

11–15	American Petroleum Institute, Chicago, Illinois
15–16	Acoustical Society of America, Chicago, Illinois
22–23	American Physical Society, Chicago, Illinois

December

2– 4	American Institute of Chemical Engineers, New Orleans, Louisiana
2– 7	Highway Research Board of National Research Council, Washington, D. C.
3– 6	American Society of Mechanical Engineers, New York, New York
26–28	American Physical Society, Philadelphia, Pennsylvania
26–28	Geological Society of America, Austin, Texas
28–30	American Association of Physics Teachers, Philadelphia, Pennsylvania
27–Jan. 2	American Association for the Advancement of Science, Philadelphia, Pennsylvania

February

21–22	American Physical Society, Cambridge, Massachusetts

April

7–11	American Chemical Society, St. Louis, Missouri

May

1– 3	American Physical Society, Washington, D. C.

June

20–21	American Physical Society, Providence, Rhode Island

Conference on Applied Nuclear Physics

October 28–November 2, 1940

A GENERAL Conference on Applied Nuclear Physics, sponsored by the American Institute of Physics in cooperation with the Massachusetts Institute of Technology, will be held during the week of October 28–November 2, 1940, at the Massachusetts Institute of Technology, Cambridge, Massachusetts. The rapidly increasing number of applications of methods and apparatus characteristic of nuclear physics in the fields of biology, radiology, chemistry, geology, and industrial physics has long emphasized the usefulness of a joint conference between physicists and their colleagues in other fields of science.

The purposes of the Conference are to bring together investigators who may be widely separated geographically, and to provide a forum for assembling and correlating present knowledge and difficulties, and for directing attention toward fundamental lines of research which should be the subject of future investigations.

The week's activities will be divided into separate sessions on applications to biology, chemistry, radiology, metallurgy, geology, and to general sessions relating to the production and use of radioactive and stable isotopes, and the protection of workers from radiation. An outline of the general program is given in the following table:

CONFERENCE ON APPLIED NUCLEAR PHYSICS

Digest of Program

Monday A.M., October 28, 1940 (two parallel sessions)

Geology I: "Techniques and Standards in Terrestrial Radioactivity Measurements."
Metallurgy I: "Tracer Studies of Metal Diffusion."

Monday P.M., October 28, 1940 (two parallel sessions)

Geology II: "Geochemical Applications of Radioactivity."
Metallurgy II: "Metallurgical Applications of Nuclear Physics."

Tuesday A.M., October 29, 1940 (three parallel sessions)

Geology III: "Radioactive Methods of Geologic Age Determinations."
Chemistry I: "Tracer Techniques in General Chemistry."
Radiology I: "General Aspects of Cancer Therapy."
Biology I: "The Study of Animal Metabolism with Radioactive Tracers."

Tuesday P.M., October 29, 1940 (three parallel sessions)

Geology IV: "Geophysical Applications of Nuclear Physics."
Chemistry II: "Tracer Techniques in Analytical Chemistry."
Radiology II: "Radium and Roentgen Therapy."
Biology II: "The Study of Animal Metabolism with Radioactive Tracers."

Wednesday A.M., October 30, 1940

General I: "Production of Radioactive and Stable Isotopes and of Penetrating Radiations."

Wednesday P.M., October 30, 1940

General II: "Measurement of Radioactive and Stable Isotopes and of Penetrating Radiations."

Thursday A.M., October 31, 1940

General III: "Protection of Workers from Injurious Effects of Radiation."

Thursday P.M., October 31, 1940 (three parallel sessions)

Chemistry III: "Synthesis of Organic Substances Containing Tracers."
Radiology III: "Neutron and Artificial Radioactivity Therapy."
Biology III: "The Study of Animal Metabolism with Radioactive Tracers."

Friday A.M., November 1, 1940 (two parallel sessions)

Radiology IV: "Dosage Measurements."
Biology IV: "Biochemical Studies with Stable and Radioactive Isotopes."

Friday P.M., November 1, 1940 (two parallel sessions)

Radiology V: "Radiobiology."
Biology V: "Tracer Studies with Radioactive Arsenic and Sulphur."

Saturday A.M., November 2, 1940 (two parallel sessions)

Biology VI: "Studies of Plant Metabolism with Stable and Radioactive Isotopes."
General IV: "Contributed Papers."

Committee in Charge of Program

Robley D. Evans, *Chairman*
Massachusetts Institute of Technology

Elmer Hutchisson, *Secretary*
University of Pittsburgh
Henry A. Barton
American Institute of Physics
Edw. U. Condon
Westinghouse Electric & Manufacturing Company
Lee A. DuBridge
University of Rochester
G. Failla
Memorial Hospital, New York
Clark Goodman
Massachusetts Institute of Technology
Ernest O. Lawrence
University of California
Harold C. Urey
Columbia University

The daily sessions will consist of short invited papers by leading investigators followed by vigorous and searching discussion by the conferees. Ample time will be allowed between and after regular sessions for personal and informal conferences. Five one-hour evening sessions will be held, in each of which an outstanding investigator will summarize the status of the several fields which are joined together by the Conference. The evening lectures will be open to the general public.

Anyone who can actively participate in or profit by the Conference is eligible and cordially invited to become a member. Advance registration (no fee) will be required to permit suitable arrangements to be made. Those wishing to attend should register by letter as soon as possible and not later than October 1. Letters and inquiries should be addressed to Professor Robley D. Evans, General Chairman, Conference on Applied Nuclear Physics, Massachusetts Institute of Technology.